ÇUKUROVA UNIVERSITY
INSTITUTE OF NATURAL AND APPLIED SCIENCES

MSc THESIS

Mehmet Onur OĞULATA

RATINGS OF VARIOUS GEAR DESIGN APPROACHES AND A TRANSLATION TECHNIQUE FOR SPIRAL BEVEL GEAR DESIGN

DEPARTMENT OF MECHANICAL ENGINEERING

ADANA-2020

ÇUKUROVA UNIVERSITY
INSTITUTE OF NATURAL AND APPLIED SCIENCES

RATINGS OF VARIOUS GEAR DESIGN APPROACHES AND A TRANSLATION TECHNIQUE FOR SPIRAL BEVEL GEAR DESIGN

Mehmet Onur OĞULATA

MSc THESIS

DEPARTMENT OF MECHANICAL ENGINEERING

We certify that the thesis titled above was reviewed and approved for the award of degree of the Master of Science by the board of jury on 28/05/2020

…….	……..	……
Prof. Dr. Necdet GEREN	Prof. Dr. Melih BAYRAMOĞLU	Prof. Dr. Uğur EŞME
SUPERVISOR	MEMBER	MEMBER

This MSc Thesis is written at the Department of Mechanical Engineering, Institute of Natural and Applied Sciences of Çukurova University.
Registration Number:

Prof. Dr. Mustafa GÖK
Director
Institute of Natural and Applied Sciences

This thesis was supported by the Scientific Research Project Unit of Çukurova University with a project number of FYL-2018-10376

ABSTRACT

MSc THESIS

RATINGS OF VARIOUS GEAR DESIGN APPROACHES AND A TRANSLATION TECHNIQUE FOR SPIRAL BEVEL GEAR DESIGN

Mehmet Onur OĞULATA

ÇUKUROVA UNIVERSITY
INSTITUTE OF NATURAL AND APPLIED SCIENCES
DEPARTMENT OF MECHANICAL ENGINEERING

Supervisor : Prof. Dr. Necdet GEREN
Year: 2020, Page: 196
Jury : Prof. Dr. Necdet GEREN
: Prof. Dr. Melih BAYRAMOĞLU
: Prof. Dr. Uğur EŞME

In this thesis, spiral bevel gear design under bending fatigue stress has been designed according to various national and international standards and machine element textbooks. Numerical analysis was performed using the analytical results (module(m) and face width(F)) obtained from the design made for each approach. Numerical analysis was done using Ansys software. The dimensionless gear rating numbers (GRi) is obtained for each approach and then the derived correlation equations are used to generate the dimensionless conversion factors (CFs). CFs allow designers and engineering students to easily conversion from one approach to ANSI/AGMA Standard. In addition, it allows the designer to optimization of gear tooth volume using GRi values.

Key Words: Spiral bevel gear design, Design approaches, Design outputs, Translation technique for spiral bevel gear

ÖZ

YÜKSEK LİSANS TEZİ

EĞRİSEL KONİK DİŞLİ TASARIMI İÇİN ÇEŞİTLİ DİŞLİ TASARIM YAKLAŞIMLARININ ORANLANMASI VE DÖNÜŞÜM FAKTÖRLERİNİN BULUNMASI

Mehmet Onur OĞULATA

ÇUKUROVA ÜNİVERSİTESİ
FEN BİLİMLERİ ENSTİTÜSÜ
MAKİNE MÜHENDİSLİĞİ ANABİLİM DALI

Danışman : Prof. Dr. Necdet GEREN
Yıl:2020, Sayfa: 196
Juri : Prof. Dr. Necdet GEREN
: Prof. Dr. Melih BAYRAMOĞLU
: Prof. Dr. Uğur EŞME

Bu tezde, spiral konik dişli tasarımı, çeşitli ulusal ve uluslararası standartlara ve makine elemanı ders kitaplarına göre tasarlanmıştır. Sayısal analiz, her yaklaşım için yapılan tasarımdan elde edilen analitik sonuçlar (modül (m) ve alın genişliği (F)) kullanılarak yapılmıştır. Nümerik analiz Ansys yazılımı kullanılarak yapılmıştır. Her yaklaşım için boyutsuz dişli derecelendirme sayıları (GRi) elde edilmiştir ve daha sonra türetilmiş korelasyon denklemleri boyutsuz dönüşüm faktörlerini (CF'ler) oluşturmak için kullanılır. CF'ler tasarımcıların ve mühendislik öğrencilerinin bir yaklaşımdan ANSI / AGMA Standardına kolayca dönüşmesini sağlar. Buna ek olarak, tasarımcının GRi değerlerini kullanarak dişli diş hacmini optimize etmesine izin verir.

Anahtar Kelimeler: Eğrisel konik dişli tasarımı, Tasarım yaklaşımları, Tasarım çıktıları, Spiral konik dişli için çeviri tekniği

EXTENDED ABSTRACT

The primary aim of this study is to obtain a dimensionless number by proportioning the design results (m and F or b) of the commonly used spiral bevel gear design approaches and to evaluate the difference between the design approaches according to the results we obtained. In this study, DIN (German Institute of Standardization), ANSI/AGMA (American Gear Manufacturers Associations), ISO (International Organization for Standardization) standards, and machine element textbooks (Fundamental of Machine Component Design 5th Edition, Juvinall R.C. and Marshek K.M., 2011 and Shigley's Mechanical Engineering Design 9th Edition (SI), Budynas R.G. and Nisbett J.K., 2011) will be studied. In this study, gear design parameters (m and F) given by design approaches for both cost and reliability will be compared.

The secondary objective of the project is to define dimensionless conversion factors to approximate conversion of gear design results in textbooks to more accurate DIN, ISO, or AGMA Standards. The conversion factors will allow the all designers including the expert designers and students who have just started gear design to convert the design results found by using the spiral bevel gear design approach with the simple formulas found in the textbooks into the design results given by the DIN, ISO, or AGMA standards design approaches. Conversion factors will enable relatively complicated and time-consuming DIN, ISO, and AGMA gear designs to be realized in less time with the textbook solutions, thus reducing convenience and design costs for designers.

This thesis provides the need to select and use appropriate spiral bevel gear design approaches that include all designers, from students who have just begun to gear design to designers who have been engaged in gear design for a long time. The selected approaches are DIN 3991, 1987 (German Institute of Standardization), ANSI/AGMA 2003-B97, 1997 (American Gear Manufacturers Associations), ISO 10300, 2001 (International Organization for Standardization)

standards, and machine element textbooks (Fundamental of Machine Component Design 5th Edition, Juvinall R.C. and Marshek K.M., 2011 and Shigley's Mechanical Engineering Design 9th Edition (SI), Budynas R.G. and Nisbett J.K., 2011).

Gear designs made with ISO, DIN and ANSI/AGMA Standards take more time since they have more complex formulations than machine element textbook (Fundamental of Machine Component Design 5th Edition, Juvinall R.C. and Marshek K.M., 2011). Therefore, conversion factors for the conversion of machine element textbook results to the verified results were developed. Conversion factors will enable relatively complicated and time-consuming DIN, ISO, and AGMA gear designs to be realized in less time with the textbook solution, thus reducing convenience and design costs for designers.

ANSYS program is used for the Finite Element Method (FEM). The numerical solutions were compared with the analytical results we obtained. There is less than 10% difference between analytical and numerical results in all approaches, except for Fundamental of Machine Component Design 5th Edition, Juvinall R.C. and Marshek K.M., 2011 at twenty degrees and twenty-five degrees of angles. This result is to reinforce the accuracy of the design.

Although the results of all design approaches differ from each other, they are very similar with excellent continuity of the charts. Dimensionless numbers as geometric rating numbers (GRi) and conversion factors (CFs), has been described and proposed to rate DIN, ISO and textbook design approaches with ANSI/AGMA 2003-B97, 1997 approach based on bending fatigue failure for spiral bevel gears. However, any approach converts to ANSI/AGMA 2003-B97, 1997 can be converted with minimum error. Beyond the investigations already available in the literature, following conclusions can be drawn in this study;

Use of radar graphics, GRi values can be read for each approach and transmitted power at a given speed ratio (1:1 to 1:8) compared to gear AGMA. It is also observed that the trend is similar even if the transmitted power changes.

When the hardness value of material increased, there was a significant decrease in the module and face width values for the DIN, ISO and J&M approaches, while the values in the AGMA approach decreased slightly. Therefore, there is a decrease in GRi values.

Dimensionless module and face width conversion factors (CFs) were generated for spiral bevel gears to convert the design results of ISO Standards, DIN Standards, and J&M machine element textbook into AGMA with low error. The formulas and values required to obtain conversion factors are given in section 4.4. If the speed ratio is an integer (1: 1 to 1: 8), CFs values can be obtained by using table 4.7 and 4.8 for the 20-degree pressure angle and table 4.9 and table 4.10 for the 25-degree pressure angle.

CFs values were confirmed by performing a case study in section 4.5. The maximum Gear Volume error (GVe) was found as 12.859% for 20-degree pressure in Table 4.17 and 11,774% for 25-degree pressure in table 4.18 with the aid of CFs. These values are for 5 kW power transmission value, 1.8:1 speed ratio, and J&M design approach. The reason for this is that it will peak between 0.5 kW and 20 kW, as can be seen in the GRi tables in Section 4.3. Looking at other study cases, the error is less than 10%. This provides the confirmability of CFs.

Shortly, this study can serve as a guide for designers interested in spiral bevel gear design. The designer may optimize the gearbox design by choosing the size according to the data in the study. Besides, for students who are new to spiral bevel gear design, they can transform the design results of easier methods into the design results of technical standards using conversion formulas without the hassle of using complex formulas. Finally, the results of this study interest all designers, from students who have just begun to gear design to designers who have been engaged in gear design for a long time.

GENİŞLETİLMİŞ ÖZET

Bu çalışmanın temel amacı, yaygın olarak kullanılan spiral konik dişli tasarım yaklaşımlarının tasarım sonuçlarını (m ve F veya b) oranlandırarak boyutsuz bir sayı elde etmek ve elde ettiğimiz sonuçlara göre tasarım yaklaşımları arasındaki farkı değerlendirmektir. Bu çalışmada, DIN (Alman Standardizasyon Enstitüsü), ANSI / AGMA (Amerikan Dişli Üreticileri Birlikleri), ISO (Uluslararası Standartlar Örgütü) standartları ve makine elemanı ders kitapları (Makine Bileşeni Tasarımı 5. Baskı, Juvinall RC ve Marshek KM, 2011 ve Shigley Makine Mühendisliği Tasarım 9. Baskı (SI), Budynas RG ve Nisbett JK, 2011) incelenecektir. Bu çalışmada, maliyet ve güvenilirlik için tasarım yaklaşımlarının verdiği dişli tasarım parametreleri (m ve F) karşılaştırılacaktır.

Projenin ikincil hedefi, dişli tasarım sonuçlarının ders kitaplarından daha doğru DIN, ISO veya AGMA Standartlarına dönüştürülmesini yaklaşık olarak ölçmek için boyutsuz dönüşüm faktörlerini tanımlamaktır. Dönüşüm faktörleri, uzman tasarımcılar ve dişli tasarımına yeni başlayan öğrenciler dahil tüm tasarımcıların, ders kitaplarında bulunan basit formüllerle eğimli konik dişli tasarım yaklaşımı kullanılarak bulunan tasarım sonuçlarını DIN tarafından verilen tasarım sonuçlarına dönüştürmelerini sağlayacaktır. , ISO veya AGMA standartları tasarım yaklaşımları. Dönüştürme faktörleri, ders kitabı çözümleriyle nispeten karmaşık ve zaman alıcı DIN, ISO ve AGMA dişli tasarımlarının daha kısa sürede gerçekleştirilmesini sağlayacak, böylece tasarımcılar için kolaylık ve tasarım maliyetlerini azaltacaktır.

Bu tez, dişli tasarımına yeni başlayan öğrencilerden uzun süre dişli tasarımına katılan tasarımcılara kadar tüm tasarımcıları içeren uygun spiral konik dişli tasarım yaklaşımlarının seçilmesi ve kullanılması ihtiyacını sağlamaktadır. Seçilen yaklaşımlar DIN 3991, 1987 (Alman Standardizasyon Enstitüsü), ANSI / AGMA 2003-B97, 1997 (Amerikan Dişli Üreticileri Birlikleri), ISO 10300, 2001 (Uluslararası Standartlar Örgütü) standartları ve makine elemanı ders kitaplarıdır

(Makinenin Temelleri) Bileşen Tasarımı 5. Baskı, Juvinall RC ve Marshek KM, 2011 ve Shigley Makine Mühendisliği Tasarım 9. Baskı (SI), Budynas RG ve Nisbett JK, 2011).

ISO, DIN ve ANSI / AGMA Standartları ile yapılan dişli tasarımları, makine elemanı ders kitabından (Temel Makine Bileşeni Tasarımı 5. Baskı, Juvinall R.C. ve Marshek K.M., 2011) daha karmaşık formülasyonlara sahip olduklarından daha fazla zaman alır. Bu nedenle, makine elemanı ders kitabı sonuçlarının doğrulanmış sonuçlara dönüştürülmesi için dönüşüm faktörleri geliştirilmiştir. Dönüşüm faktörleri, ders kitabı çözümü ile nispeten karmaşık ve zaman alıcı DIN, ISO ve AGMA dişli tasarımlarının daha kısa sürede gerçekleştirilmesini sağlayacak, böylece tasarımcılar için kolaylık ve tasarım maliyetlerini azaltacaktır.

Sonlu Elemanlar Yöntemi için ANSYS programı kullanılmıştır. Sayısal çözümler elde ettiğimiz analitik sonuçlarla karşılaştırıldı. Makine Bileşeni Tasarımı 5. Baskı, Juvinall R.C. hariç olmak üzere, tüm yaklaşımlarda analitik ve sayısal sonuçlar arasında% 10'dan az fark vardır. ve Marshek K.M., 2011'de yirmi derece ve yirmi beş derecelik açılarda. Bu sonuç tasarımın doğruluğunu güçlendirmektir.

Tüm tasarım yaklaşımlarının sonuçları birbirinden farklı olsa da grafiklerin mükemmel sürekliliği ile çok benzerler. Geometrik derecelendirme sayıları (GRi) ve dönüşüm faktörleri (CF'ler) olarak boyutsuz sayılar tarif edilmiş ve spiral, konik dişliler için eğilme yorulma başarısızlığına dayanan ANSI / AGMA 2003-B97, 1997 yaklaşımı ile DIN, ISO ve ders kitabı tasarım yaklaşımlarını derecelendirmek için önerilmiştir. Bununla birlikte, ANSI / AGMA 2003-B97, 1997'ye dönüşen herhangi bir yaklaşım minimum hata ile dönüştürülebilir. Literatürde halihazırda mevcut olan araştırmaların ötesinde, bu çalışmada aşağıdaki sonuçlar çıkarılabilir;

Radar grafiklerinin kullanılarak, GRi değerleri, her yaklaşım için okunabilir ve iletilen gücü, dişli AGMA'ya kıyasla belirli bir hız oranında (1: 1 ila 1: 8) okunabilir. Aktarılan güç değişse bile trendin benzer olduğu da gözlenmektedir.

Malzemenin sertlik değeri arttığında, DIN, ISO ve J&M yaklaşımları için modül ve yüzey genişliği değerlerinde önemli bir azalma olurken AGMA yaklaşımındaki değerler az miktarda azalmıştır. Bu nedenle, GRi değerlerinde bir azalma vardır.

ISO Standartları, DIN Standartları ve J&M makine elemanı ders kitabının tasarım sonuçlarını düşük hata ile AGMA' ya dönüştürmek için spiral konik dişliler için boyutsuz modül ve yüzey genişliği dönüşüm faktörleri (CFs) oluşturulmuştur. Dönüştürme faktörlerini elde etmek için gereken formüller ve değerler bölüm 4.4'te verilmiştir. Hız oranı tamsayı ise (1:1 ‘dan 1:8’e kadar) CF değerleri 20 derecelik basınç açısı için tablo 4.7 ve tablo 4.8 ve 25 derecelik basınç açısı için tablo 4.9 ve 4.10 kullanılarak elde edilebilir.

CFs değerleri bölüm 4.5'te vaka çalışması yapılarak doğrulanmıştır. Maksimum Dişli Hacmi hatası (GVe), Tablo 4.17' de 25 derece basınç için %12.859 ve CF'ler yardımıyla Tablo 4.18' de 25 derece basınç için %11.774 olarak bulunmuştur.

Kısacası, bu çalışma spiral konik dişli tasarımı ile ilgilenen tasarımcılar için bir rehber görevi görebilir. Tasarımcı, çalışmadaki verilere göre boyutu seçerek şanzıman tasarımını optimize edebilir. Buna ek olarak, spiral konik dişli tasarımına yeni başlayan öğrenciler için, karmaşık formüllerin sıkıntısı olmadan dönüşüm formüllerini kullanarak daha kolay yöntemlerin sonuçlarını daha standart çözümlere dönüştürebilirler. Son olarak, bu çalışmanın sonuçları, dişli tasarımına yeni başlayan öğrencilerden, uzun süredir dişli tasarımı yapan tasarımcılara kadar tüm tasarımcıları ilgilendirmektedir.

ACKNOWLEDGEMENT

First and foremost, I would like to express my deepest and heartfelt thanks as well as my most sincere appreciation to my supervisor Prof. Dr. Necdet GEREN for his consistent guidance, critical review and for commenting on the manuscript throughout the course of this research starting from proposal preparation up to the final thesis write up. His readiness in providing assistance and advice greatly helped me to carry out the study. Feeling his support, both personal and professional helped me a lot during my studies.

I would like to thank specially to Rahime Burcu OĞULATA for his continuous morale and encouraging advices starting from my undergraduate education.

Many thanks to my friends, Dr. Erkin AKDOĞAN, Sezgin Eser, Dr. Mehmet ŞAHBAZ and Sezer MORKAVUK for their help for finding tools about my study.

I am especially grateful to my mother Fatma Nurdan OĞULATA, my son and my sister, for their encouragement and persuasion about completing my thesis work.

CONTENTS **PAGE**

LIST OF TABLES **PAGE**

LIST OF FIGURES **PAGE**

1. INTRODUCTION

1.1. Gear Nomenclature

The working gear nomenclature is shown in Figure 1.1. There is a theoretical circle upon which most calculations are based, called a pitch circle. The diameter of the pitch circle called the pitch diameter. The pitch circles of a pair of mating gears are tangent other to another. In a gear pair, the small one of pair is called a pinion, and the larger one of pair is called gear. It is not essential of which is driving to another. İf the gear is the driver, the torque increases, and output speed decreases. If the gear is the driver, output speed increases, and the torque decreases.

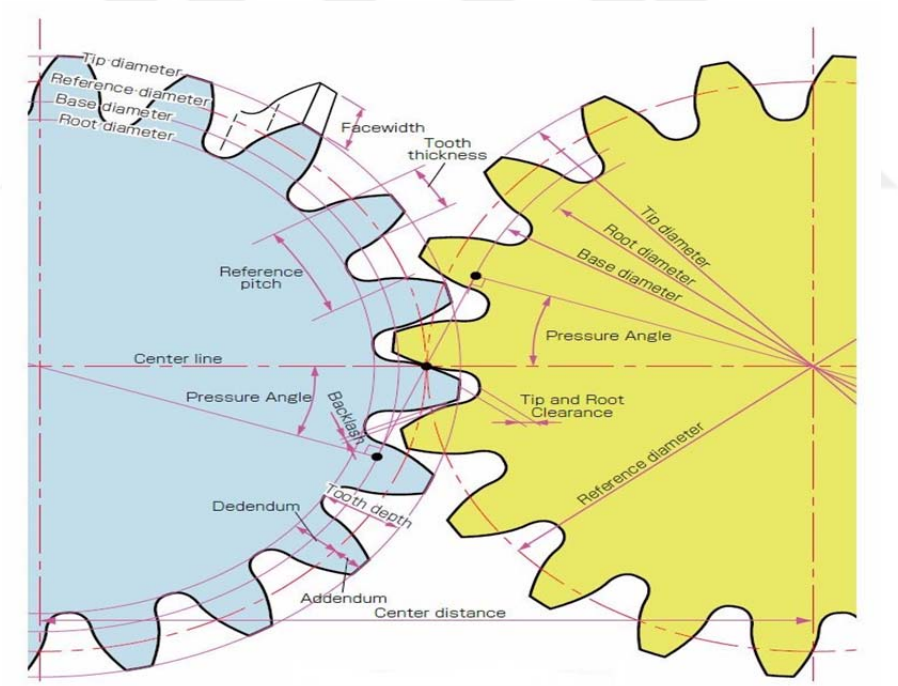

Figure 1.1. Working Gear Nomenclature (Kohara Gear Industry Co)

The circular pitch, p, is the distance that is measuring on the pitch circle from any point on one tooth to a suitable point on another adjacent tooth. Tooth thickness plus the width of space is equal to circular pitch.

The module, m in mm, equal to pitch diameter divided by the number of teeth. The module is used in the SI system. The diametral pitch (P, in inch) equals to the number of teeth divided by pitch diameter. The diametral pitch is used only with U.S. units.

The addendum, a, is the radial distance from the pitch circle and the top land. The dedendum, b, is the radial distance between the pitch circle and bottomland. Sum of the addendum and the dedendum value equals to whole depth, h_t (Budynas R.G. and Nisbett J.K., 2011).

1.2. Features of Gears Profile of Involute Gear Tooth

1.2.1. Profile of Involute Gear Tooth

Simple teeth on a cylindrical wheel changeable speed ratio and speed reduction cause several problems depending on vibration and noise, especially at elevated speeds. At the same time, a gear pair is in a mesh. Different kinds of geometrical forms can be used to eliminate these problems. However, commonly the full depth involute profile is used in most engineering practices (Juvinall R.C., Marshek K.M., 2011).

An involute of the circle is the curve generated by any point on a taut thread as it unwinds from a circle, called the base circle. The generation of two involutes is shown in Figure 1.2.

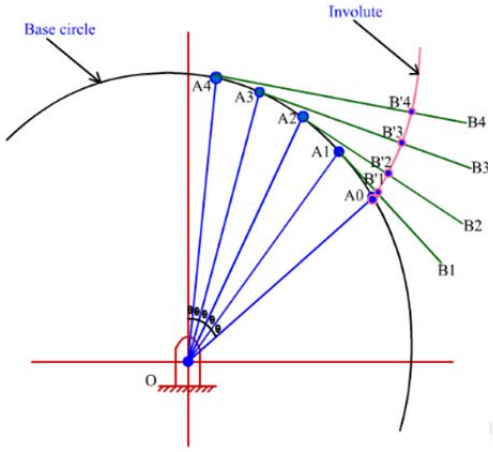

Figure 1.2. Construction of involute gear tooth (Budynas R.G. and Nisbett J.K., 2011)

As shown in Figure 1.2, divide the base circle into several equal parts, and construct radial lines OA_0, OA_1, OA_2etc. Beginning at A_1, construct perpendiculars A_1B_1, A_2B_2, A_3B_3, etc. Then along A_1B_1 lay off the distance A_1A_0, along A_2B_2 lay off twice the distance A_1A_0, etc., producing points through which the involute curve can be constructed (Budynas R.G. and Nisbett J.K., 2011).

1.2.2. Conjugate Action

It is assumed the teeth to be perfectly formed and smooth, and also absolutely rigid. Such an assumption is not correct since the force effect will cause deflections. When the tooth profiles are designed to produce a constant angular velocity ratio during meshing, this design is called conjugate action. Conjugate Gear Tooth Action is given in Figure 1.3. (Budynas R.G. and Nisbett J.K., 2011).

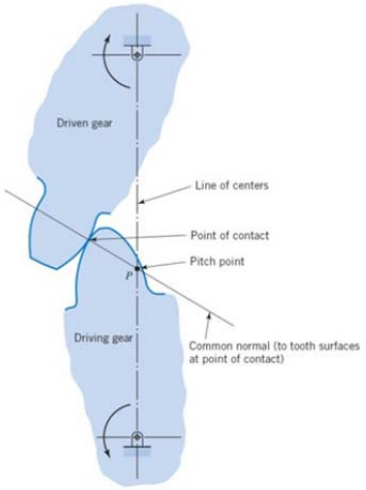

Figure 1.3. Conjugate Gear Tooth Action (Juvinall R.C., Marshek K.M., 2011)

1.3. Gear Classification

Gears can be classified in multiple ways. In particular, two different classifications can be made, with only commonly used gear types and the relationship of the shaft axes on which the gears are mounted.

Another approach is by the relationship of the shaft axes on which the gears are mounted. Shafts may be parallel, intersecting, or nonintersecting and nonparallel (Davis & associates, 2005).

One approach is only commonly used gear types are listed (Budynas R.G. and Nisbett J.K., 2011). In this study, classification was made according to common gear types.

1.3.1. Spur Gears

Spur gears, shown in Figure 1.4., is the most straightforward gear and their teeth parallel to the axis of rotation. They are used to transmit motion one shaft to another (Budynas R.G. and Nisbett J.K., 2011).

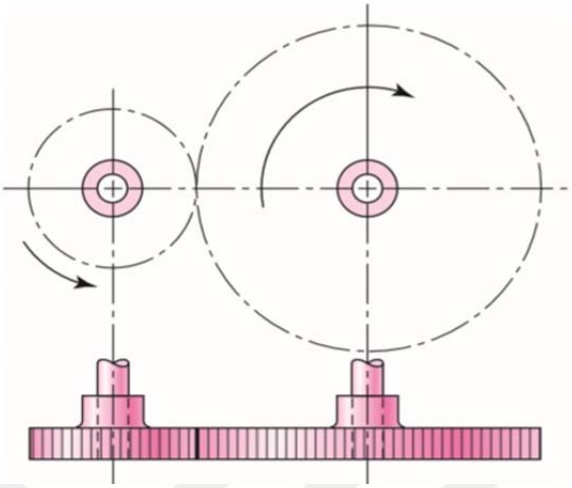

Figure 1.4. Spur Gear (Budynas R.G. and Nisbett J.K., 2011)

1.3.2. Helical Gears

Helical gears, illustrated in Figure 1.5., have teeth inclined to rotation axes. They were quieter than spur gears when helical gears in spur gear application. Because helical gears do lots of gradual engagement of the teeth during meshing. Other differences than spur gear are thrust loads and bending couples developed by the inclined tooth. They are rarely used to transmit motion between nonparallel shafts.

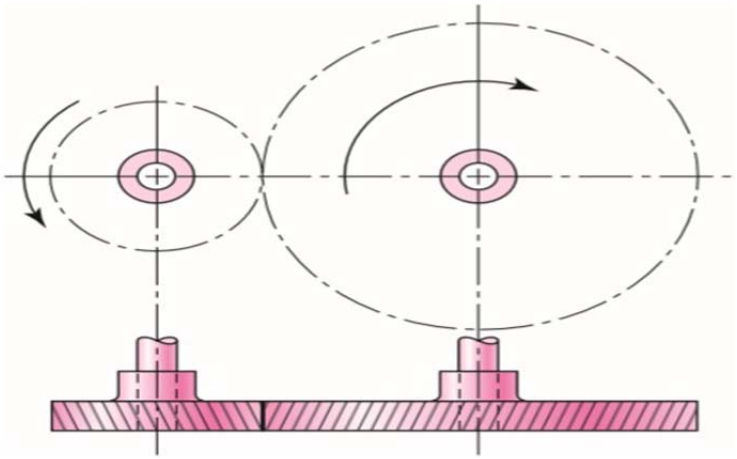

Figure 1.5. Helical Gear (Budynas R.G. and Nisbett J.K., 2011)

1.3.3. Bevel Gears

Bevel gears, illustrated in Figure 1.6., are generally used for transmitting motion between intersecting shafts and their teeth formed on conical surfaces. This figure shows straight bevel gears. Spiral bevel gears form a circular arc. Hypoid gears are so similar to spiral bevel gears, but hypoid gears shafts are offset and nonintersecting.

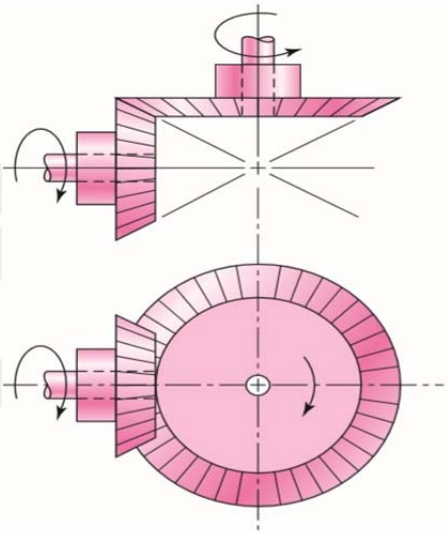

Figure 1.6. Bevel Gear (Budynas R.G. and Nisbett J.K., 2011)

1.3.4. Worm Gears

Worms and worm gears, illustrated in Figure 1.7, represent the final necessary gear type and look like a screw. The worm wheel indicates the direction of rotation for the worm gear and depends on it. It also depends on right-hand or left-hand cutting. If worm gearsets made so that the teeth of one wrap partly around the other, it is called a single enveloping worm gear set. If worm gearsets made so that the teeth of both wrap around the other, it is called double enveloping worm gear set. Worm gear sets are generally used when the speed ratios of shafts higher than 3.

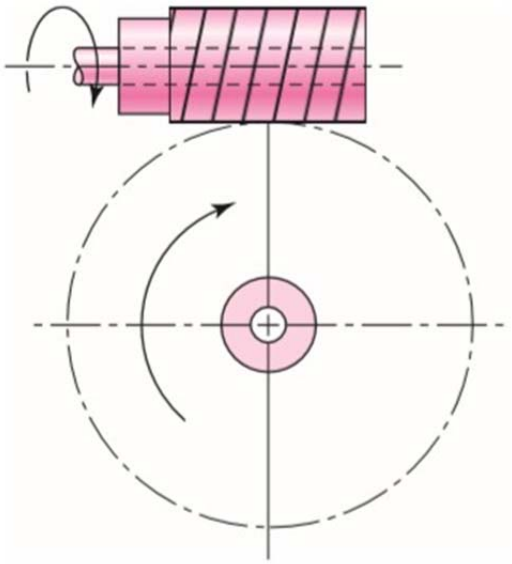

Figure 1.7. Worm Gear (Budynas R.G. and Nisbett J.K., 2011)

1.4. Spiral Bevel Gears

Gears that transmit motion between two intersecting shafts and have a conical shape are called bevel gears. One type of the bevel gear is spiral bevel gear, shown in Fig. 1.8., which the teeth are curved spirally. One of the reasons why spiral bevel gears are selected on the straight bevel gears is that curved teeth contact each other gradually and smoothly from one end to the other. The meshing of teeth is, as in straight bevel gears, rolling contacts on the pitch cone surface.

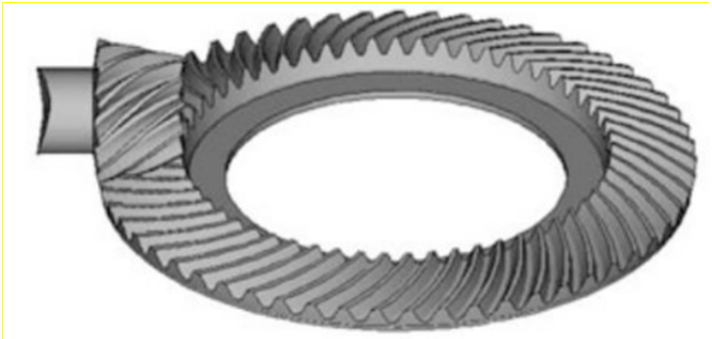

Figure 1.8. Spiral Bevel Gear (Jan Klingelnberg, 2016)

When we classify according to design and gear cutting, the Gleason type is generally used for spiral bevel gears. Nevertheless, the Klingelnberg type used with equal toe and heel tooth depth in Germany.

Spiral bevel gears have advantages and disadvantages over other gears. The first of these advantages, they are capable of grinding teeth after heat treatment, making it possible to produce high precision gears. The other advantage is they are stronger and more durable than straight bevel gears allowing for higher load operations. It is also used in high-speed applications because of lower noise and vibration in spiral bevel gears as it has a better tooth contact ratio than straight bevel gears. On the other hand, spiral bevel gears have some disadvantages. It is more challenging to manufacture spiral bevel gears and needs attention regarding the change in thrust directions depending on the rotation and twist angle. (Kohara Gear Industry Co)

As mentioned in section 1.3.2.3, hypoid gears are similar to spiral bevel gears in general appearance. The vital difference is that the pinion axis of the hypoid pair of gears is offset somewhat from the gear axis. Hypoid gears run even more smoothly and quietly than spiral bevel gears and are somewhat stronger (Davis & associates, 2005).

Zero bevel gears, as shown in Figure 1.9. have a curved tooth form like spiral bevel gears but have 0°degree spiral angle. They can be classified between spiral bevel gears and straight bevel gears (Childs. Peter R. N., 2013).

The tooth of Zero bevel gear has the same loading capacity to the tooth of straight bevel gear, but, zerol bevel gears meshing is smoother than straight bevel gear. Zero bevel gears are a type of circular arc gears. (Kohara Gear Industry Co)

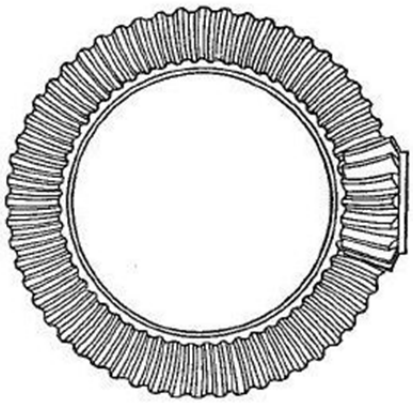

Figure 1.9. Zerol Bevel Gear (Kohara Gear Industry Co)

Hypoid and spiral bevel gears are used in the differential design in the automotive and heavy truck industries. In the space industry, spiral bevel gears and zero bevel gears are used as equipment. It is also used in transmission for marine and off-highway transmission, for example, to the working areas of spiral bevel gears (Davis & associates, 2005).

1.4.1. Tooth Shape of Spiral Bevel Gears

Spiral bevel gears are gears that have the teeth arranged on a pitch cone along curved lines, which produces a quiet operation even at high speed. Especially when the peripheral speed is more than 5 m / s, it is difficult to find gear to ensure quiet operation. At high speeds, the use of spiral bevel gears is desirable. Nomenclature of a spiral bevel gear given in Figure 1.10

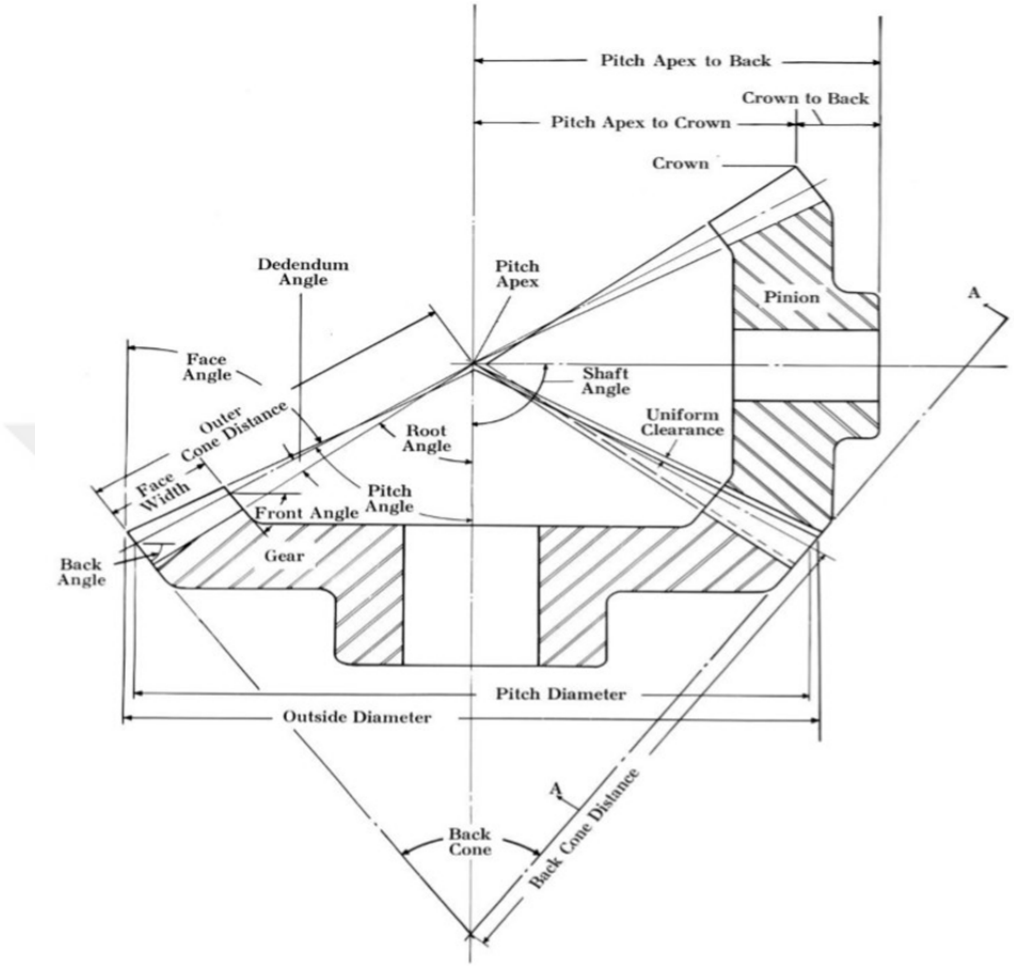

Figure 1.10. Nomenclature of spiral bevel gear (Gleason Works, 2018)

1.5. Gear Trains

Consider 2 sub-indices for pinion and 3 sub-indices for driving gear. The driven gear speed is given in formula 1.1

$$n_3 = \left|\frac{N_2}{N_3} n_2\right| \left|\frac{d_2}{d_3} n_2\right| \tag{1.1}$$

Where

n= revolution or rpm, rev/min

N= number of teeth

d= pitch diameter

Equation 1.1 can be applied to all gear types. The absolute expression is used as it may be in a negative direction according to the direction of rotation. According to the right-hand rule, counterclockwise is considered as a positive direction and clockwise as a negative direction. While the right-hand rule is used to find the direction of rotation in spur gears and parallel helical gears, the direction of rotation is found in the worm and cross helical gears as shown in Figure 1.11

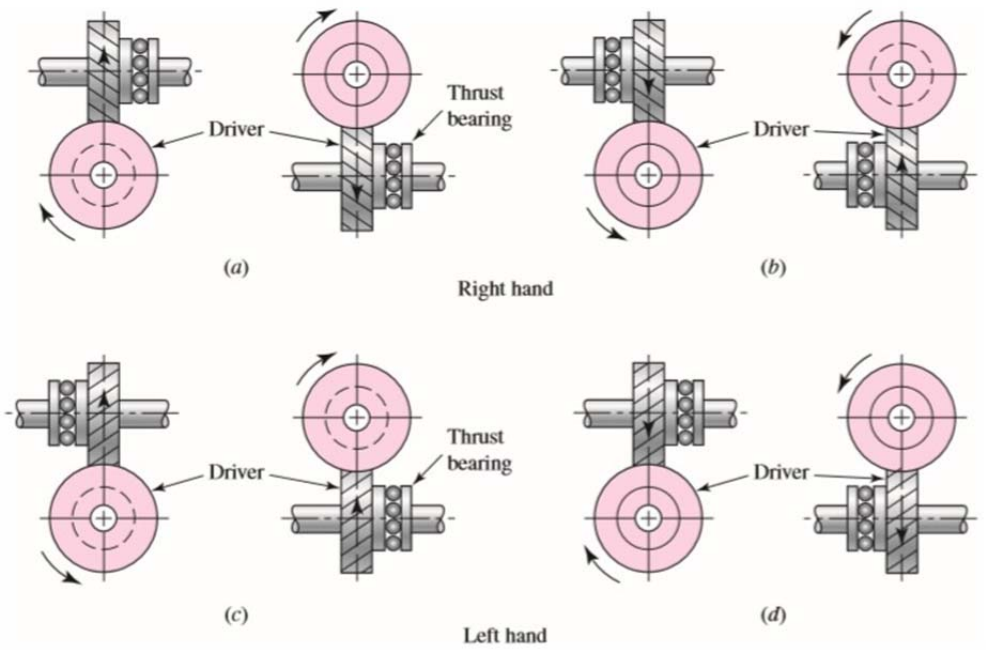

Figure 1.11. Thrust, hand relations, and rotation relations for worm gears or crossed helical gears

1.6. Aim of the Study

The primary aim of this study is to obtain a dimensionless number by proportioning the design results (m and F or b) of the commonly used spiral bevel gear design approaches and to evaluate the difference between the design approaches according to the results we obtained. In this study, DIN (German Institute of Standardization), ANSI/AGMA (American Gear Manufacturers Associations), ISO (International Organization for Standardization) standards, and machine element textbooks (Fundamental of Machine Component Design 5th Edition, Juvinall R.C. and Marshek K.M., 2011 and Shigley's Mechanical Engineering Design 9th Edition (SI), Budynas R.G. and Nisbett J.K., 2011) will be studied. In this study, gear design parameters (m and F) given by design approaches for both cost and reliability will be compared.

Also the mathematics backround of mechanical engineering students, who also work on gear design, decreases over the years. In addition, the results of the survey showed that the method that Çukurova University students were asked to use while conducting gearbox design projects was left to the students and it was seen that the students preferred the machine elements books which contain less formulas and can be solved in a shorter time compared to the national or international standards. (Geren N., Uzay Ç., Bayramoğlu M., 2020)

Then, the secondary objective of the project is to define dimensionless conversion factors to approximate conversion of gear design results in textbooks to more accurate DIN, ISO, or AGMA Standards. The conversion factors will allow the all designers including the expert designers and students who have just started gear design to convert the design results found by using the spiral bevel gear design approach with the simple formulas found in the textbooks into the design results given by the DIN, ISO, or AGMA standards design approaches. Conversion factors will enable relatively complicated and time-consuming DIN, ISO, and AGMA gear designs to be realized in less time with the textbook solutions, thus reducing convenience and design costs for designers.

2. PREVIOUS STUDIES

In the literature, there is not much work related to design an involute spiral bevel gear. Most of the works that are improving gear profile and optimization of dimensions are related to decreasing bending and surface contact stress in literature even though they are about involute helical or spur gears. Few studies are developed computer programs to draw and model the gear pairs in a Computer-Aided Design (CAD) environment, and some carried out failure analyses.

2.1. Gear Design Approaches in the Literature

The design of an involute spiral bevel gear design requires many assumptions that including different design factors. In order to gear a spiral bevel gear, national such as German Institute of Standards (DIN), international standards such as American Gear Manufacturer Association (ANSI/AGMA) and International Standard of Organization (ISO) and, or machine elements textbooks such as Fundamentals of Machine Component Design 5th Edition and Shigley's Mechanical Engineering Design 9th Edition have been provided to designers. Literature search about machine elements textbooks and standards for spiral bevel gear design is listed Table 2.1

Table 2.1. International and national standards and machine element textbooks related to the design of spiral bevel gear design

Available Design Approaches	The primary Basis of the Design approach
DIN Standards	DIN Standards
ISO Standards	DIN Standards
JGMA Standards	JGMA Standards
Fundamentals of Machine Component Design 5th Edition (Juvinall R.C., Marshek K.M., 2011)	Similar to ANSI/AGMA**
Shigley's Mechanical Engineering Design 9th Edition (Budynas R.G. and Nisbett J.K., 2011)	ANSI/AGMA Standards**
ANSI/AGMA Standards	ANSI/AGMA Standards*
Makine Elemanları ve Konstrüksiyon Örnekleri (Babalık F.C., 2010)	DIN Standards
Mechanical Design: An Integrated Approach (Ugural A.C., 2003)	ANSI/AGMA and/or Fundamental of Machine Component Design

*Most commonly used
** Introduces the design of a bevel gear clearly

2.2. General Gear Design Studies

2.2.1. Gear Design using Computer-Aided Engineering (CAE)

Most of the engineering applications made through computer programs are called computer-aided engineering (CAE). (Budynas R.G. and Nisbett J.K.,2011).

The general logic of CAE is to use complex mathematical algorithms to perform calculations. Using CAE finite element technique, the results of the simulation calculations are found. The working procedures to carry out simulations with CAE systems can be divided into three main phases, respectively, as pre-processing, calculation of the demands, post-processing.

Some engineering design software is Aries, AutoCAD, Cad Key, Solid works, Pro Engineer, I-Deas, Inventor, Mechanical Desktop, Unigraphics, Catia V5.

The finite element method (FEM) is a numerical analysis technique. It is not possible to obtain analytical mathematical solutions for many engineering problems. Using FEM, it provides numerical solutions to these engineering problems by obtaining approximate solutions. Various commercial software products are available for finite element analysis (FEA) such as Ansys, Nastran, Cosmos, LS-Dyna (Parthiban A.et al, 2013).

Geren N. and Baysal M. (2000) developed an expert system using artificial intelligence. They used this system for gearbox design by operating Delphi from Borland for an expert system development tool. This expert system has a user-friendly interface that allows the dealer to select the type of gears, the material of gears, etc. American Gear Manufacturers Association (AGMA) standard's methods and its recommendations were used for designing the spur gear. The program includes the recommended module size list box, which is the result of estimating the gear size procedure. It is stated that the developed software reduced the design duration to less than 3 minutes for an experienced designer and few minutes for an inexperienced designer, allowing the user to try different design alternatives in a short time, eliminating the errors made during the manual design process.

Gologlu C. and Zeyveli M. (2009) applied a genetic algorithm (GA) to optimize of helical gear design. It was aimed to minimize the volume of gears by using penalty functions that depend on design variables and their constraints. In this study, it is aimed to minimize the volume of gears by using boundary functions based on design variables and constraints. Although the program worked in as little as 4 seconds, the face width of the gears was generally out of limits determined by 3 to 5 times of circular pitch.

Mendi F. et al. (2010) developed a Borland Delphi 6.0 platform to execute GA to optimize helical gear design. They performed the dimensional optimization of motion and force transmitting components of a gearbox by GA. The selection of an optimum module was carried out using GA. When results were compared to analytical results, GA has given better results such as lower modules, less volume. Nevertheless, the face width calculated by GA not always in the range (3p, 5p).

2.2.2. Verification of Gear Design Results with Finite Element Analysis

For gear design, fatigue bending stress (bending fatigue) and contact stress (surface contact fatigue) must be taken into account. The tooth root is subjected to fatigue bending stress, and the tooth surfaces are subjected to fatigue contact stresses. In gear designs, the determination of gear stresses is significant. Because the failure of gear due to bending causes tooth breakage also owing to surface contact causes pitting, scoring, wear.

Vijayarangan and Ganesan (1994) investigated the results of static load distribution analyzed by 3D finite element method on composite bevel gears. These studies have shown that the static strength of the glass epoxy bevel gear is almost similar to that of the carbon steel bevel gear from the boron/epoxy bevel gear. The displacement of these gear materials is ordered from large to small, respectively, in the form of a composite bevel gear consisting of boron/epoxy, a composite bevel gear consisting of glass/epoxy, a carbon steel alloy. Boron/epoxy composite was found to be the best of the three materials.

2.2.3. The studies on the Effect of Profile Modification

Stresses in gears are vital in gear designs. By reducing these stresses, the effects of the problems during the design can be avoided or minimized by making various changes in the tooth profile.

Wu, Yong-jun et al. (2012) examined the static and dynamic behavior of a helical gear pair. With FEA results, the appropriate amount and type of tooth profile modification (TPM) are selected. Dynamic contact simulations are performed in order to observe the difference in vibration between the original helical gear pair with TPM. As a result, it has been observed that the vibration amount is reduced by the selection of the appropriate amount and type of TPM by the dynamic contact selection.

Dhavale A.S. et al. (2013) suggested that by adding stress-relieving properties to the stress zone, high stress can be reduced, which increases the

likelihood of fatigue failure at the root of spur gears. They have generated holes in the tooth root area and compared the amount of stress between original gear and modified one by using a FEM. As a result, it was found that the size of the holes and the location of the holes were as crucial as the amount of the holes. It was found in the study that two holes provided more stress reduction.

2.3. Spiral Bevel Gear Design Studies

2.3.1. Spiral Bevel Gear Design using Computer-Aided Engineering (CAE)

Galina (2007) compared the algorithms found for geometric, kinematic analysis for meshing and contact stress analysis with Hertz and non-hertz methods. While one algorithm was used for kinematic and geometric analysis of meshing analysis, two algorithms were used for surface stress analysis. The algorithms are based on grid presentation of contacting surfaces and field of distances between them. By using the codes generated based on these algorithms, contact path, transmission error, contact pressure distribution, and bearing contact values were obtained. The results showed that both of the analyzes with different misalignments could be used for all types of gear transmissions. Besides, when there is no edge contact, the gear contact pressure is obtained by using the Hertz solution. Finally, the non-hertz solution is used when there is an immediate bearing contact area near a toothed edge.

Argyris J., Fuentes A. and Litvin F.L., 2002 developed an integrated computerized approach for synthesis, analysis, and stress analysis of spiral bevel gear drives. The methods they use to develop the program are local synthesis and simulation of meshing and gear tooth surfaces. These methods reduce noise and vibration while also localized bearing contact less sensitive to errors of alignment. Using FEM, the formation of bearing contact during a cycle of meshing and stress analysis was investigated. The design of FEM and its boundary conditions were automatized. An advanced computer program for the synthesis, tooth contact analysis, and stress analysis of spiral bevel gear drives was developed. The most

time-consuming step in the application of finite element analysis, the design of contacting models by using a CAD computer program, is avoided due to automatization of the development of such models. The developed computer programs were based on the application of FORTRAN computer language for numerical computations and Visual Fortran QuickWin run-time library for graphical interpretation of results. The proposed approach was applied to the design and stress analysis of face-milled generated spiral bevel gears. The resulting approach can be used not only for spiral bevel gears but also for other types.

2.3.2. Verification of Spiral Bevel Gear Design Results with Finite Element Analysis

Bibel G.D., Kumar A., Reddy S. and Handschuh R. (1995) used FEM to generate 3D stress analysis of spiral bevel gears in mesh. FEM has been obtained by solving the equations defining the gear surface coordinates that guide the gear and pinion for the gear mesh. Suitable gap elements were used for contact boundary conditions. As a result, although FEM has achieved a general improvement, in particular, satisfactory results have not been obtained for significant stress gradients between adjacent nodes in the contact regions.

Zhang H. and Tie X. (2012) have studied the mesh performance of spiral bevel gears with new non-zero-positive modification. They claimed that using local synthesis, machining parameters with high contact rates could design non-zero-modification for spiral bevel gears. This design method could make up the shortage of low coincidence degrees resulted in increasing mesh angle in the non-zero-positive transmission designing. According to comparing the new design with the unmodified design, the max root tensile stress of pinion, max root compressive stress, max tooth surface contact stress, and root stress of gear values are also reduced the strength of the pinion increase under the same load values. The results show that the modified design's tooth profile and parameters for machinability make the gear pair having more reliability and long life.

3. MATERIAL AND METHOD

3.1. Material

In our study, the first thing to be aware of in the selection of materials is that the pinion and the gear unit must work in harmony and meet all the required service conditions.

The reason we choose cast iron is easy castability, low cost, high wear resistance, and noise damping. It generally has lower bending fatigue strength than surface fatigue strength. When designing, the results were found separately for pinion and gear, and the design results were evaluated according to the larger one. Three different pinion materials were used in the study, which had low, middle, and high strengths. It provides the mechanical properties of the selected materials shown in Table 3.1.

Table 3.1. Properties of pinion and gear materials

Material Types for Pinion and Gear and Mechanical Properties	Pinion			Gear
	Type 1: AISI 1030 Q&T @650 ℃	Type 2: AISI 4140 oil Q&T @425 ℃	Type 3: AISI 4140 oil Q&T @207 ℃	ASTM Ductile iron HT and OQ&T and ground, GR.120-90-02
Yield strength (M_{pa})	441	1140	1640	621
Ultimate tensile strength (M_{pa})	586	1280	1770	827
Brinell hardness number (HB)	207	370	510	300
Density (kg/m^3)	7850	7850	7850	7850
Poisson's Ratio	0,3	0,3	0,3	0,3
Modulus of Elasticity (G_{pa})	200	200	200	170

3.2. Method

In this thesis, the design of gears will be performed in two different ways as bending fatigue and surface contact failures according to the most common three standards and two textbook design approaches. These are;

1. ANSI/AGMA 2003-B97 Standard (1997)
2. Shigley's Mechanical Engineering Design 9th Edition (Budynas R.G. and Nisbett J.K., 2011).
3. ISO 10300:1,2 (2001), ISO-1300:3 Standards (2003),
4. DIN 3991:1,2,3 Standards (1988) and
5. Fundamentals of Machine Component Design 5th Edition (Juvinall R.C. and Marshek K.M., 2011)

Determination of module (m) and face width (F) directly, which affect the material used, were performed with the five most common design approaches mentioned above. However, since the formulas used in the Shigley's Mechanical Engineering Design 9th Edition (Budynas R.G. and Nisbett J.K., 2011) are taken from the ANSI/AGMA 2003-B97 (1997), we will consider them the same. As a result of this, four different methods were actually considered in this work. In each of the above approaches, although the bending fatigue failure and surface contact failure remained dependent on design variables affecting material strength and distortion stresses, different design approaches showed that design variables were handled in different ways in each approach.

The designs of bevel gears using the expressions of Table 3.1 are performed based on selecting the module (m) and determining the face width. This iterative process started with an initial estimation of a module and repeated until the face width reaches in an accepted range.

Moreover, two different types of stress occur as a result of gear and pinion contact, which are bending and surface contact. The most apparent difference

between them is caused by the place where the stress occurred. While bending stress occurs at the root of the tooth profile mainly, surface contact stress occurs on the surface during mating of gear and pinion teeth. Bending stress is the highest at the fillet and can cause breakage or fatigue failure of the tooth in the root region, whereas surface contact stresses occur on the surface of the tooth that may cause scoring wear, pitting fatigue failure.

First, proper values of important design parameters like a module in mm (m) or pitch diameter are searched, and the face width determined in the gear design before the material is pre-selected. Secondly, for gear and pinion, material selection should be made. We are interested in the module because, in this study, the SI unit system is used. After this stage, suitable face width is calculated according to the lowest module value. As a general requirement, the face width value must be less than ten times the selected module or 0.3 times selected ever-smaller cone distance (F (or b)) = min ($0.3A_0$, 10m). Also, different standards and different book solutions have different limitations. As shown in the flow chart, the design process for spiral bevel gear is given in Figure 3.1. The geometric rating number, GR_i, and conversion factor, CF_s, will explain respectively, section 3.2.3 and section 3.2.4. The approach for the comparison of the results obtained by following the steps for spiral bevel gear design is given in Figure 3.2.

Finally, to verify the results and to use a stable reference, a finite element method (FEM) will be used to analyses the results obtained using the analytical approaches. For this, 3-D models of bevel gears, which are created in SOLIDWORKS using GearTrax, will be imported into ANSYS Workbench 16.1. Then, the module and face widths found using each approach will be compared with the results of FEM. This approach will be used to verify each of the design approaches used in this study against ANSYS, and then more solid comparisons will be obtained.

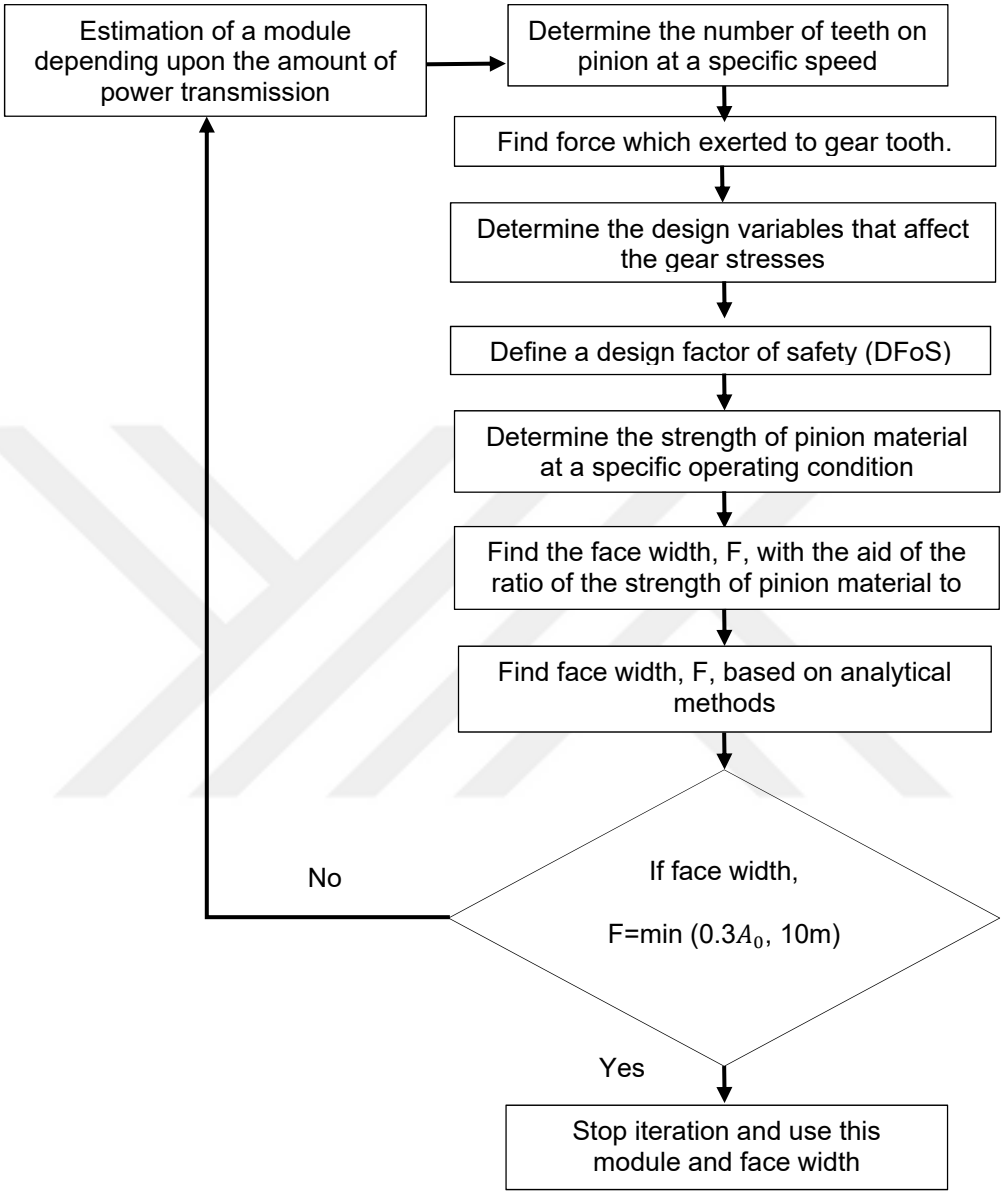

Figure 3.1. Flow chart for the design of a spiral bevel gear

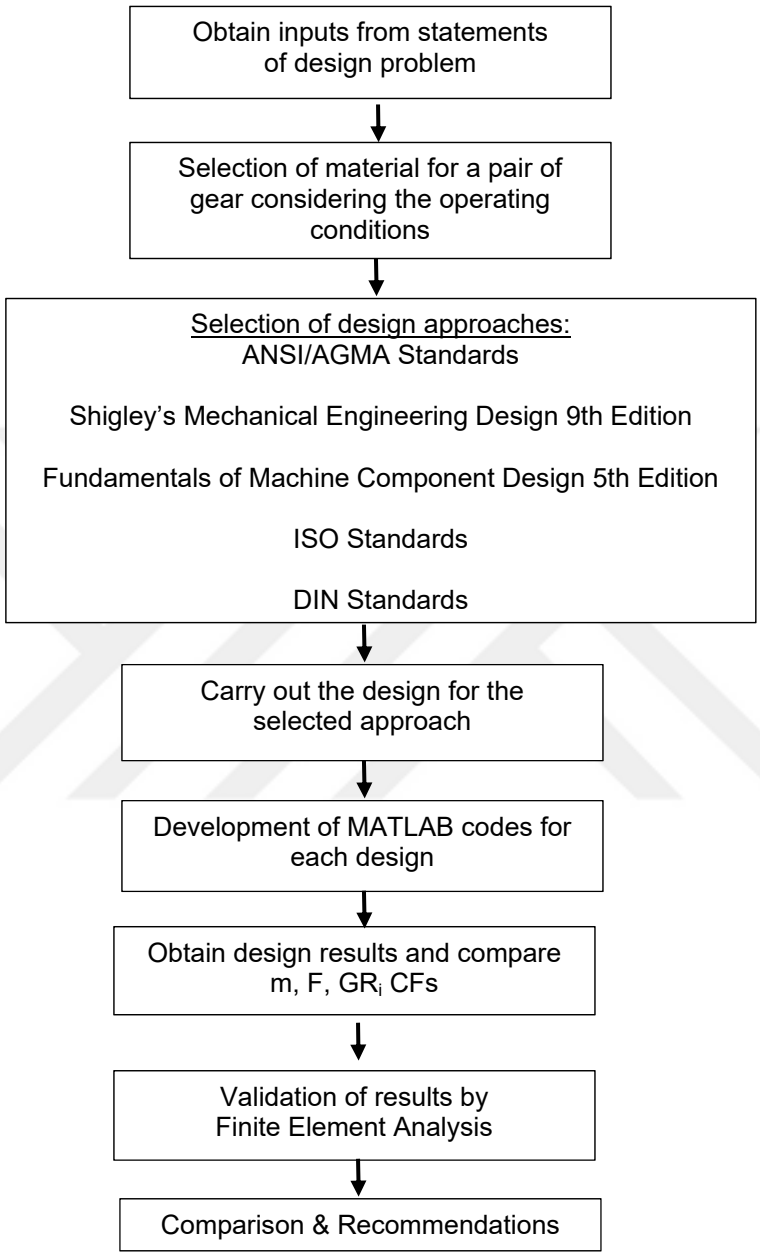

Figure 3.2. General systematic approach used for obtaining the results for the comparison of a spiral bevel gear design approaches

Design approaches given in Shigley's Machine Elements books design minimum safety factor at least 2,0 is recommended (Sgihley J.E., 1985, Budynas R.G. and Nisbett J.K., 2011). ISO 10300-1(2001) Standard recommends a factor of safety for contact stress equal or greater than one, and minimum bending-stress value should be 1.3 for spiral bevel gears. DIN 3991(1987) recommends a factor of safety for contact stress equal to one.

In the 5th Edition of Fundamentals of Machine Component Design, designs for spiral bevel gears are based on spur gears; therefore, it is recommended in 1 for spiral bevel gear, which is the lowest safety factor for spur gears. Compare the results obtained from each approach, a safety factor 2,1 was obtained, which provided the same conditions for the standards. The dimensionless number calculation has become more accurate using a specific safety factor. The design of spiral bevel gear has been defined for a life cycle of 10^8.

In Machine Component Design 5th Edition Fundamentals (Juvinall R.C. and Marshek K.M., 2011) and Shigley's Mechanical Engineering Design 9th Edition (Budynas R.G. and Nisbett J.K., 2011) books, the gear transmission quality is divided into three groups as the ground, shaved and machined. In the Fundamentals of Machine Component Design 5th Edition, the gear quality is classified as A to E (best classified as A, and the worst is E), The number 9 of the gear quality level in ANSI / AGMA standards is equal to Symbol A in the Fundamentals of Machine Component Design 5th Edition. The gear transmission quality has been divided into eight different classes for ISO 10300 Standards, as this is defined in 8 classes for ANSI/AGMA 2003-B97 Standard. In this study, the total quality of ISO and ANSI / AGMA standards should be equal to 17. This is also called the rule of 17. (Chala G., 1999) For instance, a gear quality level of 9 in ANSI/AGMA Standards is equal to a gear quality of 8 for ISO Standards.

When the gear quality increases, the ISO value decreases while the AGMA value is increasing. Since ISO 10300 standards are derived from DIN 3991, the same quality numbers are used. Gears have speed reduction ratios when designing.

In order to observe the effect of pressure angle on the work, 20° and 25° pressure angles, which are widely used in spiral bevel gear design, have been selected. For spiral bevel gear designs, since the designs for ISO and AGMA standards dictates the use of 1:1 to 1:8 speed ratio, we accepted it in the study. Moreover, the range for power transmission is selected as 0.5 kW to 1000 kW with an increase of 20kW. This means that a total of 51 designs should be performed for each of the speed ratios. All of the calculations have been carried out on MATLAB. For ease of comparison, the same type of graphics was used on Microsoft Excel pages. The results we found were drawn for each design approaches on the SOLIDWORKS 2018 program with the help of GearTrax for randomly selected 3:1 gear speed ratio, and 100 kW power transmissions. And the results were verified using the numerical finite element method on the ANSYS Workbench 18.1

3.2.1. Determination of Interference-Free Pinion Gear Teeth Number

In this thesis, the design of pinion and gear has been considered for the comparison of the results of the different approaches. Design is done according to the highest value. The minimum numbers of teeth to prevent undercuts with these angles and speed ratios have been determined and selected.

At the 20° pressure angle, the minimum teeth number for pinion according to the speed ratio for the Gleason spiral bevel gear is shown in Table 3.2. Since no data is available in the literature for 25°, the minimum number of teeth is assumed and given in Table 3.3. (Kohara Gear Industry Co)

Table 3.2. Minimum teeth number to prevent undercut on pinion for working speed ratios for 20° pressure angle and 35° spiral angle for gleason spiral bevel gear (Kohara Gear Industry Co)

Speed ratio	Minimum number of teeth on the pinion
1:1	17
2:1	13
3:1	12
4:1	12
5:1	12
6:1	12
7:1	12
8:1	12

Table 3.3. Minimum teeth number to prevent undercut on pinion for working speed ratios for 25° pressure angle and 35° spiral angle for Gleason spiral bevel gear (Kohara Gear Industry Co)

Speed ratio	Minimum number of teeth on the pinion
1:1	13
2:1	12
3:1	12
4:1	12
5:1	12
6:1	12
7:1	12
8:1	12

Now in the following sections, the design of an involute bevel pinion gear has been described for each of the design approaches.

3.2.2. Design of Spiral Bevel Gear Depend on Bending Fatigue Failure

3.2.2.1. Design Approach Using ANSI/AGMA 2003-B97 Standard

In this design approach, failure by bending will occur when the significant tooth stress equals or exceeds either the yield strength or the bending endurance strength. Allowable bending stress has been equalized to fully corrected the endurance strength of the gear tooth by considering the selected design factor of safety.

Bending stress;

$$\sigma_F = \frac{1000W_t}{b}\frac{K_A K_V}{m_{et}}\frac{Y_X K_{H\beta}}{Y_B Y_J} \quad (3.1)$$

And

σ_F: Calculated bending stress number at the root of the tooth, N/mm2

K_A: Overload Factor, shown in Table 3.4

K_V: Dynamic factor

W_t: Tangential transmitted load, in N

Y_x: Size factor for bending strength

$K_{H\beta}$: Load-Distribution Factor

b: Face width, in mm

m_{et}: Outer transverse module, in mm

Y_β: Lengthwise curvature factor for bending strength

Y_J: Geometry factor for bending strength shown in Figure 3.3 and Figure 3.4.

In bevel gear designs, when determining shaft and bearing loads, tangential or transmitted load, which is formed at the midpoint of forces of the whole tooth, is used. While the actual resultant occurs somewhere between the midpoint and the most significant point of the tooth, there is only a small error in making this assumption. Transmission load, W_t, for spiral bevel gear formula has given below,

$$W_t = \frac{6000H}{\pi dn} \quad (3.2)$$

H: Power of spiral bevel gear, kW

d: Gear diameter of spiral bevel gear, mm

n: speed of spiral bevel gear, rev/min or rpm

The factor that allows the externally applied loads to be above the nominal tangent load is called the overload factor (K_A) shown in Table 3.4. Overspeed, acceleration moments, system vibrations, and other factors cause an overload factor. Therefore, it is seen as one of the factors to be considered.

Analysis of critical speeds within the operating range of the drive is essential. If critical speeds are present, changes in the design of the overall drive system should be made to either eliminate them or to provide system damping so that gear and shaft vibrations are eliminated.

Table 3.4. Overload factors, K_A (ANSI / AGMA 2003-B97 Standard, 1997)

		The Character of Load on Driven Machinery		
The Character of Prime Mover	Uniform	Light Shock	Medium Shock	Heavy Shock
Uniform	1.00	1.25	1.50	1.75 or higher
Light shock	1.10	1.35	1.60	1.85 or higher
Medium shock	1.25	1.50	1.75	2.00 or higher
Heavy shock	1.50	1.75	2.0	2.25 or higher

The dynamic factor (K_v) The dynamic factor can be calculated according to gear quality as well as speed and load. It is generally accepted that the factors which affect the dynamic load on the gear teeth fall into five categories as design effects, manufacturing effects, transmission error, dynamic response, resonance. The dynamic factor is given by equation 3.3. It is determined by the parameters A and B, which are given by equation 3.4 and 3.5, respectively, and the pitch line velocity at the operating pitch diameter, which can be seen in equation 3.6.

$$K_V = \left[\frac{A}{A + \sqrt{200V_{et}}}\right]^{-B} \quad \text{for } 5 \leq Q_v \leq 11 \tag{3.3}$$

$$A = 50 + 56(1.0 - B) \tag{3.4}$$

$$B = 0.25\ \llbracket(12 - Q\_v)\rrbracket\text{^}0.667 \tag{3.5}$$

Q_v: the transmission accuracy level number

$$V_{et} = 5.236\ X\ 10^{-5} d_1 n_1 \tag{3.6}$$

Y_X is called size factor, without sufficient experience, is determined as being dependent on the module.

$$Y_X = \begin{Bmatrix} 0{,}5 & m_{et} < 16\ mm \\ 0{,}4867 + 0{,}008339 m_{et} & 1{,}6 \le m_{et} \le 50 mm \end{Bmatrix} \tag{3.7}$$

The load distribution factor ($K_{H\beta}$) modifies the rating formulas to reflect the non-uniform distribution of the load along the tooth length. The use of the load distribution factor equations assumes a tooth contact pattern per 3.8 under full load operating conditions.

$$K_{H\beta} = K_{mb} + 5{,}6(10^{-6})b^2 \tag{3.8}$$

K_{mb} is load distribution modifier;

$$K_{mb} = \begin{Bmatrix} 1.00 & \text{both members straddle mounted} \\ 1.10 & \text{one member straddle mounted} \\ 1.25 & \text{neither member straddle mounted} \end{Bmatrix} \tag{3.9}$$

Figure 3.3 shows the geometry factor for spiral bevel gears (J) with a 20° pressure angle, 35° spiral angle, and 90° shaft angle. Figure 3.4 shows the geometry factor for spiral bevel gears (J) with a 25° pressure angle, 35° spiral angle, and 90° shaft angle.

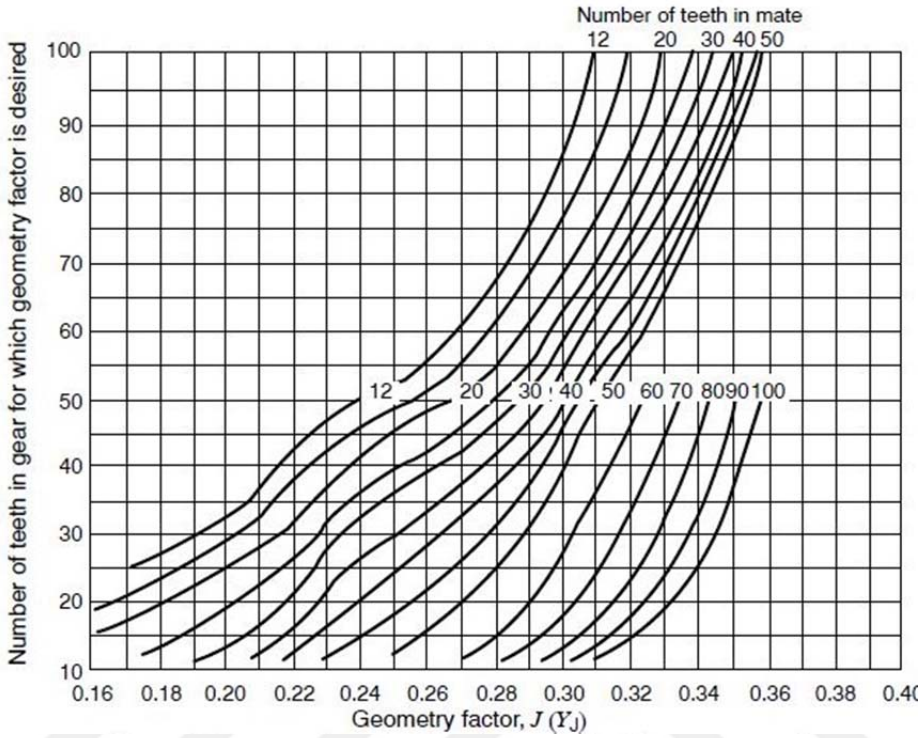

Figure 3.3. Geometry factor for spiral bevel gears (J) with a 20° pressure angle, 35° spiral angle and 90° shaft angle (ANSI / AGMA 2003-B97 Standard, 1997)

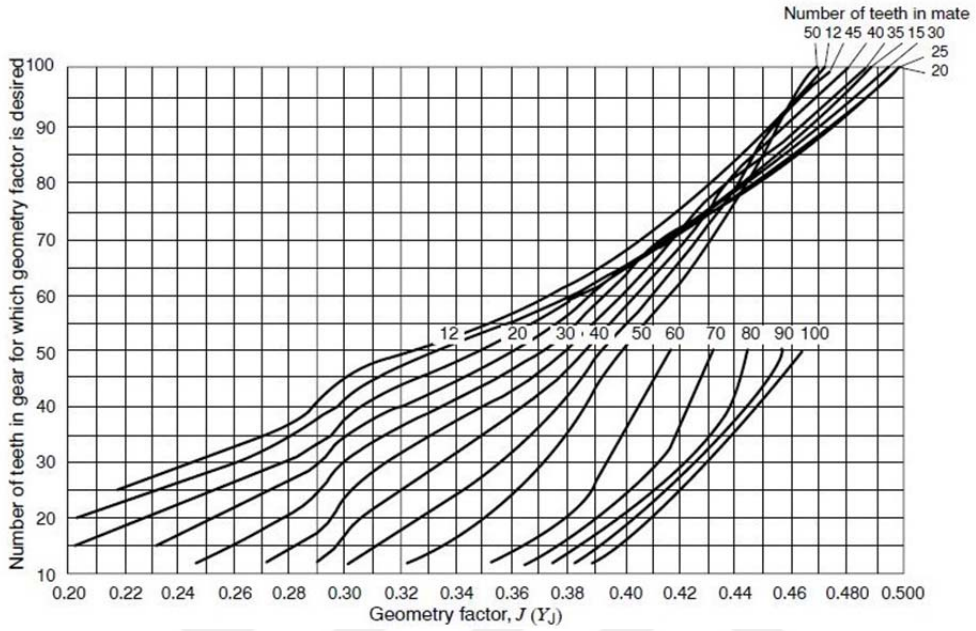

Figure 3.4. Geometry factor for spiral bevel gears (J) with a 25° pressure angle, 35° spiral angle and 90° shaft angle (ANSI / AGMA 2003-B97 Standard, 1997)

Permissible bending stress number is given formula 3.10.

$$\sigma_{FP} = \frac{\sigma_{F\,lim} Y_{NT}}{S_F K_\Theta Y_z} \tag{3.10}$$

Where

σ_{FP}: Permissible bending stress number, N/mm2

$\sigma_{F\,lim}$: Bending stress number (allowable) given in Table 3.5 and Figure 3.5, N/mm2

S_F: Bending safety factor

Y_{NT}: Stress cycle factor, given in Fig. 3.7 and formula 3.11;

K_Θ: Temperature factor, given in formula 3.12

Y_z: Reliability factor, given in Table 3.7 and formula 3.13;

The allowable number of stresses, σ_{FP}, varies for reasons such as the quality of the material selected for the design, the microstructure, residual stress, material composition, processing applications, and cleanliness. The hardness values are given in Table 3.6 below (ANSI / AGMA 2003-B97 Standard, 1997).

Table 3.5. Allowable bending stress number for steel gears, $\sigma_{F\ lim}$ (ANSI / AGMA 2003-B97 Standard, 1997)

Material designation	Heat treatment	Minimum surface hardness	Allowable bending stress number $\sigma_{F\ lim}$ $\frac{N}{mm}^2$		
			Grade 1	Grade 2	Grade 3
Steel	Through hardened	See figure 3.5	See figure 3.5	See figure 3.5	
	Flame or induction				
	Hardened	50 HRC	85	95	--
	un-hardened roots	--	154	--	--
	hardened roots	See Table 8 at AGMA/ANSI	205	240	275
	Carburized & case hardened				
AISI 4140	Nitrided	84.5 HR15N	--	150	--
Nitralloy 135M	Nitrided	90.0 HR15N	--	165	--

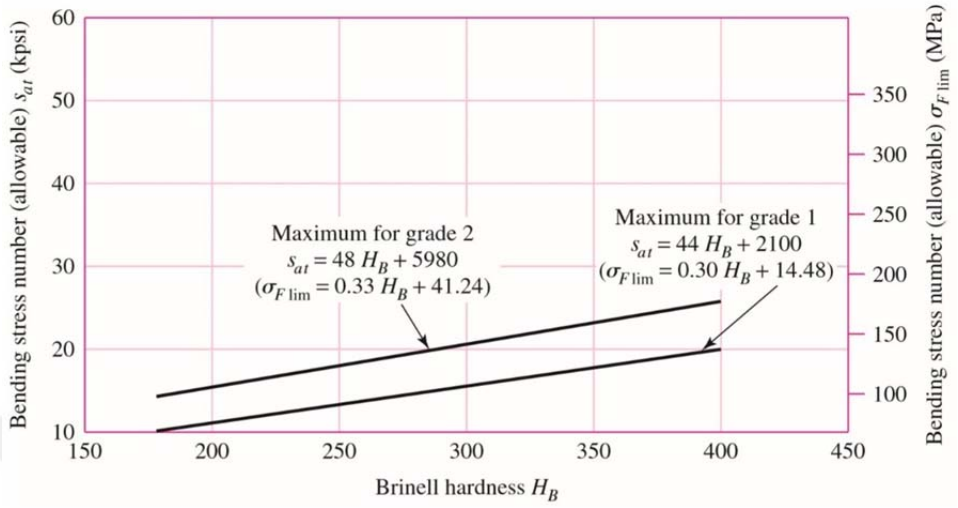

Figure 3.5. Allowable bending stress number, $\sigma_{F\ lim}$, for through-hardened steel bevel gears (ANSI / AGMA 2003-B97 Standard, 1997)

Table 3.6. Allowable bending stress number for iron gears (ANSI / AGMA 2003-B97 Standard, 1997)

Material	Material designation		Heat treatment	Typical minimum surface hardness	Allowable bending stress number $\sigma_{F\ lim}\ \frac{N}{mm}^2$
	ASTM	ISO			
Cast iron	ASTM A48 Class 30 Class 40	ISO/DR 185 Grade 200 Grade 300	As cast As cast	175 HB 200 HB	30 45
Ductile (nodular) iron	ASTM A536 Grade 80-55-06 Grade 120-90-02	ISO/DIN 1083 Grade 600-370-03 Grade 800-480-02	Quench. & temp.	180 HB 300 HB	70 95

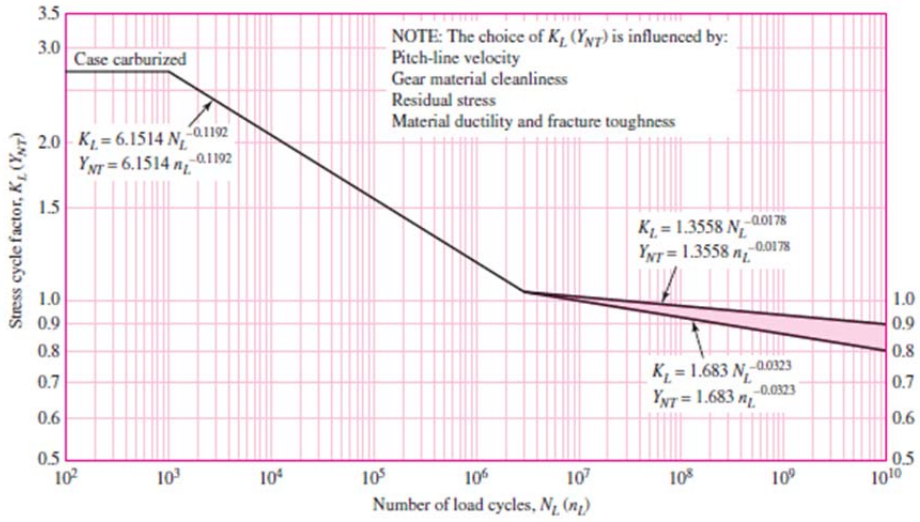

Figure 3.6. Stress cycle factor for bending strength K_L (Y_{NT}) for carburized case-hardened steel bevel gears (ANSI / AGMA 2003-B97 Standard, 1997)

$$Y_{NT} = \begin{Bmatrix} 2.7 & 10^2 \le nL < 10^3 \\ 6.1514 n_L^{-0.1182} & 10^3 \le nL < 3(10^6) \\ 1.6831 n_L^{-0.0323} & 3(10^6) \le nL \le 10^{10} \\ 1.3558 n_L^{-0.0323} & 3(10^6 \le nL \le 10^{10} \end{Bmatrix} \quad (3.11)$$

Temperature Factor (K_θ);

$$K_\theta = \begin{Bmatrix} 1 & 0℃ \le \theta \le 120℃ \\ (273+\theta)/393 & \theta > 120℃ \end{Bmatrix} \quad (3.12)$$

Under normal conditions where the operating gear blank temperature is between 32°F and 250°F (0°C and 120°C), the temperature factor (K_Θ) for both pitting resistance and bending strength is taken as 1.0.

The safety factors S_H and S_F, as defined in 2003-B97, are adjustments to the strength, not to the load. Therefore, it cannot be used (by comparison) to assess whether the threat is contact fatigue or bending fatigue. Since Wt has the same value for pinion and gear, √SH is assumed to be equal to SF.

Table 3.7. Reliability factors, Y_Z (ANSI/AGMA 2003-B97)

Requirements of application	Y_z [1)]
Fewer than one failure in 10 000	1.5
Fewer than one failure in 1000	1.25
Fewer than one failure in 100	1.00
Fewer than one failure in 10	0.85 [2)]
Fewer than one failure in 2	0.7 [3)]
NOTES: 1)Tooth breakage is sometimes considered a more significant hazard than pitting. In such cases, the higher value of Y_z is selected for bending. 2)At this value, a plastic flow might occur rather than pitting 3)From test data extrapolation.	

$$Y_Z = \begin{Bmatrix} 0.5 - 0.25\log(1-R) & 0.99 \le R \le 0.999 \\ 0.7 - 0.15\log(1-R) & 0.9 \le R \le 0.99 \end{Bmatrix} \quad (3.13)$$

3.2.2.2. Design Approach Using Fundamentals of Machine Component Design 5th Edition

Juvinall and Marshek give the design approach slightly different from the previous ones for bending fatigue failure. The design calculations of bevel gear tooth bending and surface fatigue strengths are even more complicated than for spur and helical gears. The treatment given here is very brief. This approach mostly recommends that in the absence of more specific information, the factors affecting gear tooth bending stress;

The equation for spiral bevel gear based on the spur gear equation:

$$\sigma = \frac{F_t}{mbj} K_v K_o K_m \quad (3.14)$$

Where

σ: Bending fatigue stress,

b: Face width, mm

F_t: Tangential load

m: module, mm

J: Bevel gear geometry factor, determined from Figure 3.7

K_v: Velocity factor. Same with the spur gear. Gears with shaved or ground profile, it is calculated from Equation 3.3 or shown in Figure 3.8

K_o: Overload factor, from Table 3.9

K_m: Mounting factor, from Table 3.8

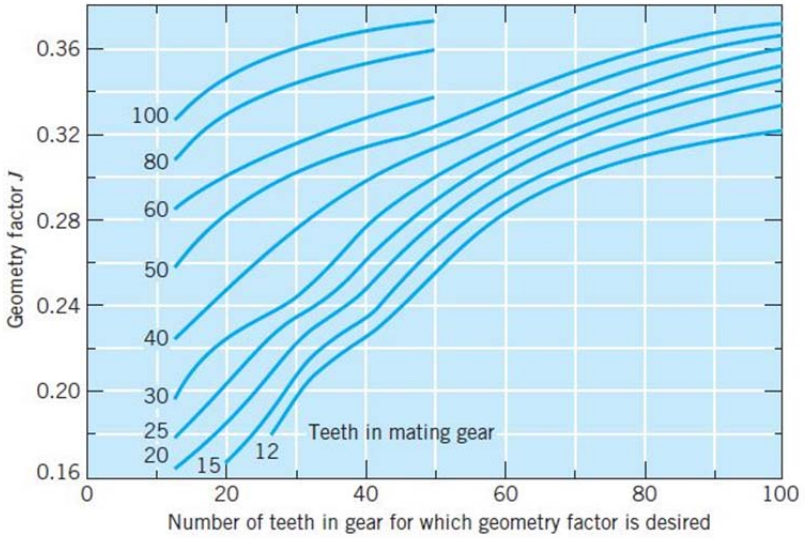

Figure 3.7. Geometry factors (J) for spiral bevel gears. Pressure angle = 20°, spiral angle = 35°, shaft angle = 90° (From AGMA Information Sheet 226.01; also see ANSI/AGMA 2003-A86.)

Table 3.8. Mounting correction factor, Km for bevel gears (Juvinall R.C., Marshek K.M., 2011)

Mounting Type	Mounting Rigidity, Max to Questionable
Both gears straddle-mounted	1.0 to 1.25
One gear straddle-mounted, the other overhung	1.1 to 1.4
Both gears overhung	1.25 to 1.5

Table 3.9. Overload correction factor, Ko (Juvinall R.C., Marshek K.M., 2011)

	Driven Machinery		
Source of Power	Uniform	Moderate Shock	Heavy Shock
Uniform	1	1.25	1.75
Light shock	1.25	1.5	2.00
Medium shock	1.5	1.75	2.25

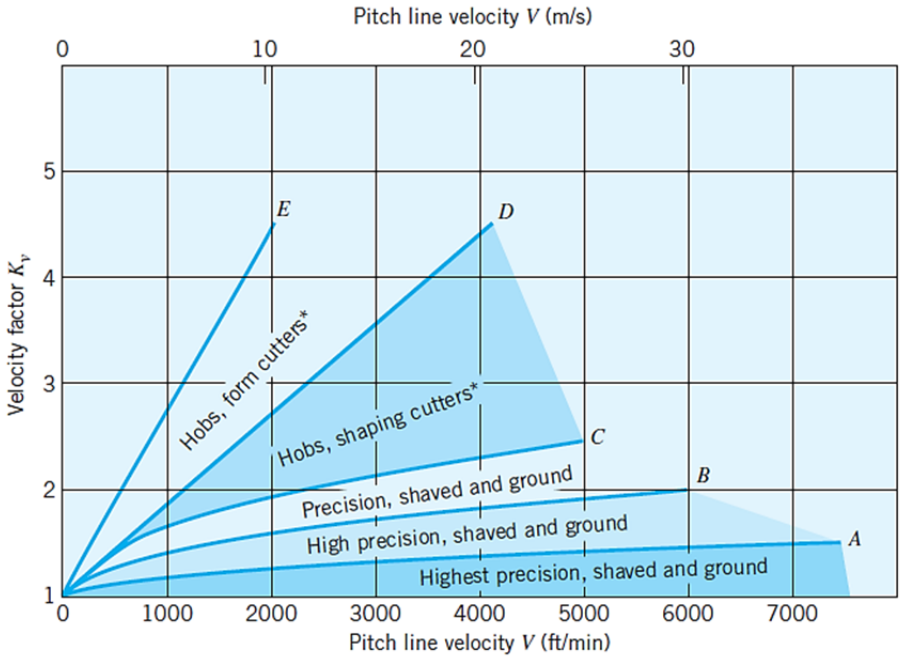

Figure 3.8. Velocity factor K_v (Juvinall R.C., Marshek K.M., 2011)

The effective fatigue stress from the below equation must be compared with the corresponding fatigue strength (S_n). The appropriate endurance limit for making infinite life design can be obtained from the following equation:

$$S_n = S'_n C_L C_G C_S C_T C_R \quad (3.15)$$

Which, for these steel members are usually;

$$S_n = (0.5S_u)C_L C_G C_S C_T C_R \quad (3.16)$$

Where

S'_n: Standard R. R. Moore endurance limit

For steel S'_n= (0,5). S_{ut} and

for other ductile materials S'_n= (0,7). S_{ut}

$C_{L:}$ Load factor equals to 1,0 for bending loads

$C_{G:}$ Gradient factor equals to 1,0 for P>5 (m<5,08), and 0,85 for P≤5 (m≥5,08)

C_S: Surface factor from Figure 3.9.

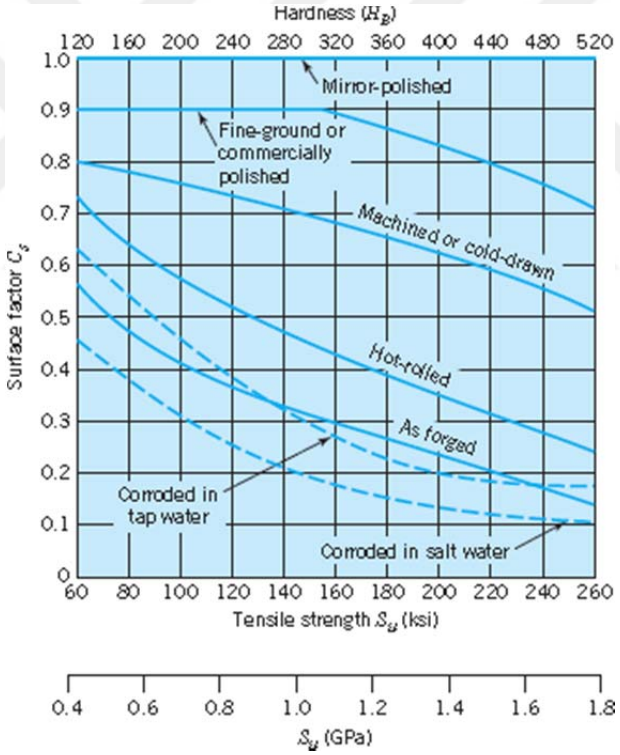

Figure 3.9. Surface factor C_s (Juvinall R.C., Marshek K.M., 2011)

k_t: Temperature factor, C_T, steel gears temperature factor equals to 1.0 for T<160°F. The main formula is given formula 3.17

$$k_t = \frac{620}{460 + T} \text{for T} > 160\ °\text{F} \tag{3.17}$$

k_r: Reliability factor, C_R, For convenience, values corresponding to an endurance limit standard deviation of 8 percent are given in table 3.10;

Table 3.10. Reliability factor, k_r (Juvinall R.C., Marshek K.M., 2011)

Reliability (%)	50	90	99	99.9	99.99	99.999
Factor k_r	1.000	0.897	0.814	0.753	0.702	0.659

k_{ms}: Mean stress factor.

k_{ms}= 1,0 for two way bending also known as idler gears

k_{ms}= 1,4 for one way bending also known as input and output gears

This approach recommends that the design factor of safety for bending fatigue can be taken as the ratio of fatigue strength to fatigue stress. Since the coefficients K_o, Km, and k_r are used, the safety factor does not have to be too much. When we accept 99.9% reliability, it is might that the safety factor is 1.5. Safety coefficient 2.1 was taken to carry out the study under similar conditions in all solutions. (Juvinall R.C., Marshek K.M., 2011).

3.2.2.3. Design Approach Using DIN 3991 Standards - Part 3

The following equations are provided in DIN 3991 Standards – Part 3 for the spiral bevel gear design (DIN 3991-1 Standard, 1988). Tooth root stress, σ_F, is the maximum tensile stress at the surface in the root.

$$\sigma_F = \sigma_{FO} K_A K_V K_{F\beta} K_{F\alpha} \leq \sigma_{FP} \tag{3.18}$$

Where

σ_{FO}: The local tooth root stress defined as the maximum tensile stress arising at the tooth root due to the nominal torque when a perfect gear is loaded, given in formula 3.20.

K_A: External force and application factor, shown in Table 3.14

K_V: Dynamic factor, formula 3.19 and formula 3.19 values shown in Table 3.11

$K_{F\beta}$: Face load factor, shown in Table 3.13

$K_{F\alpha}$: Transverse load factor, shown in Table 3.12

σ_{FP}: The permissible tooth root stress

$$K_V = \left(\frac{K_1 K_2}{\frac{F_{mt}}{b_{eH} K_A}} + K_3 \right) \frac{z_1 v_{mt}}{100} \sqrt{\frac{u^2}{u^2 + 1}} + 1 \text{ (3.19)} \qquad (3.19)$$

Table 3.11. Dynamic factor values, K_v, (DIN 3991-1 Standard, 1988)

Factors	Gear quality according to standards of the DIN 3965 series	Straight toothing	Helical and spiral teeth
K1	3	2,19	
	4	3,18	
	5	5,48	
	6	9,5	
	7	15,34	
	8	27,02	
	9	58,43	
	10	106,64	
	11	146,08	
	12	219,12	
K2	3 to 12	1,0645	1
K3	3 to 12	0,0193	0,01

Table 3.12. Transverse load factor, $K_{F\alpha}$ (DIN 3991-1 Standard, 1988)

Specific loading K_aF_{mt}/b_e			≥100N/mm							< 100N/mm
Gear accuracy grade			5 and finer	6	7	8	9	10	11 and coarser	all accuracy grades
Surface hardened	Straight bevel gears	$K_{F\alpha}$	1,0		1,1	1,2	$1/Y_\varepsilon$ or 1,2, whichever is greater			
	Helical and spiral bevel gears	$K_{F\alpha}$	1,0	1,1	1,2	1,4	$\varepsilon_{v\alpha n}$ or 1,4, whichever is greater			
Not surface hardened	Straight bevel gears	$K_{F\alpha}$	1,0			1,1	1,2	$1/Y_\varepsilon$ or 1,2, whichever is greater		
	Helical and spiral bevel gears	$K_{F\alpha}$	1,0		1,1	1,2	1,4	$\varepsilon_{v\alpha n}$ or 1,4, whichever is greater		

Table 3.13. Face load factor, $K_{F\beta}$,(ISO 10300-1 Standard, 2001)

Verification of contact pattern	Mounting conditions of pinion and gear		
Contact pattern is checked	Neither member cantilever mounted	One-member cantilever mounted	Both members cantilever mounted
For each gear set in its housing under full load	1,00	1,00	1,00
For each gear set under light test load	1,05	1,10	1,25
For a sample gear set and estimated for a full load.	1,20	1,32	1,50
NOTE Based on optimum tooth contact pattern under maximum operation load, as evidenced by the results of a deflection test on the gear in their mountings.			

Table 3.14. Application factor $K_{A,}$ values (ISO 10300-1 Standard, 2001)

	Working characteristics of the driven machine			
Working characteristics of the driving machine	Uniform	Light shocks	Medium shocks	Heavy shocks
Uniform	1,00	1,25	1,50	1,75
Light shocks	1,10	1,35	1,60	1,85
Medium shocks	1,25	1,50	1,75	2,00
Heavy shocks	1,50	1,75	2,00	2,25

$$\sigma_{F0} = \frac{F_{mt}}{b_{eF} m_{mn}} Y_{Fa} Y_{Sa} Y_{\varepsilon} Y_K Y_{\beta} \tag{3.20}$$

$$b_{eF} = b_{eH} = 0{,}85b \tag{3.21}$$

F_{mt}: The nominal tangential force at the reference cone at mid-face width;

b: the face width;

Y_{Fa}: The tooth form factor, which accounts for the influence of the tooth form on the nominal bending stress for load application at the tooth tip;

Y_{Sa}: The stress correction factor, which accounts for the conversion of the nominal bending stress for load application at the tooth tip to the corresponding local tooth root stress. Thus Y_{Sa} accounts for the stress-increasing effect of the notch (in the root fillet), as well as for the fact that the stress condition in the critical root section is complicated, but not for the influence of the bending moment arm;

Y_{FS}: It is obtained by multiplying Y_{Fa} and Y_{Sa}, shown in Figure 3.10

Y_{ε}: The contact-ratio factor, which accounts for the conversion of the local stress determined for the load application at the tooth tip to the determinant position, given in formula 3.22;

Y_K: The bevel-gear factor, which accounts for smaller values for $l_b{}'$ compared to total face width b and the inclined lines of contact, with the current state of knowledge, one can set $Y_K = 1$.

Y_β: Schrägen factor, given in formula 3.24

$$Y_\varepsilon = 0{,}25 + \frac{0{,}75}{\varepsilon_{v\alpha n}} \quad (3.22) \tag{3.22}$$

$$\text{For } \varepsilon_{v\alpha n} \geq 2 \text{ take } \varepsilon_{v\alpha n} = 2 \tag{3.23}$$

$$Y_\beta = 1 - \varepsilon_{v\beta} \frac{\beta_m}{120°} \tag{3.24}$$

$$\text{If } \varepsilon_{v\beta} > 1, \text{ take } \varepsilon_{v\beta} = 1; \tag{3.25}$$

$$\text{If } \beta_m > 30, \text{take } \varepsilon_{v\beta} = 30 \tag{3.26}$$

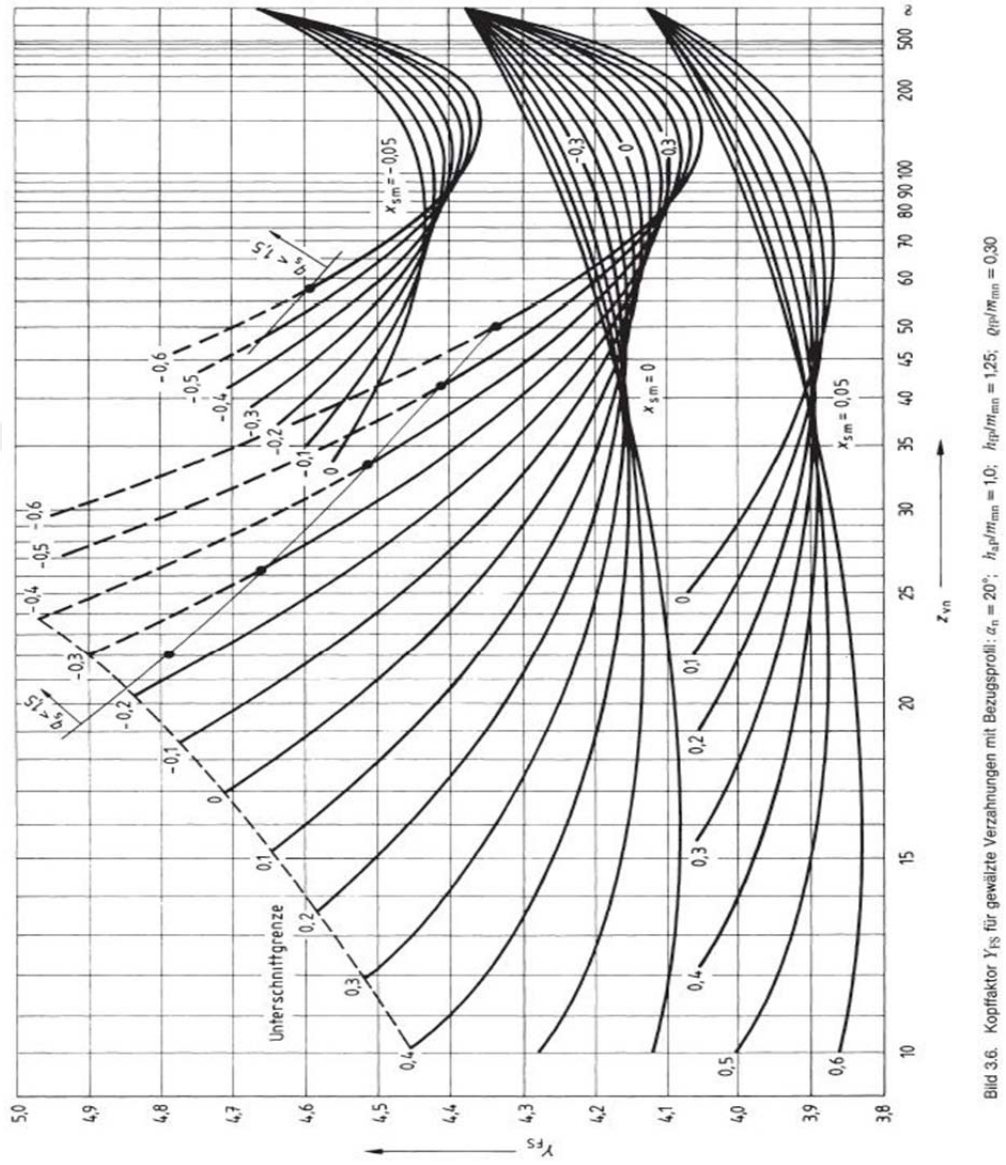

Figure 3.10. Combined tooth form factor $\boldsymbol{Y_{FS}}$= $\boldsymbol{Y_{Fa}Y_{Sa}}$ for gears generated by basic rack $\boldsymbol{p_{a0}}$= 0,3 $\boldsymbol{m_{mn}}$ (DIN 3991-3 Standard, 1988)

$$\sigma_{FP} = \frac{\sigma_{F\,lim} Y_{ST}}{S_{F\,min}} Y_{\delta\,rel\,T} Y_{R\,rel\,T} Y_X \quad (3.27) \qquad (3.27)$$

$\sigma_{F\ lim}$: the bending stress number for the nominal stress in bending of the test gear, which accounts for material, heat treatment, and surface influence at test gear dimensions, shown in Figure 3.11, Figure 3.12 and Figure 3.13 according to the type of material;

Y_{ST}: The stress-correction factor for the dimensions of the standard test gear $Y_{ST} = 2{,}0$;

$S_{F\ min}$: The minimum safety factor;

$Y_{\delta\ rel\ T}$: The relative sensitivity factor for the allowable stress number, related to the conditions at the standard test gear ($Y_{\delta\ rel\ T} = Y_{\delta} Y_{\delta T}$ accounts for the notch sensitivity of the material);

$Y_{R\ rel\ T}$: The relative surface condition factor ($Y_{R\ rel\ T} = Y_R Y_{RT}$ accounts for the surface condition at the root fillet, related to the conditions at the test gear);

Y_X: The size factor for tooth root strength, which accounts for the influence of the module on the tooth root strength;

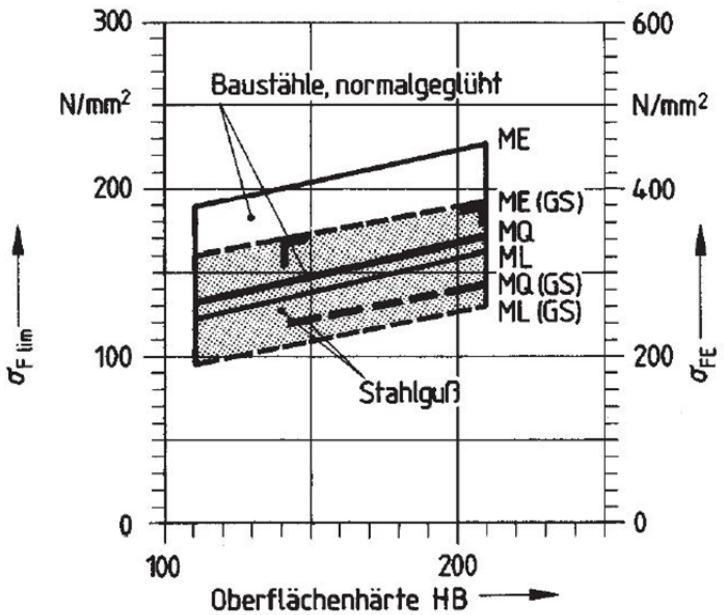

Figure 3.11. Allowable Bending Stress Number for Steel Gears, $\sigma_{F\ lim}$, for structural steel, normalized and steel, tooth root strength (DIN 3991-3 Standard, 1988)

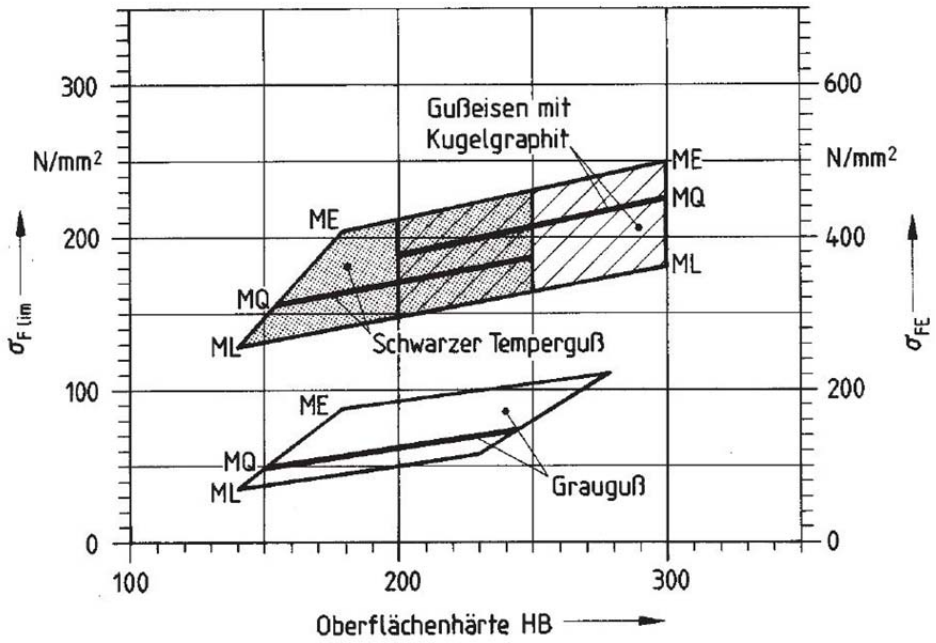

Figure 3.12. Allowable Bending Stress Number for Steel Gears, $\sigma_{F\,lim}$, for nodular cast iron (DIN 3991-3 Standard,1988)

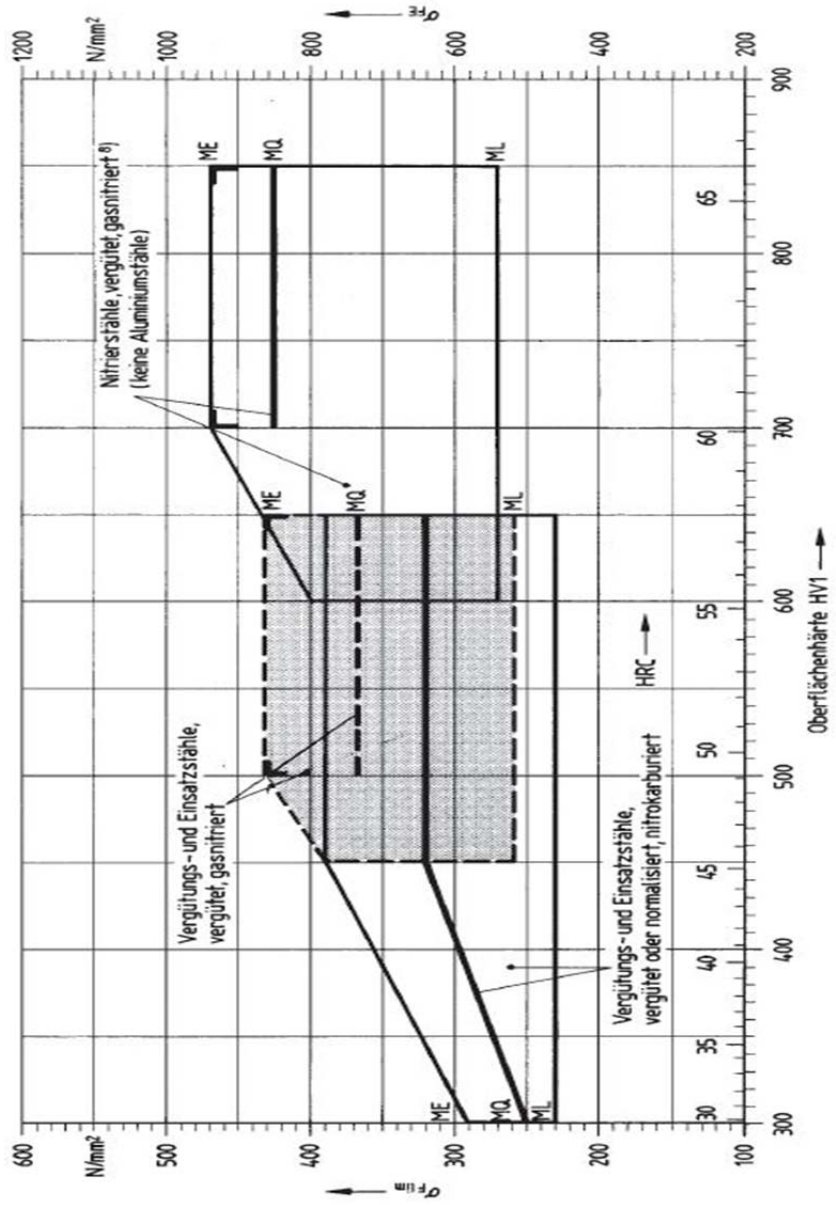

Figure 3.13. Allowable Bending Stress Number for Steel Gears, $\sigma_{F\ lim}$, for nitrided and nitrocarburized parts, tooth root fatigue strength (DIN 3991-3 Standard, 1988)

This method is generally sufficiently exact for industrial gears. In the case of gears with $q_s \geq 1{,}5$ it is set as:

$$Y_{\delta\, rel\, T} = 1{,}0$$

For $q_s \geq 2{,}5$, the calculation is on the safe side.

The reduction of the allowable tooth root stress expected in case of $q_s < 13$ is accounted for by:

$$Y_{\delta\, rel\, T} = 0{,}95$$

The relative surface condition factor, $Y_{R\, rel\, T}$, determined by tests with test specimens.

Range $R_z < 1$ µm**:**

For through-hardened and case-hardened steels:

$$Y_{R\, rel\, T} = 1{,}12$$

For soft steels:

$$Y_{R\, rel\, T} = 1{,}07$$

For grey cast iron, nitrided, and nitro-carburized steels:

$$Y_{R\, rel\, T} = 1{,}025$$

Range 1 µm < R_z < 40 µm**:**

For through-hardened and case-hardened steels:

$$Y_{R\, rel\, T} = \frac{Y_R}{Y_{RT}} = 1{,}674 - 0{,}529(R_z + 1)^{0{,}1}$$

For soft steels:

$$Y_{R\, rel\, T} = \frac{Y_R}{Y_{RT}} = 5{,}306 - 4{,}203(R_z + 1)^{0{,}01}$$

For grey cast iron, nitrided, and nitro-carburized steels:

$$Y_{R\, rel\, T} = \frac{Y_R}{Y_{RT}} = 4{,}299 - 3{,}259(R_z + 1)^{0{,}005}$$

The size factor, Y_X**,** accounts for the decrease in strength with increasing size (size effect), shown in Table 3.15.

The main factors such as the size of the tooth, ratio of tooth size to diameter, the diameter of the part, the stress area, the selected material and the applied heat treatment, ratio of case depth to tooth thickness directly affect the size factor.

Table 3.15 The size factor for tooth root strength, Y_X (DIN 3991-3 Standard, 1988)

Material		Normal module m_n	Size factor Y_X
St, V, GGG (perl., bai.), GTS (perl.)	For Fatigue Strength	$m_n \leq 5$ $5 < m_n < 30$ $30 \leq m_n$	$Y_X = 1{,}0$ $Y_X = 1{,}03 - 0{,}006 * m_n$ $Y_X = 0{,}85$
Eh,IF (grund), NTV		$m_n \leq 5$ $5 < m_n < 25$ $25 \leq m_n$	$Y_X = 1{,}0$ $Y_X = 1{,}05 - 0{,}01 * m_n$ $Y_X = 0{,}8$
GG, GGG (ferr.)		$m_n \leq 5$ $5 < m_n < 25$ $25 \leq m_n$	$Y_X = 1{,}0$ $Y_X = 1{,}075 - 0{,}015 * m_n$ $Y_X = 0{,}7$
All materials for static strength		-	$Y_X = 1{,}0$

3.2.2.4. Design Approach Using ISO 10300 Standards - Part 3

Although the main formula used for bending stress calculations is provided in 10300-3, values and formulas are taken from 10300-1 and 6336-6 standards. Tooth root stress, σ_F, is the maximum tensile stress at the surface in the root.

$$\sigma_F = \sigma_{FO} K_A K_V K_{F\beta} K_{F\alpha} \leq \sigma_{FP} \quad (3.28)$$

Where

σ_{FO}: Nominal tooth root stress, which is the maximum local principal stress produced at the tooth root

σ_F: Permissible bending stress

K_A: External force and application factor, shown in Table 3.16

K_V: Dynamic factor, given in formula 3.29

$K_{F\beta}$: Face load factor

$K_{F\alpha}$: Transverse load factor

σ_{FP}: The permissible tooth root stress

Table 3.16. Application factor, K_A (ISO 10300-1 Standard, 2001)

	Working characteristics of the driven machine			
Working characteristics of the driving machine	Uniform	Light shocks	Medium shocks	Heavy shocks
Uniform	1,00	1,25	1,50	1,75 or higher
Light shocks	1,10	1,35	1,60	1,85 or higher
Medium shocks	1,25	1,50	1,75	2,00 or higher
Heavy shocks	1,50	1,75	2,00	2,25 or higher

The dynamic factor K_V is given by equation 3.29 and is determined by the parameters A and B, which are given by equation 3.30 and 3.31, thees respectively, and the pitch line velocity at the operating pitch diameter, which can be seen in equation 3.32.

$$K_V = \left[\frac{A}{A + \sqrt{200V_{et}}}\right]^{-B} \tag{3.29}$$

For $6 \leq C \leq 9$,

$$\mathrm{A} = 50 + 56(1.0 - \mathrm{B}) \tag{3.30}$$

$$\mathrm{B} = 0.25(C - 5)^{0.667} \tag{3.31}$$

C: the transmission accuracy level number

$$V_{et} = v_{mt}\frac{d_{e1,2}}{d_{m1,2}} \tag{3.32}$$

$K_{F\beta}$ is defined as the ratio between the maximum tooth root stress and the mean tooth root stress over the face width and is given by equation 3.33;

$K_{H\beta}$ is defined as the ratio between the maximum load per unit face width and the mean load per unit face width, and is given by table 3.17;

$$K_{F\beta} = K_{H\beta}/K_{F0} \quad (3.33)$$

We assume $K_{F0} = 1$

Table 3.17. Mounting factor, $K_{H\beta-be}$ (ISO 10300-1 Standard, 2001)

Verification of contact pattern	Mounting conditions of pinion and gear		
Contact pattern is checked	Neither member cantilever mounted	One-member cantilever mounted	Both members Cantilever Mounted
For each gear set in its housing under full load	1,00	1,00	1,00
For each gear set under light test load	1,05	1,10	1,25
For a sample gear set and estimated for a full load.	1,20	1,32	1,50
NOTE Based on optimum tooth contact pattern under maximum operation load, as evidenced by the results of a deflection test on the gear in their mountings.			

In order to compensate for a sufficient face width under full load b_e less than 85% of the face width b, the face load factor is to be corrected. Because of that, the decisive load distribution factor $K_{H\beta-C}$ is given by equation 3.34;

$K_{H\beta-C}$: Face load factor

$$K_{H\beta-C} = 1{,}5K_{H\beta-be}.\frac{0.85b}{b_e} \quad \text{for} b_e < 0{,}85b \ (3.34) \quad (3.34)$$

And $K_{H\alpha-C}$ and $K_{F\alpha-C}$ shall be taken from Table 3.18;

Table 3.18. Transverse load distribution factors, $K_{H\alpha-C}$ and $K_{F\alpha-C}$ (ISO 10300-1 Standard, 2001)

Specific loading K_aF_{mt}/b_e			≥100N/mm							< 100N/mm
Gear accuracy grade			6 and better	7	8	9	10	11	12	all accuracy grades
Surface hardened	Straight bevel gears	$K_{F\alpha}$	1,0		1,1	1,2	$1/Y_\varepsilon$ or 1,2, whichever is greater			
	Helical and spiral bevel gears	$K_{F\alpha}$	1,0	1,1	1,2	1,4	$\varepsilon_{v\alpha n}$ or 1,4, whichever is greater			
Not surface hardened	Straight bevel gears	$K_{F\alpha}$	1,0			1,1	1,2	$1/Y_\varepsilon$ or 1,2, whichever is greater		
	Helical and spiral bevel gears	$K_{F\alpha}$	1,0		1,1	1,2	1,4	$\varepsilon_{v\alpha n}$ or 1,4, whichever is greater		

$$\sigma_{F0} = \frac{F_{mt}}{bm_{mn}} Y_{Fa} Y_{Sa} Y_\varepsilon Y_K Y_{LS} \ (3.35) \qquad (3.35)$$

Where;

σ_{F0}: is the local tooth root stress defined as the maximum tensile stress arising at the tooth root due to the nominal torque when a perfect gear is loaded.

F_{mt}: The nominal tangential force at the reference cone at mid-face width;

b*:* the face width;

Y_{Fa}: The tooth form factor, which accounts for the influence of the tooth form on the nominal bending stress for load application at the tooth tip;

Y_{Sa}: The stress correction factor, which accounts for the conversion of the nominal bending stress for load application at the tooth tip to the corresponding local tooth root stress. Thus Y_{Sa} accounts for the stress-increasing effect of the notch (in the root fillet), as well as for the fact that the stress condition in the critical root section is complicated, but not for the influence of the bending moment arm;

Y_{FS}: It is obtained by multiplying Y_{Fa} and Y_{Sa}, shown in Figure 3.14

Y_{ε}: The contact-ratio factor (see clause 8), which accounts for the conversion of the local stress determined for the load application at the tooth tip to the determinant position, given in 3.36;

Y_K: The bevel-gear factor, which accounts for smaller values for $l_b{}'$ compared to total face width b and the inclined lines of contact;

Y_{LS}: The load sharing factor, which accounts for load distribution between two or more pairs of teeth.

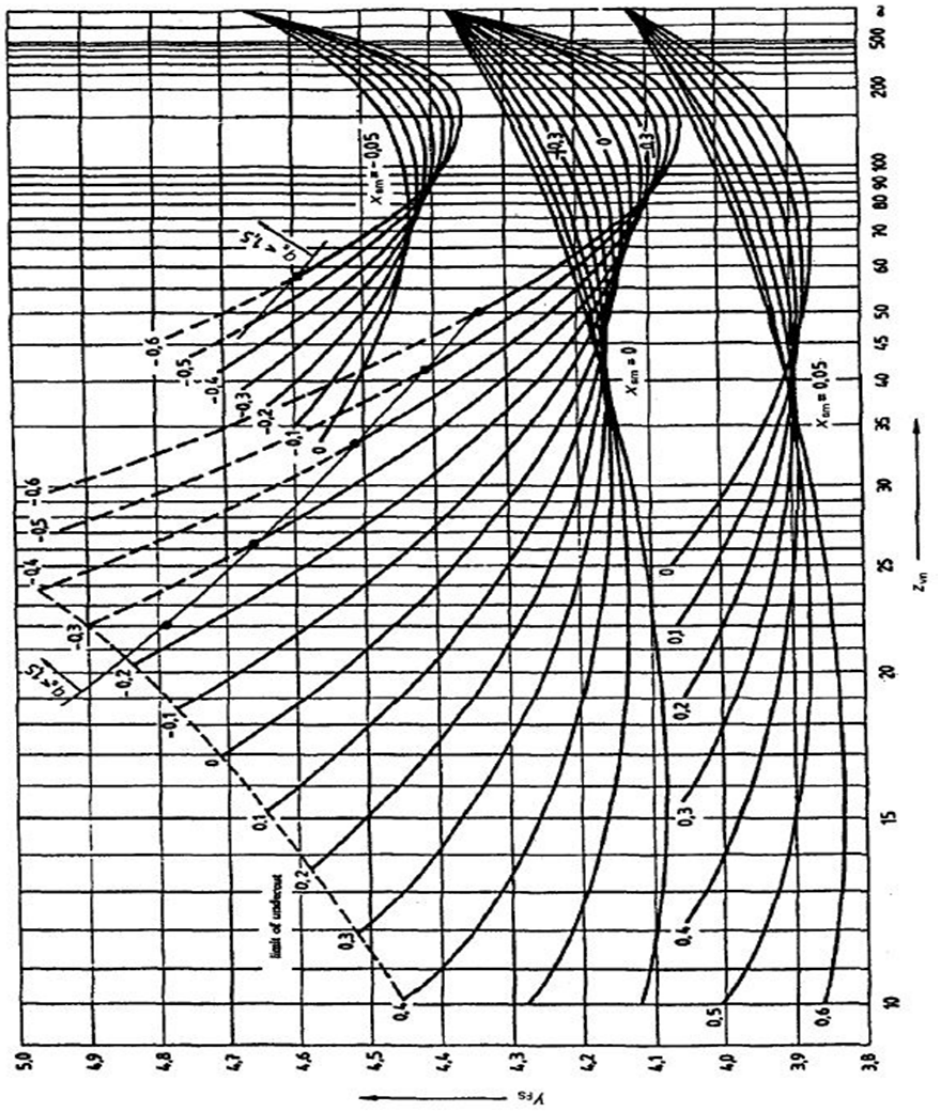

Figure 3.14. Combined tooth form factor $\boldsymbol{Y_{FS}}$= $\boldsymbol{Y_{Fa}Y_{Sa}}$ for gears generated by basic rack $\boldsymbol{p_{a0}}$= 0,3 $\boldsymbol{m_{mn}}$ (ISO 10300-3 Standard, 2003)

The contact-ratio factor, Y_{ε}, converts the load application at the tooth tip (here the tooth form factor, Y_{Fa}, and stress correction factor(Y_{Sa})**,** apply) to the decisive point of load application.

$$Y_\varepsilon = 0{,}25 + \frac{0{,}75}{\varepsilon_{v\alpha}} \geq 0{,}625 \text{ for } \varepsilon_{vb} = 0 \quad (3.36)$$

$$Y_\varepsilon = 0{,}625 \text{ for } \varepsilon_{vb} > 1$$

l'_{bm}: The projected length of the middle line of contact

The load sharing factor, Y_{LS}, accounts for load sharing between two or more pairs of teeth.

$$Y_{LS} = {Z_{LS}}^2$$

$$\sigma_{FP} = \frac{\sigma_{F\,lim} Y_{ST} Y_{NT}}{S_{F\,min}} Y_{\delta\,rel\,T} Y_{R\,rel\,T} Y_X \quad (3.37)$$

$\sigma_{F\,lim}$: The bending stress number for the nominal stress in bending of the test gear, which accounts for material, heat treatment, and surface influence at test gear dimensions, shown in Table 3.19;

Y_{ST}: The stress-correction factor for the dimensions of the standard test gear $Y_{ST} = 2.0$;

$S_{F\,min}$: The minimum safety factor;

$Y_{\delta\,rel\,T}$: The relative sensitivity factor for the allowable stress number, related to the conditions at the standard test gear ($Y_{\delta\,rel\,T} = Y_\delta Y_{\delta T}$ accounts for the notch sensitivity of the material);

$Y_{R\,rel\,T}$: The relative surface condition factor ($Y_{R\,rel\,T} = Y_R Y_{RT}$ accounts for the surface condition at the root fillet, related to the conditions at the test gear);

Y_X: The size factor for tooth root strength, which accounts for the influence of the module on the tooth root strength;

Y_{NT}: The life factor, which accounts for the influence of required numbers of cycles of operation, given in Fig. 3.15.

As a result of testing the gears taken as reference, the number of nominal stresses, $\sigma_{F\,lim}$, is obtained, shown in Table 3.19. It is the bending stress limit value relevant to the influences of the material, the heat treatment, and the surface roughness of the test gear root fillets. ISO 6336-Part 5 provides information on

commonly used gear materials, methods of heat treatment, and the influence of gear quality on values for nominal stress numbers, which are used for nominal stress.

$$\sigma_{F\,lim} = A * x + B \tag{3.38}$$

Table 3.19. Calculation of σ_{Flim} (ISO 6336-5 Standard, 2003)

No	Material	Type	Abbrev-iation	Quali-ty	A	B	Hard-ness	Min. hard-ness	Max hard-ness
1	Normalized low carbon steels/cast steels	wrought normalized low carbon steels	St	ML/ MQ	0,455	69	HB	110	210
2				ME	0,386	147		110	210
3		cast steels	St(cast)	ML/ MQ	0,313	62	HB	140	210
4				ME	0,254	137		140	210
5	Cast iron materials	black malleable cast iron	GTS (perl.)	ML/ MQ	0,345	77	HB	135	250
6				ME	0,403	128		175	250
7		nodular cast iron	GGG	ML/ MQ	0,350	119	HB	175	300
8				ME	0,380	134		200	300
9		grey cast iron	GG	ML/ MQ	0,256	8	HB	150	240
10				ME	0,200	53		175	275
11	Through hardened wrought steels	carbon steels	V	ML	0,250	108	HV	115	215
12				MQ	0,240	163		115	215
13				ME	0,283	202		115	215
14		alloy steels	V	ML	0,423	104	HV	200	360
15				MQ	0,425	187		200	360
16				ME	0,358	231		200	390
17	Through hardened cast steels	carbon steels	V (cast)	ML/ MQ	0,224	117	HV	130	215
18				ME	0,286	167		130	215
19		alloy steels	V (cast)	ML/ MQ	0,364	161	HV	200	360
20				ME	0,356	186		200	360

Table 3.19. Calculation of σ_{Flim} (ISO 6336-5 Standard, 2003) (Countined)

21	Case Hardened		Eh	ML	0,000	312	HV	600	800
22	Wrought steels	≥ 25 HRC, Lower		MQ	0,000	425		660	800
23		≥ 25 HRC, Upper			0,000	461		660	800
24		≥ 30 HRC,			0,000	500		660	800
25				ME		525		660	800
26	Flame or		IF	ML	0,305	76	HV	485	615
27	induction			MQ	0,138	290		500	570
28	hardened				0,000	369		570	615
29	wrought and cast steels			ME	0,271	237		500	615
30	Nitrided Wrought steels/nitriding steels /through hardening steels nitrided	nitriding steels (a)	NV (nitro-car.)	ML	0,000	270	HV	650	900
31				MQ	0,000	420		650	900
32				ME	0,000	468		650	900
33		through hardening steels	NV (nitro-car.)	ML	0,000	258	HV	450	650
				MQ	0,000	363		450	650
34				ME	0,000	432		450	650
35									
36	wrought	Through	NV	ML	0.000	224	HV	300	650
37	steels nitro-carburised	Hardening steels	(nitro-car)	MQ/ ME	0,653	94		300	450
38					0,000	388		450	650

This method is generally sufficiently exact for industrial gears. In the case of gears with

$q_s \geq 1{,}5$ it is set as:

$$Y_{\delta\, rel\, T} = 1{,}0$$

For $q_s \geq 2{,}5$, the calculation is on the safe side.

The reduction of the allowable tooth root stress expected in case of $q_s < 13$ is accounted for by:

$$Y_{\delta\, \mathrm{rel\, T}} = 0{,}95$$

The relative surface condition factor, $Y_{R\, rel\, T}$

Range $R_z < 1$ µm:

For through-hardened and case-hardened steels:

$$Y_{R\,rel\,T} = 1{,}12$$

For soft steels:

$$Y_{R\,rel\,T} = 1{,}07$$

For grey cast iron, nitrided, and nitro-carburized steels:

$$Y_{R\,rel\,T} = 1{,}025$$

Range 1 µm < R_z< 40 µm:

For through-hardened and case-hardened steels:

$$Y_{R\,rel\,T} = \frac{Y_R}{Y_{RT}} = 1{,}674 - 0{,}529(R_z + 1)^{\frac{1}{10}}$$

For soft steels:

$$Y_{R\,rel\,T} = \frac{Y_R}{Y_{RT}} = 5{,}306 - 4{,}203(R_z + 1)^{1/100}$$

For grey cast iron, nitrided, and nitro-carburized steels:

$$Y_{R\,rel\,T} = \frac{Y_R}{Y_{RT}} = 4{,}299 - 3{,}259(R_z + 1)^{1/200}$$

The size factor, Y_X, accounts for the decrease in strength with increasing size (size effect).

The main factors such as the size of the tooth, ratio of tooth size to diameter, the diameter of the part, the stress area, the selected material and the applied heat treatment, ratio of case depth to tooth thickness directly affect the size factor. Size factor formulas for structural and through-hardened steels, spheroidal cast iron, pearlitic malleable cast iron are given in Formula 3.39, 3.40, 3.41.

$$Y_X = 1{,}03 - 0{,}006m_{mn} \tag{3.39}$$

with the restriction 0,85≤Y_X≤1,0

For case, flame, induction-hardened steels, nitrided or nitro-carburized steels

$$Y_X = 1{,}05 - 0{,}01m_{mn} \tag{3.40}$$

With the restriction 0,80≤Y_X≤1,0

For grey cast iron

$$Y_X = 1{,}075 - 0{,}015 m_{mn} \tag{3.41}$$

with the restriction $0{,}70 \leq Y_X \leq 1{,}0$

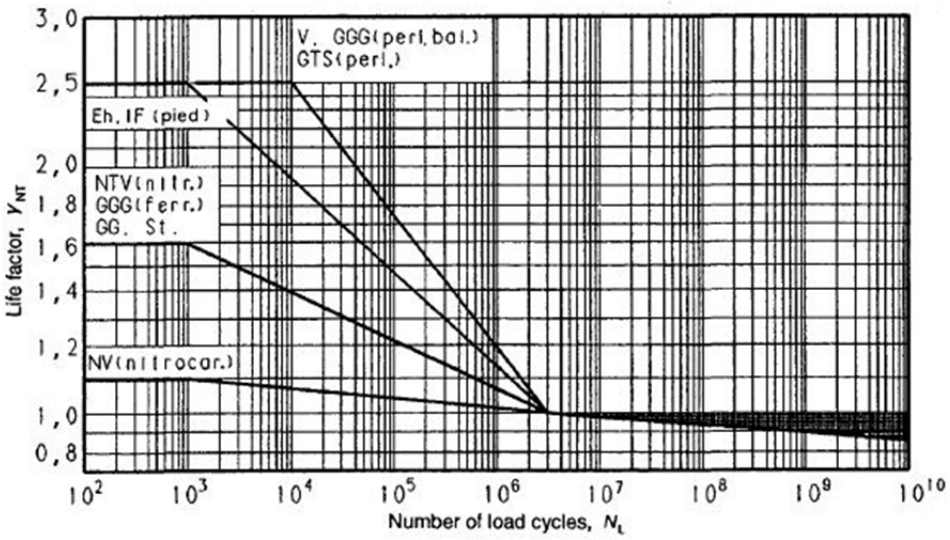

Figure 3.15. Life factor, Y_{NT} (ISO 10300-3 Standard, 2003)

3.2.3. Defining Geometric Rating Numbers (GR_i) for Design Approaches

Geometric rating numbers are dimensionless numbers obtained by using m and F values determined from various combinations of power values and speed ratios using formulas of standards and machine element book solutions. More specifically, GR_i is obtained by the ratio of the results obtained by multiplying half of the circular pitch and the face width for different approaches, as defined in equation 3.42. GR_i is more like a geometrical value, which may be used as a representative for the cross-sectional area at the pitch diameter. Half of the circular pitch ($\frac{p}{2} = \pi \frac{m}{2}$) is used because it is equal to the tooth thickness in the SI unit system. (Geren N., Uzay Ç, 2016).

$$GR_i = \frac{\frac{\pi m_i F_i}{2}}{\frac{\pi m_o F_o}{2}} = \frac{m_i F_i}{m_o F_o} \tag{3.42}$$

Where m_i and F_i are the module and face width obtained from each of the gear design approaches respectively, and m_0 and F_0 obtained module and face width respectively, which are obtained according to the selected technical design standard. In this study, the values of all approach solutions are divided into ANSI / AGMA 2003-B97 gear standards, and the geometric rating numbers GR_i is found.

3.2.4. Defining Conversion Factors (CFs) for Design Approaches

The most crucial aim of this thesis work is to find out a correlation between all design approaches (ISO, DIN, J&M, or AGMA) and selected one (ISO, DIN, J&M, or AGMA). In this thesis, as mentioned in Section 3.2.3, Conversion Factors (CF_s) will be calculated based on the AGMA standard. Therefore, conversion factors are generated to convert module (m) and face width (F) obtained from each design approaches (ISO, B&N, J&M) to the AGMA standard. Under the same conditions, the dimensionless number obtained by dividing the module obtained from any design approach into the module obtained by AGMA is indicated by the m_i^* . If the ratio were set to face width, it would be indicated by F_i^*. The mean values of conversion factors for the module ($\overline{CF}_{mi}$) and face width ($\overline{CF}_{Fi}$) with their standard deviations are given in Table 3.20 (Geren N., Uzay Ç., Bayramoğlu M., 2017)

Table 3.20. Formulas to obtain mean conversion factors and standard deviation of conversion factors for a module and face width (Geren N., Uzay Ç., Bayramoğlu M., 2017)

Conversion factor	Mean	Standard deviation
Module	$\overline{CF}_{mi} = \frac{1}{N}\sum_{j=1}^{N} {m_i}^*$	$\sigma_{\overline{CF}_{mi}} = \sqrt{\frac{1}{N}\sum_{j=1}^{N}({m_i}^* - \overline{CF}_{mi})^2}$
Face width	$\overline{CF}_{Fi} = \frac{1}{N}\sum_{j=1}^{N} {F_i}^*$	$\sigma_{\overline{CF}_{Fi}} = \sqrt{\frac{1}{N}\sum_{j=1}^{N}({F_i}^* - \overline{CF}_{Fi})^2}$

Where

The subscript “i”: each of the design approaches (AGMA, ISO, DIN, J&M)

The subscript “c”: convert primary value to desired value

N: number of points at selected transmitted power

${m_{ij}}^*$: the value of ${m_i}^*$ at a specific transmitted power

${F_{ij}}^*$: the value of ${F_i}^*$ at a specific transmitted power

Dimensionless numbers of $\overline{CF}_{mi}$ and $\overline{CF}_{Fi}$ obtained using expressions given in Table 3.20 may be used to convert the design results of the target approach to AGMA if we have m_i and F_i values for a gear designed using any of ISO, B&N, or J&M design approaches. As a result, any gear designer or a student designing gear to find converted values “$m_{c,AGMA}$” and “$F_{c,AGMA}$” using simple expressions. This is easily done by using equation 3.43 and equation 3.44.

$$m_{c,AGMA} = \frac{m_i}{\overline{CF}_{mi}} \tag{3.43}$$

$$F_{c,AGMA} = \frac{F_i}{\overline{CF}_{Fi}} \tag{3.44}$$

The error between the conversion formulas and the actual value is obtained using the gear volume error formula (GV_e) as a percentage, as given in equation 3.45.

$$GV_e = \left[\frac{(m\,F)_{c,AGMA} - (m\,F)_{AGMA}}{(m\,F)_{AGMA}}\right] 100 \tag{3.45}$$

A flow chart has been introduced to obtain GR_i and CF_s in Figure 3.16 to exhibite the step by step procedure used in this thesis.

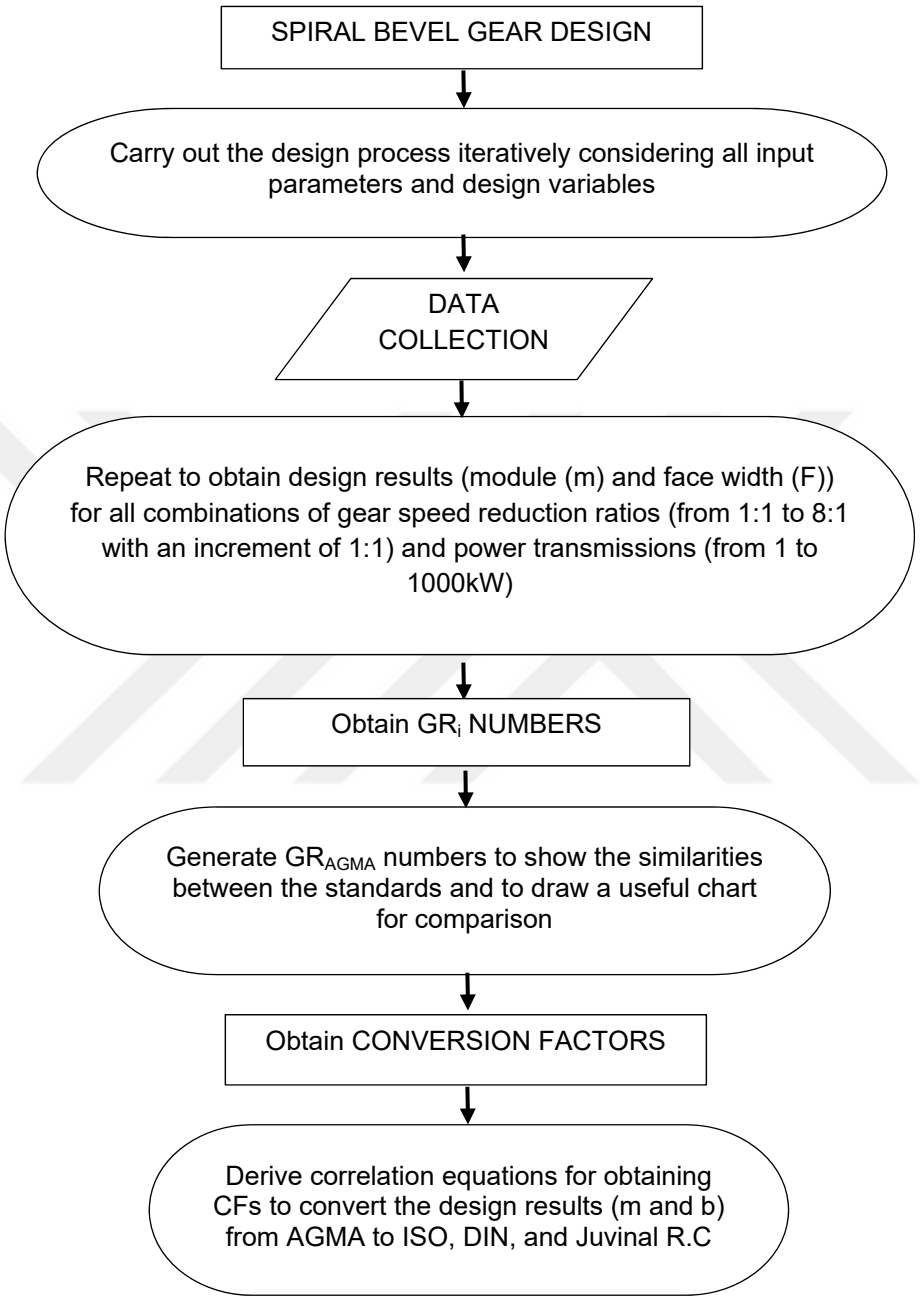

Figure 3.16. A general systematic approach to obtaining GR_i and CFs

3.2.5. Finding Tooth Stresses Using Finite Element Method (FEM)

In this study, module and facewidth results are found analytically using standards and machine elements books. The results are numerically solved with ANYSY Workbench 18.1 software. The reliability of the design is verified by comparing analytical and numerical results. The ANSYS program needs a structural model to perform numerical analysis. To provide this model, the 3D solid model of the pinion is drawn in the SolidWorks 2018 program using the GearTrax 2018 program with the values we obtain from analytical results.

Structural analysis requires three steps generally: pre-processing, solver and post-processing. In pre-processing, the geometry of the structure is made and creating mesh elements, solver is the definition of boundary conditions and lastly in post-processing analysis results are obtained.

In Section 4.2, ANSYS results give gear bending stress values for each approach. 3:1 speed ratio and 100 kW power values are chosen as the analysis parameters, since they usually give average module and face width values.

3.2.6. Summary

The direct formula, which gives the face width (F) value for each approach, was obtained using the formulas given in the previous sections and is given in Table 3.21.

Table 3.21. Face width equations of the design approaches based on bending fatigue stress failure criteria

Design Approaches	Face Width
ANSI/AGMA 2003-B97 Standard (Shigley's Mechanical Engineering Design 9th Ed.)	$F = \frac{1000Wt}{\sigma_{Flim}Y_{NT}} \frac{K_A K_V}{m_{et}} \frac{Y_X K_{H\beta}}{Y_B Y_J} S_F K_\Theta Y_z$
Fundamental of Machine Component Design 5th Ed.	$F = \frac{F_t}{mS'_n C_L C_G C_S C_T C_R J} K_v K_O K_m$
ISO Standards 10300	$F = \frac{F_{mt} Y_{F\alpha} Y_{S\alpha} Y_\varepsilon Y_K Y_{LS} K_v K_A K_{F\alpha} K_{F\beta} S_{Fmin}}{\sigma_{lim} m_{mn} Y_{\delta\, rel\, T} Y_{R\, rel\, T} Y_x Y_{ST} Y_{NT}}$
DIN 3991 Standards	$F = \frac{F_{mt} Y_{F\alpha} Y_{S\alpha} Y_\varepsilon Y_K Y_\beta K_v K_A K_{F\alpha} K_{F\beta} S_{Fmin}}{0{,}85\sigma_{lim} m_{mn} Y_{\delta\, rel\, T} Y_{R\, rel\, T} Y_x Y_{ST}}$

4. RESULTS AND DISCUSSIONS

The most critical design parameters for gear design are module and face width. As mentioned in Chapter 3, these have been determined considering the bending stress using four different types of design approaches, given by ANSI/AGMA 2003-B97 standards, Juvinall R.C., Marshek K.M. (2011), DIN Standards 3991-(Part 1-3),1987 and ISO Standards 10300-(Part 1-3), 2001.

For selected standards and machine design books, equations for face width "F" based on bending stress have been obtained, considering the four types of gear design formulations given in Table 3.21.

Figure 3.2 in Chapter 3 has also described the iterations needed for proper module selection and face width determination. For pinion and gear, geometry criteria, working conditions, and material properties were determined and then iteration started. The defined input parameters have not been changed until each iteration is completed. The values considered in this study and the input parameters are shown in Table 4.1, and these are kept the same for all types of design approaches in order to compare the design results fairly. By keeping the input parameters constant, iterations are performed until the difference between the input module and the result module is acceptable. The calculations were carried out and the face width calculations were performed using the recommended value of $F = 0.3A_0$ or $F = 10m$, whichever is smaller, then face width and the module were obtained. Face width "F" and module "m" are obtained for 4 design approaches (for the technical standards and machine elements textbooks) with different power transmissions and speed ratios. 51 different power transmission values are used for each speed ratio and for each design approach. Each design approaches have 8 different speed ratios which give 816 design results for just one case. 3264 design results for 4 different design approaches are calculated for only type 1 material. Since 3 different types of material for 20^o and 25^o are used, 19584 design results are obtained, in total.

Table 4.1. Values of the selected input parameters for the design

Input Parameters	Value
Pressure angle, α_n	20° and 25°
Spiral angle, β_m	35°
Type of gear profile	Involute
Input speed of a power source, rpm	1200
Number of life cycles, N	10^8
Design factor of safety, n_d	2,1
Reliability, %	99,9
Operating temperature, T_G	Moderate or low (~120°C)
The quality number for gear	ISO 10300 standards and DIN 3991 standards: 8 ANSI/AGMA 2003-B97 standards; 9 Juvinall R.C., Marshek K.M.,2011: shaved or ground
Material properties of gear pair	see Table 3.1
Working characteristics of driving and driven machines	Uniform
Selected transmitted power range kW	0,5 kW-1000 kW
Selected Gear speed ratio range, m_G	1:1, 2:1, 3:1, 4:1, 5:1, 6:1, 7:1, 8:1

4.1. Comparison of Module Selection and Face Width Results of the Design Approaches

Whether the material type, design approaches, pressure angle, and other input parameters change, gear volume change due to module and face width can be easily seen in the MATLAB page. Figure 4.1 shows an example for the MATLAB page prepared for spiral bevel gear design based on bending fatigue design using ANSI / AGMA 2003-B97, 1997 technical standard.

It consists of input parameters, design variables, and the most important design parameters that are module and face width. When the input parameters

change, the results change directly. The values of the design input parameters and the values of the design variables related to each design are found, with equations, tables or figure readings.

Gear design always begins with module selection and then the iterations are carried out until the correct module is found. However, this can be very time consuming, and the design can lead to erroneous results for the inexperienced designer. Thus, MATLAB program codes pages were arranged to carry out the design calculations.

4.1.1. Comparison of Face With and Module Results

In the graphics given in this section, the effect of increasing transmitted power values on the module and face width is examined, and its general trend is found.

Related graphics for comparison of face width and module results are giving Appendix A.1 for type 2 material and twenty-degree pressure angle, Appendix B.1 for type 2 material and twenty-degree pressure angle, Appendix C.1 for type 1 material and twenty-five-degree pressure angle, D.1 for type 2 material and twenty-five-degree pressure angle, E.1 for type 3 material and twenty-five-degree pressure angle.

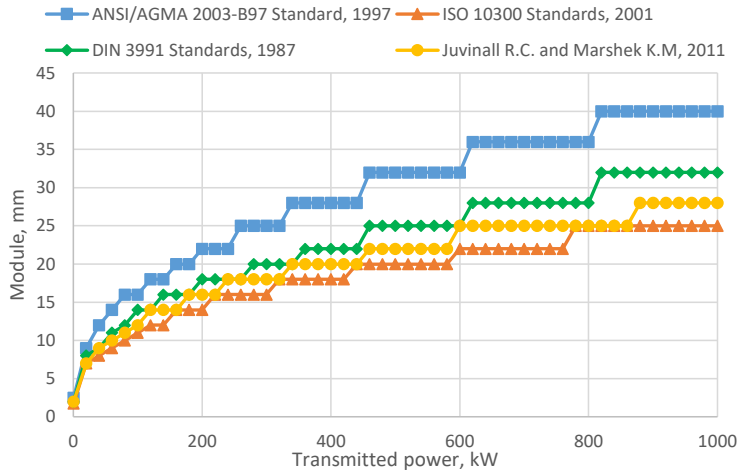

Figure 4.1. Module values under various transmitted power at 1:1 speed ratio for α_n=20° and material type 1

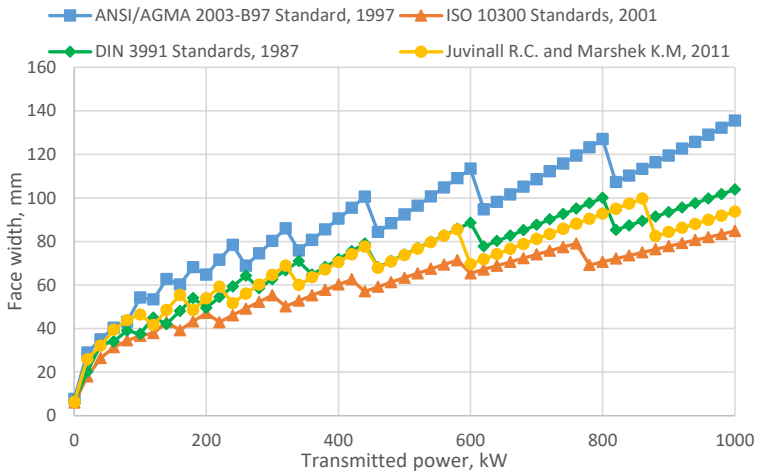

Figure 4.2. Face width values under various transmitted power at 1:1 speed ratio for α_n=20° and material type 1

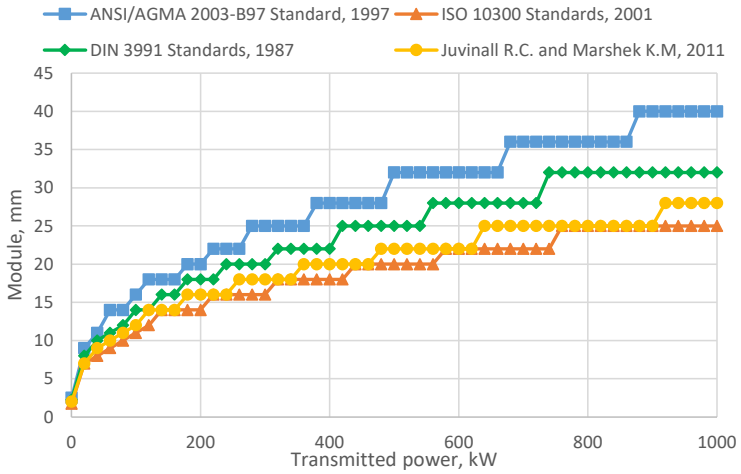

Figure 4.3. Module values under various transmitted power at 2:1 speed ratio for α_n=20° and material type 1

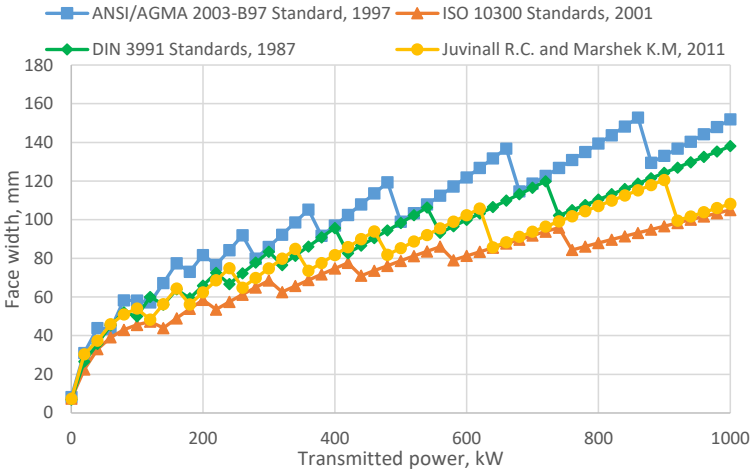

Figure 4.4. Face width values under various transmitted power at 2:1 speed ratio for α_n=20° and material type 1

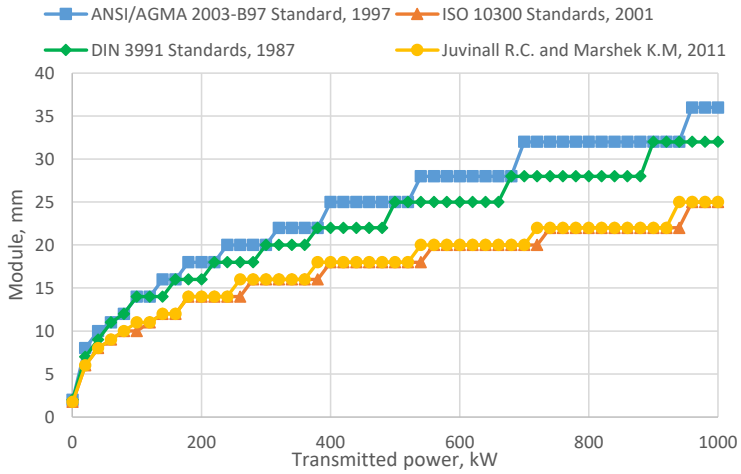

Figure 4.5. Module values under various transmitted power at 3:1 speed ratio for α_n=20° and material type 1

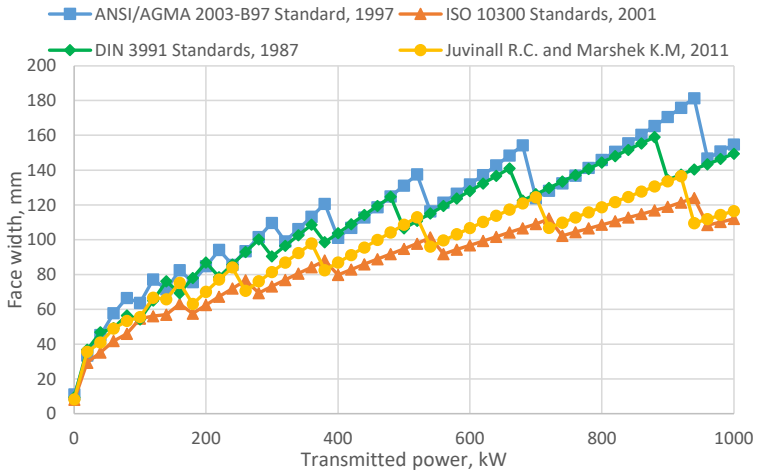

Figure 4.6. Face width values under various transmitted power at 3:1 speed ratio for α_n=20° and material type 1

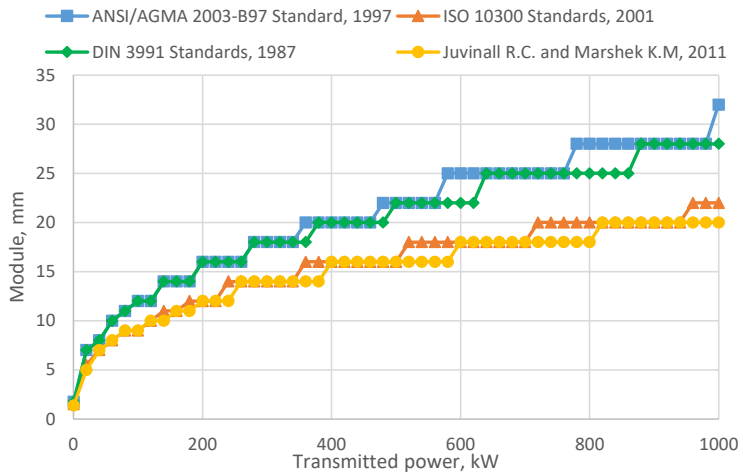

Figure 4.7. Module values under various transmitted power at 3:1 speed ratio for α_n=20° and material type 1

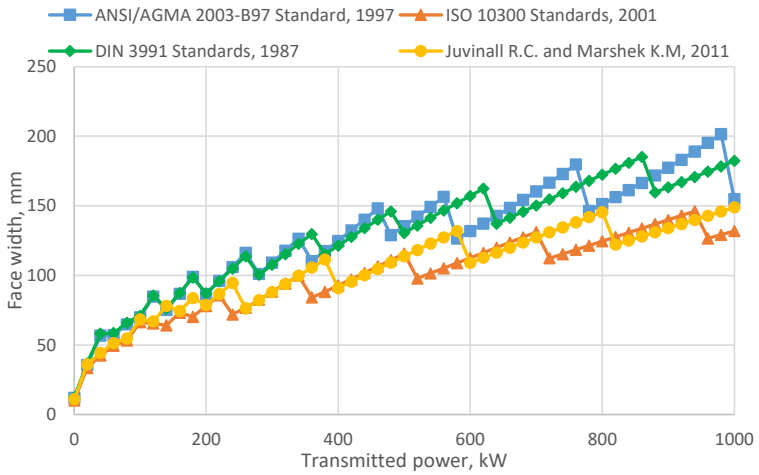

Figure 4.8. Module values under various transmitted power at 4:1 speed ratio for α_n=20° and material type 1

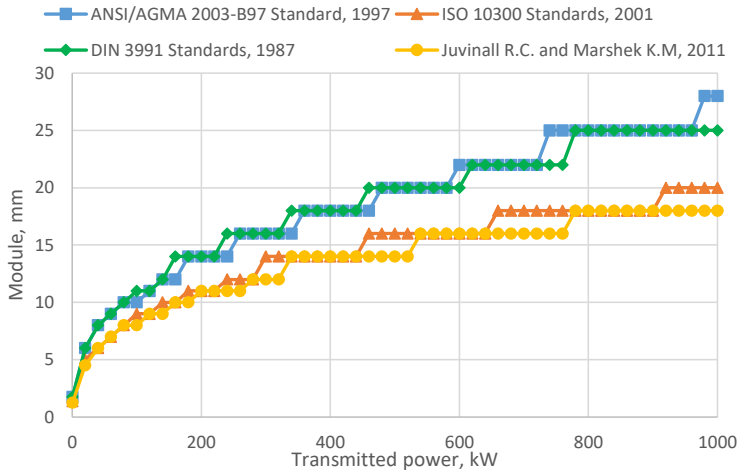

Figure 4.9. Module values under various transmitted power at 5:1 speed ratio for α_n=20° and material type 1

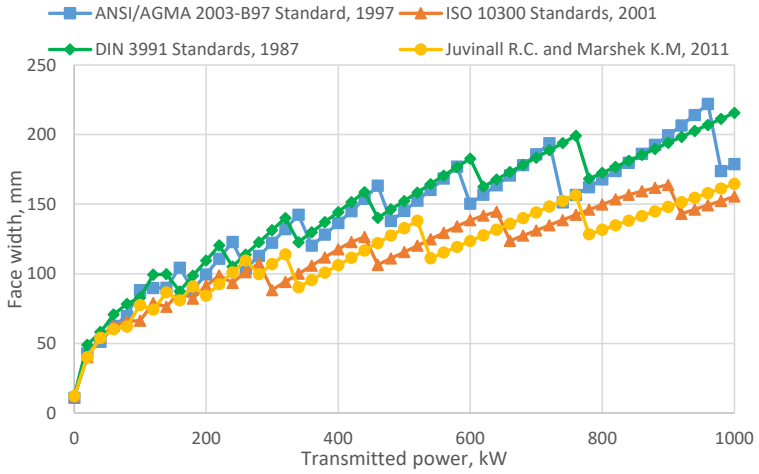

Figure 4.10. Face width values under various transmitted power at 5:1 speed ratio for α_n=20° and material type 1

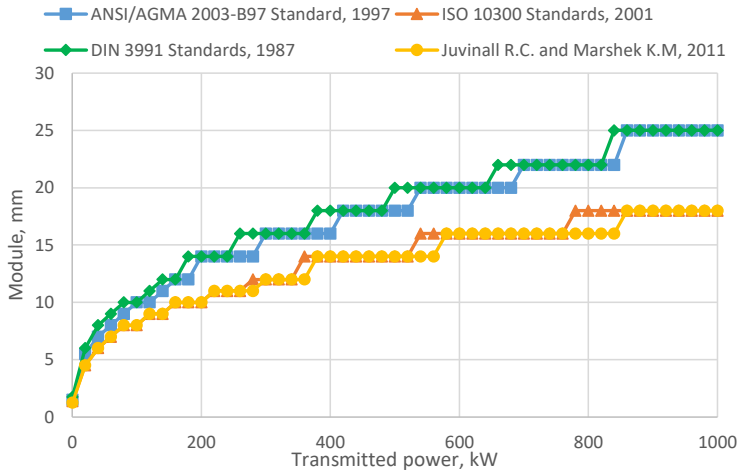

Figure 4.11. Module values under various transmitted power at 6:1 speed ratio for α_n=20° and material type 1

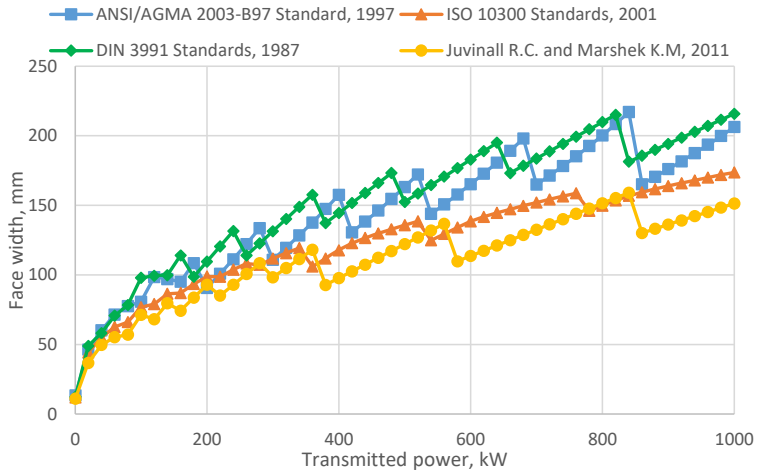

Figure 4.12. Face width values under various transmitted power at 6:1 speed ratio for α_n=20° and material type 1

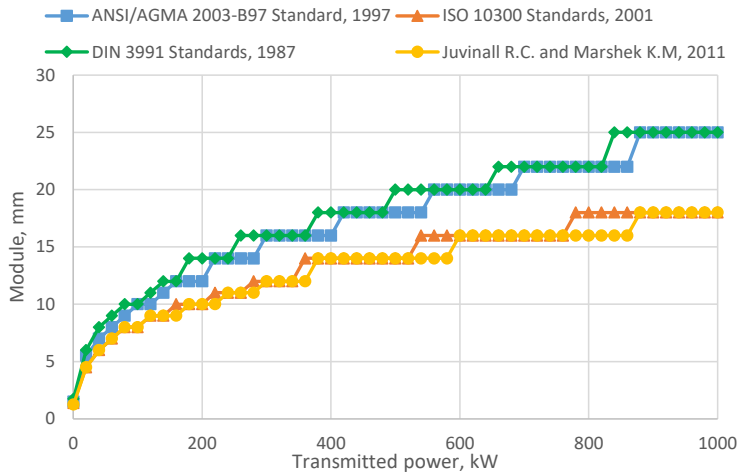

Figure 4.13. Module values under various transmitted power at 7:1 speed ratio for α_n=20° and material type 1

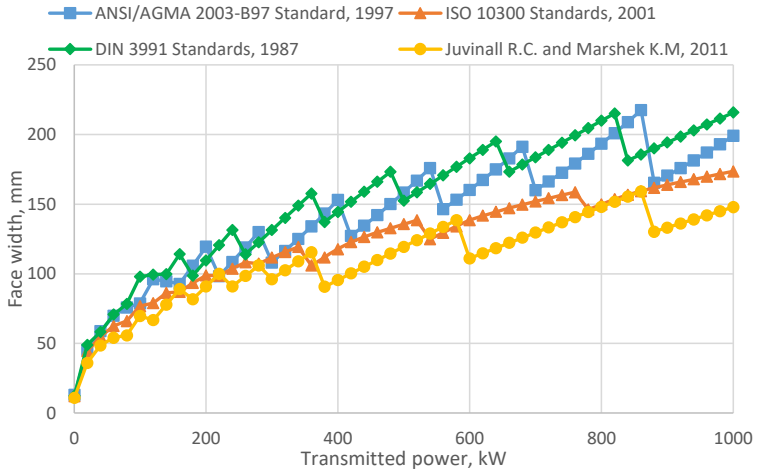

Figure 4.14. Face width values under various transmitted power at 7:1 speed ratio for α_n=20° and material type 1

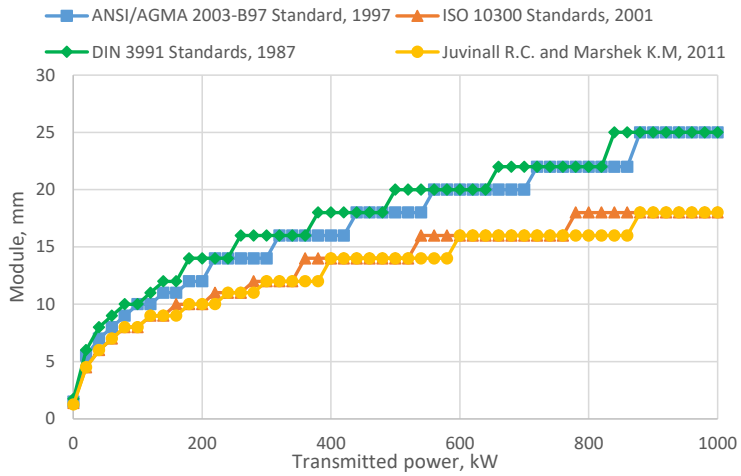

Figure 4.15. Module values under various transmitted power at 8:1 speed ratio for α_n=20° and material type 1

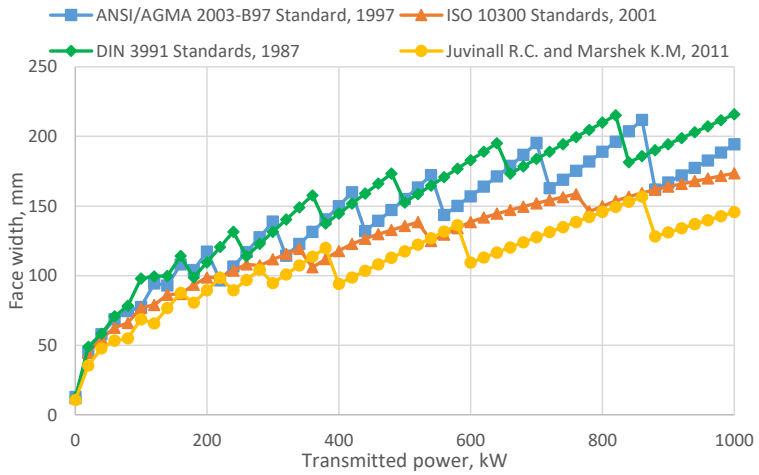

Figure 4.16. Face width values under various transmitted power at 8:1 speed ratio for α_n=20° and material type 1

As seen in Figure 4.1 to Figure 4.16, all approaches in 1:1 speed ratio gave the maximum module and minimum face widths.

The same trend can also be seen from the given module and face width figures (4.1 to 4.16) for all speed ratios. As the speed ratio increased (1:1 to 1:8), It

was observed that while the speed ratio increased, the module decreased for each design approach, while the face width increased. At speed ratios from 6:1 to 8:1, the module and face width values are almost the same. In these figures, the maximum results of module and face widths have been given by ANSI/AGMA 2003-B97 standard for 1:1, 2:1, 3:1 speed ratio. Between 4:1 and 8:1 speed ratio, AGMA and DIN approach, gave similar results for the module and face width values, and these values are the highest.

4.1.2. Comparison of the Module Results Considering Speed Ratio for the Selected Power Transmissions

In the graphics given in this section, the effect of speed ratio for the selected power transmissions on the module is examined, and its general trend is found. Table 4.3 gives locations of the obtained results in this work.

Related graphics for comparison of face width and module results are giving Appendix A.2 for type 2 material and twenty-degree pressure angle, Appendix B.2 for type 2 material and twenty-degree pressure angle, Appendix C.2 for type 1 material and twenty-five-degree pressure angle, D.2 for type 2 material and twenty-five-degree pressure angle, E.2 for type 3 material and twenty-five-degree pressure angle.

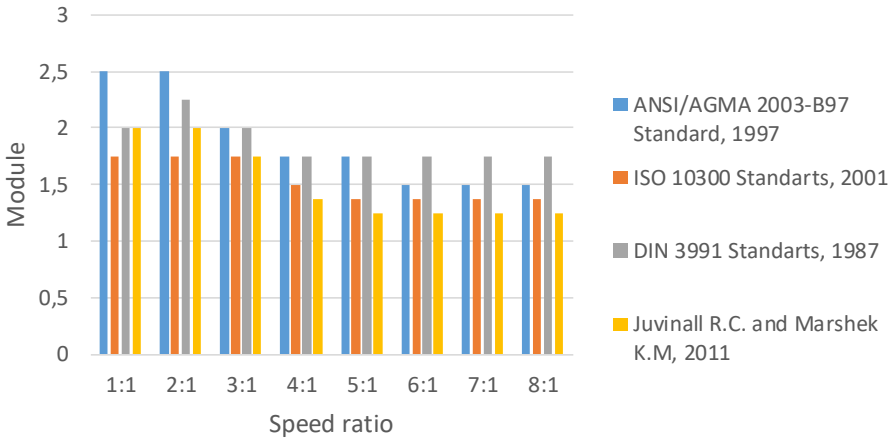

Figure 4.17. The speed ratio effect on the module at 0,5 kW power transmission for α_n=20° and material type 1

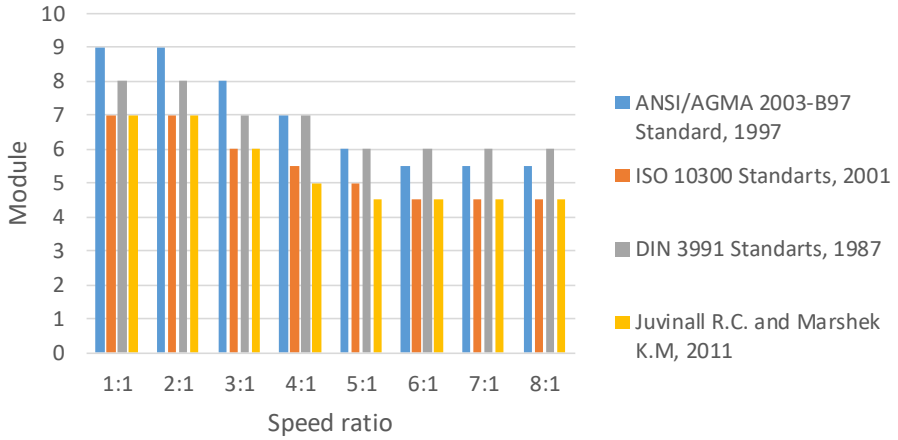

Figure 4.18. The speed ratio effect on the module at 20 kW power transmission for α_n=20° and material type 1

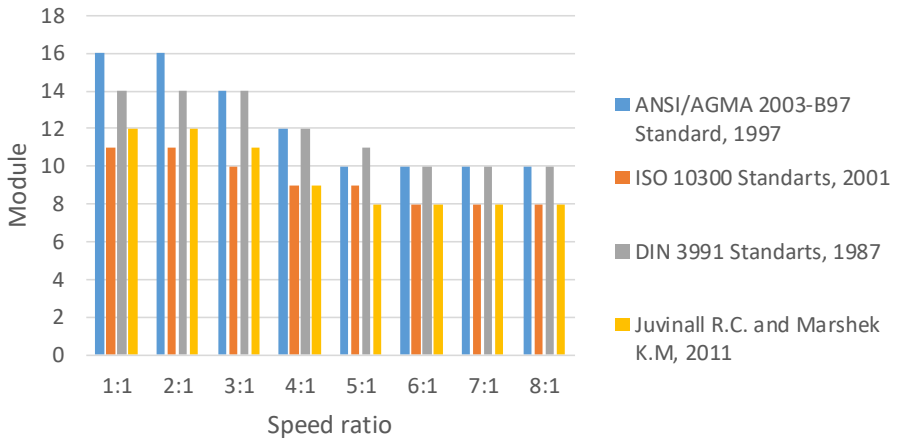

Figure 4.19. The speed ratio effect on the module at 100 kW power transmission for α_n=20° and material type 1

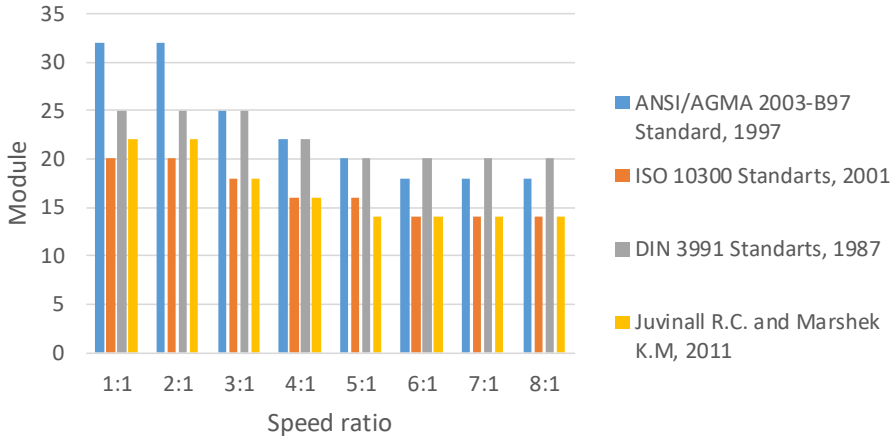

Figure 4.20. The speed ratio effect on the module at 500 kW power transmission for α_n=20° and material type 1

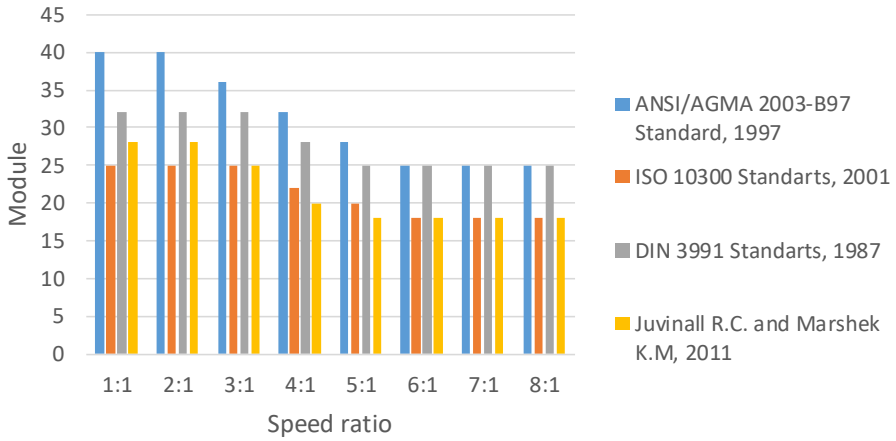

Figure 4.21. The speed ratio effect on the module at 1000 kW power transmission for α_n=20° and material type 1

The above graphs were examined, and the following results were obtained.

DIN Standard gives the highest module when the speed ratio is 2:1 at 0.5 kW transmitted power value. DIN standard gives the same and highest module value in 1:1 and 2:1 speed ratio in other selected speed ratios.

For the other technical standards, the module values remain the same at 1:1

and 2:1 speed ratio. In addition, the highest module value among the selected speed ratios is in these two speed ratios.

The module value decreases when the speed ratio increases from 2:1 to 6:1 for each standard, while the module remains constant at speed ratios from 6:1 to 8:1.

4.2. Comparisons of Analytical and Numerical solutions of Gear Tooth Bending Stresses

Comparing analytical and numerical solutions is a parameter that shows the accuracy of the design. As mentioned in section 3.2.5, the module and face width results obtained by the approaches, numerical values for 3:1 speed ratio and 100 kW transmitted power are obtained using ANSYS software. Following major steps and boundaries are involved in pre-processing stage in ANSYS Workbench 18.1. Boundary conditions are;

- Fixed support is defined to shaft contact surface of pinion and
- Frictionless support is defined to lateral surface of pinion (see Figure 4.23).

Major steps are;

- Material properties are defined in Workbench 18.1 according to material type 1, data taken from Table 3.1.
- Resultant Force are applied on pitch line of pinion teeth as shown in Figure 4.22.

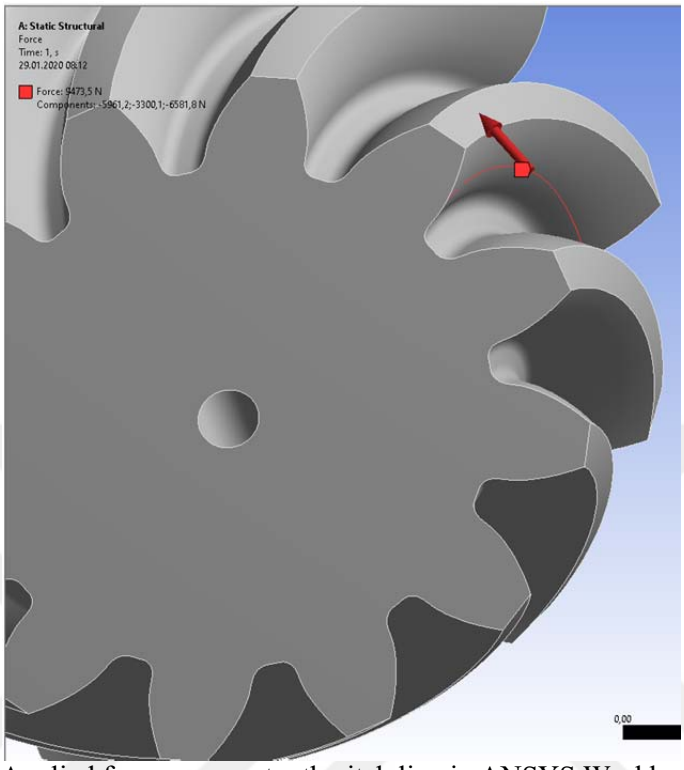

Figure 4.22. Applied force on gear tooth pitch line in ANSYS Workbench 18.1

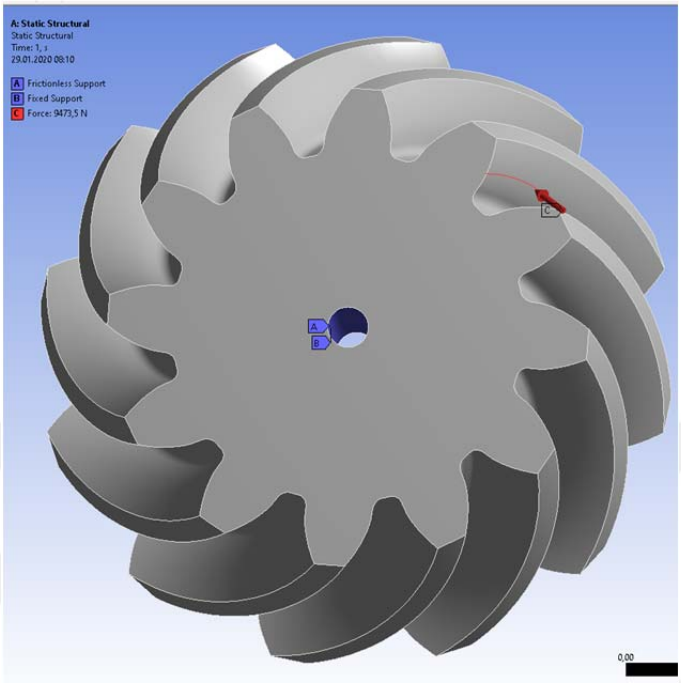

Figure 4.23. Pre-processing step in ANSYS Workbench 18.1

3D body of pinion is meshed with 2 mm triangle mesh size given in Figure 4.24.

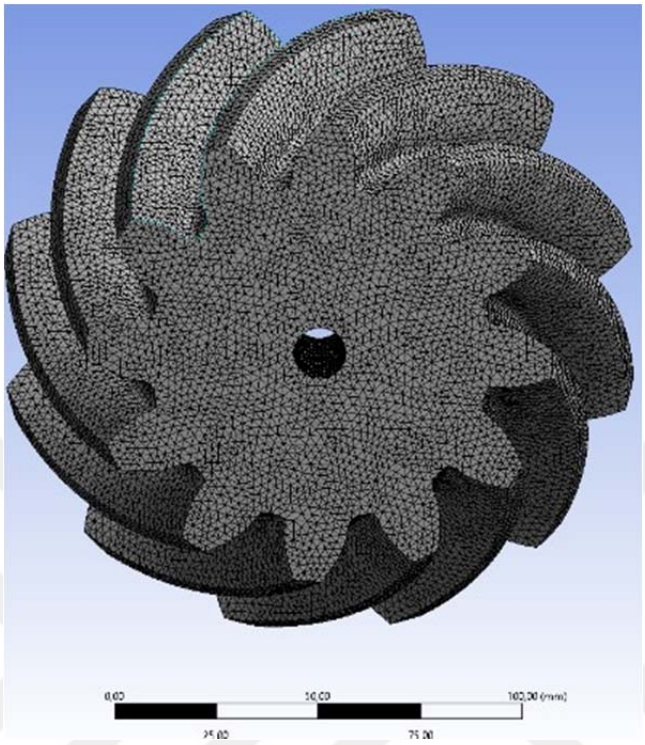

Figure 4.24. Meshing of body in pre-processing steps in ANSYS Workbench 18.1

In Figure 4.25, the result of bending stress distribution is exhibited along the gear tooth root according to Finite Element Analysis (FEA) is shown.

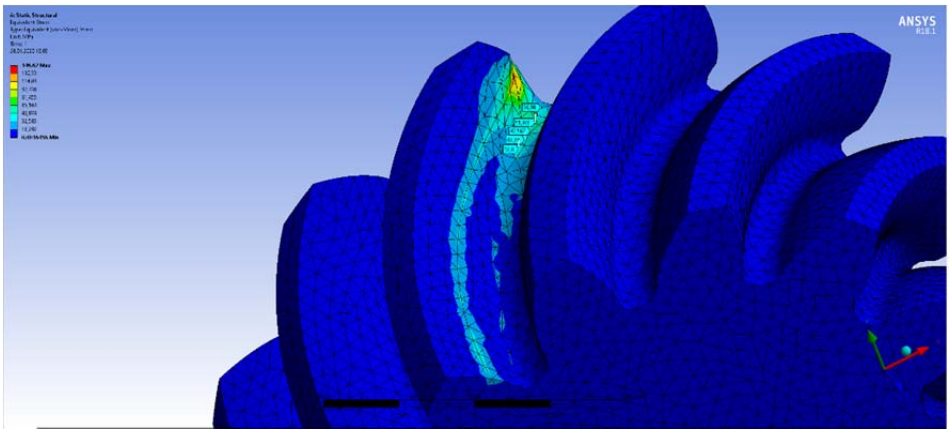

Figure 4.25. Numerical Von Mises stress results in ANSYS Workbench 18.1

Module and face width results are found analytically using the technical standards and machine elements textbooks. The results are numerically solved with ANYSY Workbench 18.1 software. The reliability of each analytical design approach is verified by comparing analytical and numerical results. The results are provided in Table 4.2 and Table 4.3. It is observed that the numerical results are higher than analytical results.

Table 4.2. Comparison of tooth bending stresses obtained from the analytical approaches and numerical method for α_n=20° and Type 1.

Design Approaches	**ANSI/AGMA 2003-B97 Standards**	**DIN 3991 Standard**	**ISO 10300 Standards**	**Juvinall R.C. and Marshek K.M.**
Module (mm)	14	14	10	11
Face Width (mm)	63,668	54,215	54,636	55,566
Number of Pinion	12	12	12	12
Tangential Force (kN)	9,474	9, 474	13,263	12,057
Analytical (MPa)	38,779	56,962	69,092	112.52
Numerical (MPa)	42,317	63,165	72,328	93,278
Difference (%)	9,123	10,89	4,68	17,11

Table 4.3. Comparison of tooth bending stresses obtained from the analytical approaches and numerical method for α_n=25° and Type 1.

Design Approaches	**ANSI/AGMA 2003 B97 Standards**	**DIN 3991 Standard**	**ISO 10300 Standards**	**Juvinall R.C. and Marshek K.M.**
Module (mm)	12	14	10	10
Face Width (mm)	66,314	58,467	54,36	53,162
Number of Pinion	12	12	12	12
Tangential Force (kN)	11,052	9,474	13,263	13,263
Analytical (MPa)	38,745	56,962	69,087	112.52
Numerical (MPa)	36,141	57,317	71,861	99,345
Difference (%)	6,72	0,623	4,015	11,71

The error rate between numerical and analytical values shown in Tables 4.4 and 4.5 showed that it is at most around 10%. This error rate indicates that the analytical values of the design are of sufficient accuracy.

4.3. Obtaining Geometric Rating Numbers (GRi) for All Design Approaches

In this section, GR_i values are provided considering the reference approach (AGMA) and using the formula given in Section 3.2.3.

Comparison of Geometric rating numbers (GR_i) results that are obtained by using all design approaches are presented by preparing radar charts. The charts are plotted and presented for the 1:1 to 1:8 speed ratios for the transmitted power values. With the radar charts, the ratio of each approach to the AGMA approach can be examined under a single graph. The locations of the GR_i results for all the design approaches are given in Table 4.6.

Figures in between 4.26 to 4.33 show that the trend for all approaches are very similar with excellent continuity of the results for the design approaches 20° pressure angle and material type 1. As a result of this, ranking can be achieved for ANSI/AGMA 2003-B97 standard, ISO Standards 10300 standards, Juvinall R.C., Marshek K.M., and DIN 3991 standards approach ratings.

Related graphics for comparison of face width and module results are giving Appendix A.2 for type 2 material and twenty-degree pressure angle, Appendix B.2 for type 2 material and twenty-degree pressure angle, Appendix C.2 for type 1 material and twenty-five-degree pressure angle, D.2 for type 2 material and twenty-five-degree pressure angle, E.2 for type 3 material and twenty-five-degree pressure angle.

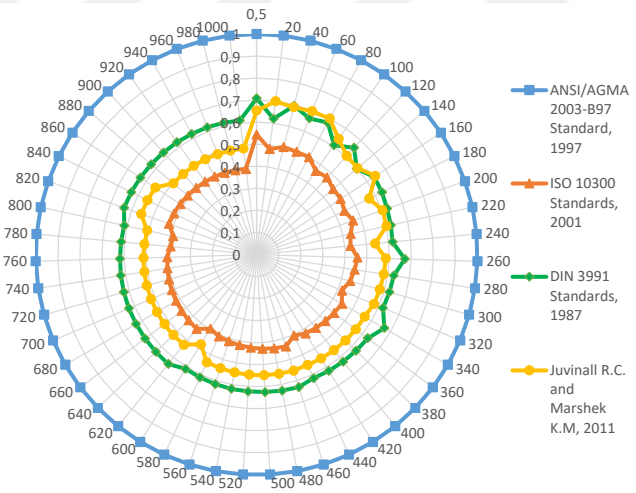

Figure 4.26. Results of GR_i for all approaches at 1:1 speed ratio for α_n=20° and material type 1

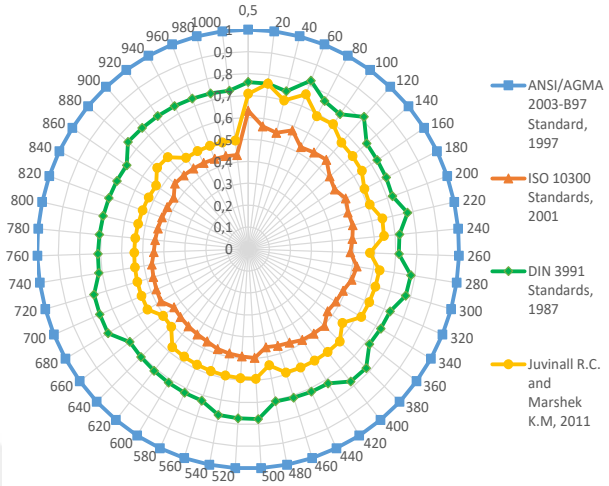

Figure 4.27. Results of GR_i for all approaches at 2:1 speed ratio for α_n=20° and material type 1

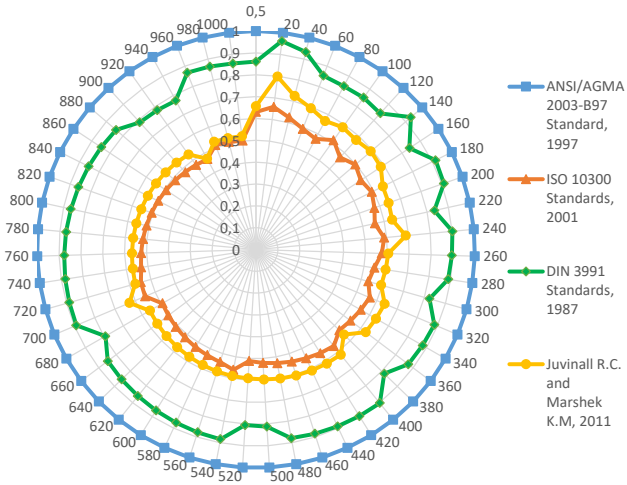

Figure 4.28. Results of GR_i for all approaches at 3:1 speed ratio for α_n=20° and material type 1

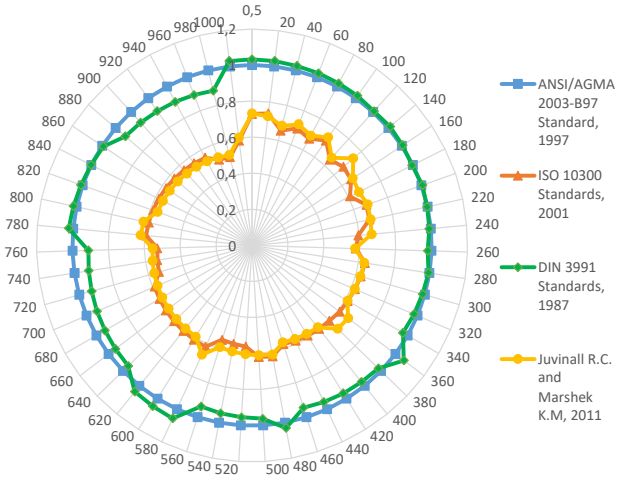

Figure 4.29. Results of GR_i for all approaches at 4:1 speed ratio for α_n=20° and material type 1

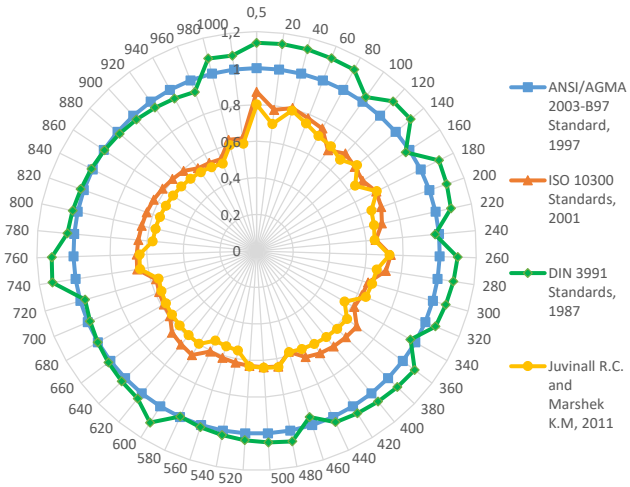

Figure 4.30. Results of GR_i for all approaches at 5:1 speed ratio for α_n=20° and material type 1

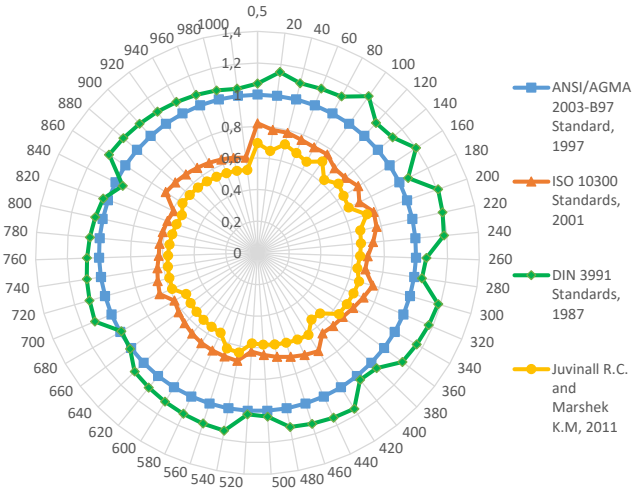

Figure 4.31. Results of GR_i for all approaches at 6:1 speed ratio for α_n=20° and material type 1

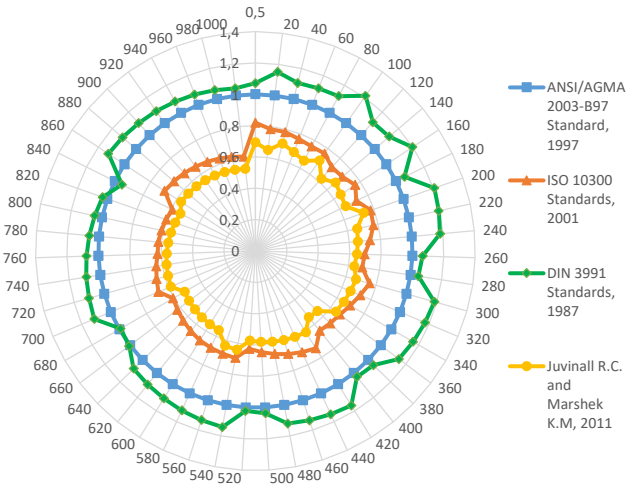

Figure 4.32. Results of GR_i for all approaches at 7:1 speed ratio for α_n=20° and material type 1

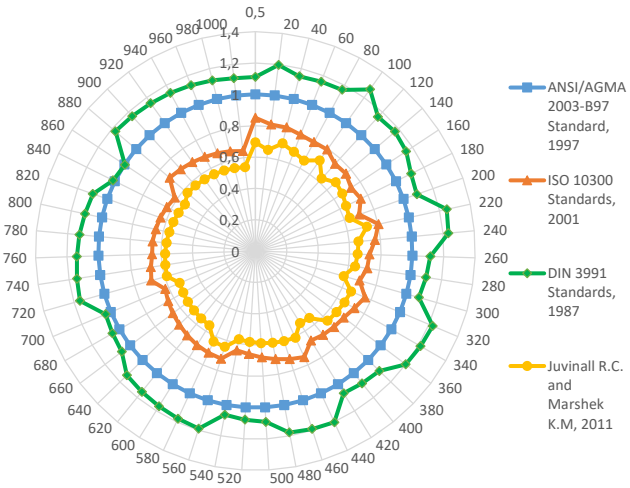

Figure 4.33. Results of GR_i for all approaches at 8:1 speed ratio for α_n=20° and material type 1

Mean GR_i numbers for various design approaches for each speed ratio with 20° and 25° pressure angle, respectively, are given in Table 4.4 and Table 4.5.

Table 4.4. Mean GR_i results for all design approaches and each speed ratio with $\alpha_n = 20^o$

α_n=20°	Material Type 1			Material Type 2			Material Type 3		
Speed ratio	ISO	DIN	J&M	ISO	DIN	J&M	ISO	DIN	J&M
1:1	0,432	0,631	0,558	0,381	0,614	0,558	0,381	0,598	0,558
2:1	0,483	0,739	0,590	0,361	0,624	0,505	0,351	0,521	0,505
3:1	0,542	0,865	0,603	0,407	0,728	0,460	0,396	0,608	0,376
4:1	0,605	0,980	0,614	0,454	0,832	0,466	0,442	0,693	0,367
5:1	0,656	1,045	0,619	0,487	0,883	0,465	0,474	0,736	0,368
6:1	0,686	1,101	0,601	0,515	0,942	0,458	0,501	0,786	0,360
7:1	0,700	1,124	0,605	0,524	0,958	0,459	0,509	0,800	0,361
8:1	0,707	1,137	0,603	0,531	0,971	0,459	0,516	0,810	0,361
Average	0,601	0,953	0,599	0,458	0,819	0,479	0,446	0,694	0,407
Std.	0,105	0,190	0,019	0,067	0,146	0,036	0,064	0,108	0,078

Table 4.5. Mean GR_i results for all design approaches and each speed ratio with $\alpha_n = 25^o$

α_n=25°	Material Type 1			Material Type 2			Material Type 3		
Speed ratio	ISO	DIN	J&M	ISO	DIN	J&M	ISO	DIN	J&M
1:1	0,575	0,793	0,540	0,507	0,654	0,540	0,507	0,654	0,540
2:1	0,603	0,936	0,595	0,449	0,780	0,497	0,436	0,647	0,497
3:1	0,656	1,103	0,622	0,487	0,918	0,467	0,473	0,767	0,383
4:1	0,716	1,227	0,632	0,533	1,038	0,478	0,518	0,860	0,375
5:1	0,766	1,308	0,630	0,568	1,098	0,475	0,551	0,915	0,375
6:1	0,784	1,326	0,612	0,590	1,134	0,468	0,574	0,943	0,369
7:1	0,809	1,370	0,616	0,607	1,167	0,468	0,591	0,970	0,368
8:1	0,825	1,399	0,619	0,620	1,193	0,473	0,604	0,992	0,370
Average	0,717	1,183	0,608	0,545	0,998	0,483	0,532	0,844	0,410
Std.	0,095	0,220	0,030	0,061	0,196	0,025	0,059	0,138	0,068

It was seen in Tables 4.4 and 4.5 that high standard deviation values depending on speed ratio shows that a ratio cannot be established with average values, so conversion formulas should be obtained using polynomial equations.

The average speed ratio values from 1:1 to 1:8 given in Table 4.5. and the mean GR_i values for each approach, all type of materials and all pressure angles are given in Table 4.6.

Table 4.6. Mean GR_i numbers for all design approaches, all type of materials and all pressure angles

Design approaches	$\alpha_n = 20^o$			$\alpha_n = 25^o$		
	Type 1	Type 2	Type 3	Type 1	Type 2	Type 3
ISO	0,601	0,458	0,446	0,717	0,545	0,532
DIN	0,953	0,819	0,694	1,183	0,998	0,992
J&M	0,599	0,479	0,407	0,608	0,483	0,410
ANSI/AGMA	1.000	1.000	1.000	1.000	1.000	1.000

Considering the 20° pressure angle, the mean GR_i values are as follows from the largest to the smallest.

For Type 1: AGMA > DIN > ISO > J&M;

For Type 2: AGMA > DIN > J&M >ISO;

For Type 3: AGMA > DIN > ISO > J&M.

The same study has been carried out for 25° pressure angle. The mean GR_i values are as follows from the largest to the smallest.

For Type 1: DIN > AGMA > ISO > J&M;

For Type 2: AGMA > DIN > ISO > J&M;

For Type 3: AGMA > DIN > ISO > J&M.

As a result, although the ISO approach gives the lowest mean GR_i for twenty degrees of pressure angle and material type 2, the J&M approach gives the lowest mean GR_i for each material at 20° pressure angle for material type 1 and 3,

and each material at 25^{o} degrees of pressure angle. AGMA approach gives the highest GR_i except for the type 1 and pressure angle 20^{o}

4.4. Obtaining AGMA Conversion Factors (CFs) for Module and Face Width

The results obtained from the conversion factors and standard deviations of the conversion factors using the formulas given in Section 3.2.4 are given in Table 4.7 for material type 1 and 20° pressure angle and Table 4.10 for material type 1 and 25° pressure angle.

Standard deviations values for module ($\sigma_{\overline{CF}_{mi}}$) and for face widths ($\sigma_{\overline{CF}_{Fi}}$) given in Table 4.7 for material type 1 and 20° pressure angle and Table 4.10 for material type 1 and 25° pressure angle. It shows that the module and face width results obtained from the design approaches (ISO, DIN, J&M) can be converted to AGMA standard approach with a reasonable error at the selected speed ratios from 1:1 to 8:1 and selected transmitted power from 0.5 kW and 1000 kW. Correlation polynomial up to fourth-order (C_p) expressions were obtained and given in Table 4.7 for material type 1 and 20° pressure angle and Table in 4.10 for material type 1 and 25° pressure angle.

Table 4.7. Conversion factors for module and face width for $\alpha_n = 20°$, material type 1

From Design approaches to AGMA		From ISO to AGMA				From DIN to AGMA				From J&M to AGMA			
$\mathbf{m_G}$	N_p	$\overline{CF_m}$	$\sigma_{\overline{CF_m}}$	$\overline{CF_F}$	$\sigma_{\overline{CF_F}}$	$\overline{CF_m}$	$\sigma_{\overline{CF_m}}$	$\overline{CF_F}$	$\sigma_{\overline{CF_F}}$	$\overline{CF_m}$	$\sigma_{\overline{CF_m}}$	$\overline{CF_F}$	$\sigma_{\overline{CF_F}}$
1:1	17	0,649	0,039	0,667	0,052	0,791	0,031	0,799	0,050	0,712	0,040	0,786	0,078
2:1	13	0,676	0,047	0,716	0,070	0,850	0,049	0,874	0,082	0,725	0,047	0,815	0,081
3:1	12	0,723	0,049	0,751	0,053	0,920	0,053	0,944	0,085	0,733	0,049	0,824	0,073
4:1	12	0,771	0,051	0,787	0,078	0,976	0,046	1,008	0,087	0,741	0,053	0,831	0,091
5:1	12	0,785	0,051	0,839	0,102	1,002	0,054	1,048	0,097	0,743	0,049	0,836	0,108
6:1	12	0,791	0,055	0,869	0,077	1,041	0,060	1,063	0,097	0,775	0,054	0,778	0,077
7:1	12	0,797	0,055	0,880	0,077	1,049	0,064	1,077	0,106	0,774	0,053	0,784	0,078
8:1	12	0,804	0,057	0,882	0,077	1,058	0,064	1,080	0,107	0,778	0,055	0,778	0,077

Table 4.8. Conversion factors for face width and module at any speed ratio for $\alpha_n = 20^o$, material type 1

	From design approach to AGMA	C_p Expressions for Module (m_i) (to AGMA) regressions for $\overline{CF_{mi}}$	R^2
1kW - 1000kW	ISO to AGMA	$\overline{CF_{m.I-A}}$ =-0,0041m_G^2+0,0592m_G+0,5865	0.99
	DIN to AGMA	$\overline{CF_{m.D-A}}$ =-0,0055m_G^2+0,0885m_G+0,7038	0.98
	J&M to AGMA	$\overline{CF_{m.J-A}}$ =-0,0001m_G^2+0,011m_G+0,7009	0.94
	C_p Expressions for Face Width (F) (to AGMA) regressions for $\overline{CF_{Fi}}$		
1kW - 1000kW	ISO to AGMA	$\overline{CF_{F.I-A}}$ =-0,0033m_G^2+0,0619m_G+0,6036	0.99
	DIN to AGMA	$\overline{CF_{F.D-A}}$ =-0,0071m_G^2+0,1043m_G+0,6988	0.99
	J&M to AGMA	$\overline{CF_{F.J-A}}$ =0,0003m_G^4-0,0051m_G^3+0,0197m_G^2-0,0041m_G+0,7758	0.84

Table 4.9. Conversion factors and their corresponding standard deviations for module and face width for $\alpha_n = 25^o$, material type 1

From Design approaches to AGMA		From ISO to AGMA				From DIN to AGMA				From J&M to AGMA			
m_G	N_p	$\overline{CF_m}$	$\sigma_{\overline{CF_m}}$	$\overline{CF_F}$	$\sigma_{\overline{CF_F}}$	$\overline{CF_m}$	$\sigma_{\overline{CF_m}}$	$\overline{CF_F}$	$\sigma_{\overline{CF_F}}$	$\overline{CF_m}$	$\sigma_{\overline{CF_m}}$	$\overline{CF_F}$	$\sigma_{\overline{CF_F}}$
1:1	13	0,741	0,043	0,778	0,062	0,879	0,030	0,904	0,049	0,710	0,044	0,762	0,080
2:1	12	0,758	0,050	0,799	0,072	0,956	0,056	0,984	0,094	0,735	0,051	0,812	0,080
3:1	12	0,792	0,056	0,831	0,066	1,034	0,057	1,072	0,092	0,741	0,044	0,841	0,071
4:1	12	0,837	0,047	0,857	0,079	1,099	0,058	1,122	0,107	0,748	0,045	0,847	0,091
5:1	12	0,863	0,052	0,891	0,085	1,121	0,049	1,170	0,089	0,759	0,054	0,835	0,097
6:1	12	0,861	0,057	0,914	0,089	1,140	0,051	1,167	0,088	0,784	0,052	0,783	0,088
7:1	12	0,873	0,054	0,929	0,080	1,156	0,059	1,189	0,099	0,781	0,052	0,792	0,085
8:1	12	0,882	0,052	0,938	0,085	1,169	0,064	1,202	0,114	0,781	0,048	0,797	0,095

Table 4.10. Conversion factors for face width and module (irrespective of speed ratio) at any speed ratio for $\alpha_n = 25^o$, material type 1

	From design approach to AGMA	C_p Expressions for Module (m_i) (to AGMA) regressions for $\overline{CF_{mi}}$	R^2
1kW - 1000kW	ISO to AGMA	$\overline{CF_{m.\mathrm{I}-A}}$ = -0,0028m_G^2+0,0466m_G+0,6876	0.97
	DIN to AGMA	$\overline{CF_{m.\mathrm{D}-A}}$ =0,0006m_G^3-0,0146m_G^2+ 0,132m_G+0,756	0.99
	J&M to AGMA	$\overline{CF_{m.J-A}}$ = -0,001m_G^2+0,0189m_G++0,694	0.95
C_p Expressions for Face Width (F) **(to AGMA) regressions for $\overline{CF_{Fi}}$**			
1kW - 1000kW	ISO to AGMA	$\overline{CF_{F.\mathrm{I}-A}}$ =-0,0014m_G^2+0,036m_G+0,7365	0.99
	DIN to AGMA	$\overline{CF_{F.\mathrm{D}-A}}$ = -0,0075m_G^2+ 0,1084m_G+ 0,8043	0.99
	J&M to AGMA	$\overline{CF_{F.J-A}}$ =0,0003m_G^4-0,0037m_G^3+0,0032m_G^2+0,0632m_G+0,6984	0.93

The conversion factor differences for 20° and 25° pressure angles are given in Table 4.11 for module and in Table 4.12 and for face width to find the correlation for pressure angles. DIN approaches with the highest CFs values and J&M approaches to the smallest CFs values are given in Figure 4.34 to understand the effect of pressure angle on CFs easly. The tables and figures show that differences in conversion factors caused by different pressure are at most 14,267 and at least 0,282. Since conversion factor values are different in pressure angle, different formulas are needed for each pressure angle.

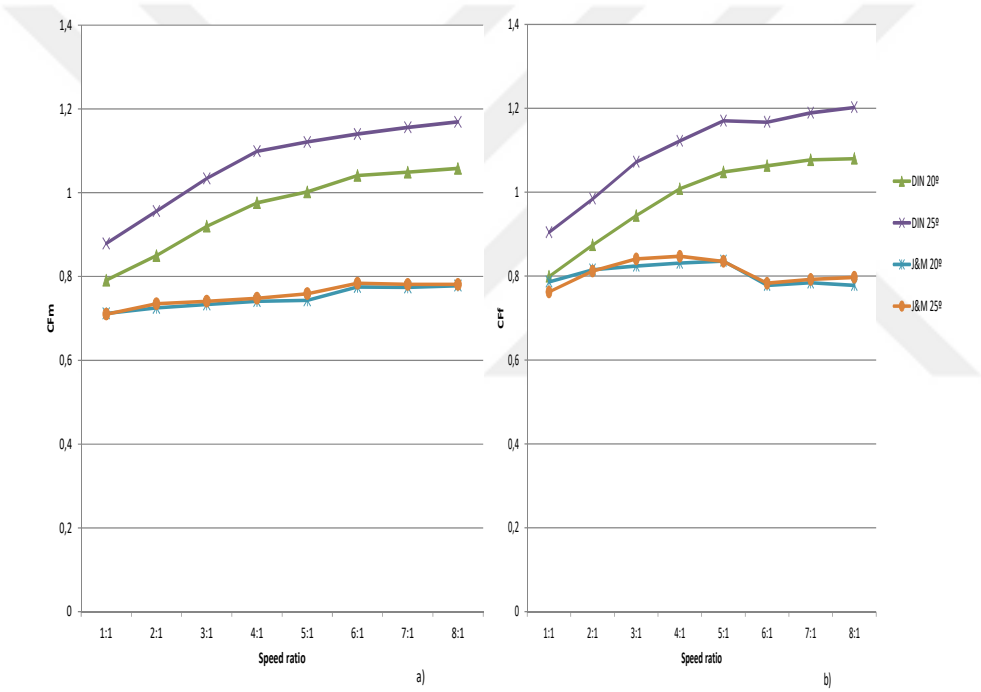

Figure 4.34. The effect of pressure angle on CFs values depending on speed ratios, $a) CF_m$, $b) CF_F$

Table 4.11. Module conversion factor differences between pressure angles of α_n=20° and α_n=25°

Speed ratio	From ISO to AGMA			From DIN to AGMA			From J&M to AGMA		
	$\overline{CF_m}$, α_n=20°	$\overline{CF_m}$, α_n=25°	Difference (%)	$\overline{CF_m}$, α_n=20°	$\overline{CF_m}$, α_n=25°	Difference (%)	$\overline{CF_m}$, α_n=20°	$\overline{CF_m}$, α_n=25°	Difference (%)
1:1	0,649	0,741	12,416	0,791	0,879	10,011	0,712	0,710	-0,282
2:1	0,676	0,758	10,818	0,850	0,956	11,088	0,725	0,735	1,361
3:1	0,723	0,792	8,712	0,920	1,034	11,025	0,733	0,741	1,080
4:1	0,771	0,837	7,885	0,976	1,099	11,192	0,741	0,748	0,936
5:1	0,785	0,863	9,038	1,002	1,121	10,616	0,743	0,759	2,108
6:1	0,791	0,861	8,130	1,041	1,140	8,684	0,775	0,784	1,148
7:1	0,797	0,873	8,706	1,049	1,156	9,256	0,774	0,781	0,896
8:1	0,804	0,882	8,844	1,058	1,169	9,495	0,778	0,781	0,384

Table 4.12. Face width conversion factor differences between pressure angles of α_n=20° and α_n=25°

Speed ratio	From ISO to AGMA			From DIN to AGMA			From J&M to AGMA		
	$\overline{CF}_F$, α_n=20°	$\overline{CF}_F$, α_n=25°	Difference (%)	$\overline{CF}_F$, α_n=20°	$\overline{CF}_F$, α_n=25°	Difference (%)	$\overline{CF}_F$, α_n=20°	$\overline{CF}_F$, α_n=25°	Difference (%)
1:1	0,667	0,778	14,267	0,799	0,904	11,615	0,786	0,762	-3,150
2:1	0,716	0,799	10,388	0,874	0,984	11,179	0,815	0,812	-0,369
3:1	0,751	0,831	9,627	0,944	1,072	11,940	0,824	0,841	2,021
4:1	0,787	0,857	8,168	1,008	1,122	10,160	0,831	0,847	1,889
5:1	0,839	0,891	5,836	1,048	1,170	10,427	0,836	0,835	-0,120
6:1	0,869	0,914	4,923	1,063	1,167	8,912	0,778	0,783	0,639
7:1	0,880	0,929	5,274	1,077	1,189	9,420	0,784	0,792	1,010
8:1	0,882	0,938	5,970	1,080	1,202	10,150	0,778	0,797	2,384

Finally, the verification of design results was performed by using the module and face width values we obtained with bending fatigue failure formulas in surface contact failure formulas. And the verification results for 20° and 25° pressure angles and material type 1 are given in tables between Table 4.13 and Table 4.16 below;

Table 4.13. Verifying safety factor for contact stress (S_H) results based on AGMA 2003-B97, 1997 Standard for α_n=20° and α_n=25°

	α_n =20°				α_n =25°			
Power (kW)	Module (m)	Face width (F)	Safety factor (S_H)	Result of design	Module (m)	Face width (F)	Safety factor (S_H)	Result of design
0,5	2,5	7,633	0,8711	not safe	2,75	6,901	0,9084	not safe
20	9	28,884	0,987	not safe	10	25,717	1,0158	safe
100	16	54,157	1,143	safe	18	47,386	1,168	safe
500	32	92,378	1,418	safe	36	81	1,453	safe
1000	40	135,6	1,566	safe	45	121,6	1,684	safe

Table 4.14. Verifying safety factor for contact stress (S_H) results based on Juvinall R.C., Marshek K.M. for α_n=20° and α_n=25°

	α_n =20°				α_n =25°			
Power (kW)	Module (m)	Face width (F)	Safety factor (S_H)	Result of design	Module (m)	Face width (F)	Safety factor (S_H)	Result of design
0,5	2	6,23	0,613	not safe	2,25	5,373	0,43	not safe
20	7	24,47	0,645	not safe	8	21,668	0,652	not safe
100	12	46,431	0,665	not safe	14	37,132	0,651	not safe
500	22	73	0,662	not safe	25	61,815	0,649	not safe
1000	28	93	0,662	not safe	32	77,6	0,648	not safe

Table 4.15. Verifying safety factor for contact stress (S_H) results based on DIN 3991, 1987 Standards for α_n=20° and α_n=25°

	α_n =20°				α_n =25°			
Power (kW)	Module (m)	Face width (F)	Safety factor (S_H)	Result of design	Module (m)	Face width (F)	Safety factor (S_H)	Result of design
0,5	2	6,758	0,321	not safe	2,5	6,27	0,389	not safe
20	7	24,028	0,303	not safe	9	23,009	0,4015	not safe
100	14	37,564	0,2174	not safe	16	42,035	0,451	not safe
500	25	73,974	0,223	not safe	32	72,164	0,488	not safe
1000	32	130,8	0,257	not safe	40	106,5	0,507	not safe

Table 4.16. Verifying safety factor for contact stress (S_H) results based on ISO 10300, 2001 Standards for α_n=20° and α_n=25°

	α_n =20°				α_n =25°			
Power (kW)	Module (m)	Face width (F)	Safety factor (S_H)	Result of design	Module (m)	Face width (F)	Safety factor (S_H)	Result of design
0,5	1,75	7,682	1,122	safe	2,25	5,879	0,715	not safe
20	6	28,244	1,154	safe	8	20,939	0,728	not safe
100	10	52,515	1,2124	safe	14	37,139	0,744	not safe
500	18	91,198	1,221	safe	25	66,571	0,772	not safe
1000	25	107,7	1,186	safe	32	87,1	0,794	not safe

4.5. Case Studies: Testing the Confirmability of CFs

In this section, randomly selected speed ratio and power transmitted values are used to testing confirmability of the conversion factors obtained using Table 4.9 for twenty degrees pressure angle and Table 4.10 for twenty-five pressure angle. Module (m_i) and face width (F_i) values are obtained for the selected power and speed ratios. The values obtained are converted to m_{AGMA} and F_{AGMA} by conversion factors ($\overline{CF}_{mi}$ and $\overline{CF}_{Fi}$). The gear volume errors (GV_e) are calculated and the results are given in Table 4.17 for material type 1 and 20° pressure angle, and in Table 4.18 for material type 1 and 25° pressure angle.

Table 4.17. Validating and proving conversion factors with the percentage errors in the range of 0,5 kW to 1000 kW (α_n =20°, Material type 1)

Case: Design approach, m (speed ratio), Power (kW)	m_i	F_i	m_{AGMA}	F_{AGMA}	mF_{AGMA}	m_i and F_i converted to $m_{c,AGMA}$ and $F_{c,AGMA}$							
						$\overline{CF}_{mi}$	$m_{c,AGMA}$	$\frac{m_i}{}$ Error (%)	$\overline{CF}_{Fi}$	$F_{c,AGMA}$	$\frac{F_i}{}$ Error (%)	$(mx F)_{c,AGMA}$	GV_e (%)
ISO (2.4:1) 100 kW	11	48,49	16	63,668	1018,69	0,705	7,093	-2,477	0,733	0,733	3,885	1018,688	1,312
ISO (5.4: 1) 375 kW	14	110,35	16	151,13	2418,1	0,787	15,604	11,235	0,842	0,842	-13,244	2333,517	-3,498
J&M (1.8:1) 5 kW	4,5	15,132	5,5	18,9	103,96	0,720	6,247	13,577	0,806	18,782	-0,623	117,3278	12,859
J&M (3.2:1) 185 kW	14	63,655	16	94,682	1514,9	0,735	20,586	28,660	0,829	0,829	-18,877	1581,153	4,373
DIN (4.4:1) 465 kW	20	141,591	20	143,354	2867,1	0,987	20,269	1,346	138,779	1,048	-3,192	2812,931	-1,89
DIN (6.6:1) 870 kW	25	187,857	25	164,249	4106,2	1,020	23,848	-4,609	174,28	1,078	6,107	4156,171	1,217

Table 4.18. Validating and proving conversion factors with the percentage errors in the range of 0.5 kW to 1000 kW (α_n =25°, Material type 1)

Case: Design approach, m (speed ratio), Power (kW)	m_i	F_i	m_{AGMA}	F_{AGMA}	mF_{AGMA}	mi and Fi converted to mc, AGMA, and Fc, AGMA							
						$\overline{CF}_{mi}$	$m_{c,AGMA}$	m_i Error (%)	$\overline{CF}_{Fi}$	$F_{c,AGMA}$	F_i Error (%)	$(mx F)_{c,AGMA}$	GV_e (%)
ISO (2.4:1) 100 kW	11	49,547	14	57,052	798,723	0,783	14,043	0,307	0,815	60,806	6,581	853,8962	6,908
ISO (5.4:375) 80 kW	14	109,066	16	121,204	1939,3	0,858	16,325	2,030	0,890	122,536	1,099	2000,367	3,149
J&M (1.8:1) 5 kW	4,5	13,464	5	18,602	93,011	0,725	6,209	24,176	0,804	16,744	-9,986	103,9619	11,774
J&M (3.2:1) 185 kW	12	67,138	16	72,95	1167,2	0,744	16,124	0,774	0,844	79,583	9,092	1283,181	9,937
DIN (4.4:1) 465 kW	20	151,51	18	136,042	2448,8	1,105	18,095	0,530	1,136	133,364	-1,969	2413,264	-1,451
DIN (6.6:1) 870 kW	25	201,22	22	171,187	3776,1	1,164	21,483	-2,351	1,193	168,662	-1,475	3623,323	-4,046

The maximum GV_e values are 12,859 for material type 1 and 20° pressure angle and 11,774 for material type 1 and 20° pressure angle. These values are for 5 kW power transmission value, 1.8 speed ratio and J&M design approach. The reason for this is that it will peak between 0.5 kW and 20 kW as can be seen in the GRi tables in Section 4.3. Looking at other case studies, the error is less than %10. Lower than %10 error is reasonable to provides the confirmability of CFs.

5. CONCLUSION

This thesis provides the need to select and use appropriate spiral bevel gear design approaches that include all designers, from students who have just begun to gear design to designers who have been engaged in gear design for a long time. The selected approaches are DIN 3991, 1987 (German Institute of Standardization), ANSI/AGMA 2003-B97, 1997 (American Gear Manufacturers Associations), ISO 10300, 2001 (International Organization for Standardization) standards, and machine element textbooks (Fundamental of Machine Component Design 5th Edition, Juvinall R.C. and Marshek K.M., 2011 and Shigley's Mechanical Engineering Design 9th Edition (SI), Budynas R.G. and Nisbett J.K., 2011).

Design of gears using ISO, DIN, and ANSI/AGMA Standards take more design time since they have more complex formulations than those that are available in machine element textbooks (Fundamental of Machine Component Design 5th Edition, Juvinall R.C. and Marshek K.M., 2011). Therefore, conversion factors have been developed to convert the results obtained from the machine element textbook into the standard approaches. Conversion factors will enable relatively complicated and time-consuming DIN, ISO, and AGMA gear designs to be realized in less time combining simplicity of the textbook solution with the accuracy of technical gear design approaches thus providing convenience and reducing design time, which coincidently reduces costs for the design.

ANSYS program is also used for the Finite Element Method (FEM). The numerical solutions were compared with the analytical results that were obtained for all design approaches. The results of the study show that there is less than 10% difference between analytical and numerical results in all approaches, except for Fundamental of Machine Component Design 5th Edition, Juvinall R.C. and Marshek K.M., 2011 at twenty degrees and twenty-five degrees of angles.

Although the results of all design approaches differ from each other, they are very similar to the excellent continuity of the charts. Dimensionless numbers as geometric rating numbers (GRi) have been described and proposed to rate DIN, ISO, and textbook design approaches with ANSI/AGMA 2003-B97, (1997), approach based on bending fatigue failure for spiral bevel gears. In addition to that, conversion factors (CFs) have been derived. This provides the conversion of any textbook design approach results into ANSI/AGMA 2003-B97, (1997), with minimum error. Beyond the investigations already available in the literature, the following conclusions can be drawn in this study;

Use of radar graphics, GRi values can be read for each approach and transmitted power at a given speed ratio (1:1 to 1:8) can be compared according to gear AGMA. It is also observed that the trend is similar even if the transmitted power changes.

Differences in GR_i numbers provide a relative comparison between each approach. For example, mean values of

GR_{AGMA} minus GR_{ISO} (1,00-0,601=0,399) is 0,399

GR_{AGMA} minus $GR_{J\&M}$ (1,00-0,599=0,401) is 0,401

GR_{AGMA} minus GR_{DIN} (1,00-0,953=0,047) is 0,047

GRi (obtained from F times m) values are compared according to the AGMA approach for pressure angle of 20° and material type 1. ISO, J&M, DIN approaches have a lower gear tooth volume compared to AGMA with a rate of 39,9%, 40,1%, and 4,7%, respectively.

The difference between the GRi values shows the percentage gear tooth volume difference according to the AGMA design comparatevily for each design. These values show that if we use the design approaches other than AGMA, we can gain material advantage for gear tooth volume for twenty-degree pressure angles.

Likewise, for pressure angle of 25° and material type 1, mean values of

GR_{AGMA} minus GR_{ISO} (1,00-0,711=0,289) is 0,289

GR_{AGMA} minus $GR_{J\&M}$ (1,00-0,608=0,392) is 0,392

GR_{AGMA} minus GR_{DIN} (1,00-1,183=-0,183) is -0,183

GRi (obtained from F times m) values are compared according to the AGMA approach for pressure angle of 25° and material type 1. ISO, J&M approaches have a lower gear tooth volume compared to AGMA with a rate of 28,9%, 39,2%, and respectively. DIN approach has a higher gear tooth volume compared to AGMA with a rate of 18,3. These values show that if we use the design approaches other than DIN, we can gain an advantage for gear tooth volume in the case of using twenty-five-degree pressure angles.

Similar trend can be seen in both pressure angles (20° and 25°) depending on speed ratio, as shown in Table 4.11, Table 4.12 and Figure 4.34. Although the pressure angle of J&M to AGMA conversion values changes, the difference between CFs values according to pressure angle is 3.1% at most. This may be because the J&M approach refers to the AGMA standard. However, this situation shows up to 14.3% difference for conversion of ISO and DIN standard approaches to AGMA CFs. This result showed that CFs formulas must be created for each pressure angle.

When the hardness of material increased, there was a significant decrease in the module and face width values for the DIN, ISO and J&M approaches, while the module and face width in the AGMA approach decreased slightly. Therefore, there is a decrease in GRi values.

Conversion formulas based on speed ratio at 20 degrees pressure angle conversion factor of face width for J&M appraoch to AGMA approach equation gave a result of at least 0.84 R^2 value shown in Table 4.8. Other results at 20 degrees pressure angle are above 0.94 R^2 value. Conversion formulas at 25 degrees pressure angle, R^2 values are between 0.93 and 0.99 shown in Table 4.10. High R^2 values support the accuracy of formulas.

Dimensionless module and face width conversion factors (CFs) were generated for spiral bevel gears to convert the design results of ISO Standards, DIN Standards, and J&M machine element textbook into AGMA with low error. The formulas and values required to obtain conversion factors are given in section 4.4. If the speed ratio is an integer (1: 1 to 1: 8), CFs values can be obtained by using table 4.7 and 4.8 for the 20-degree pressure angle and table 4.9 and table 4.10 for the 25-degree pressure angle respectively.

The accuracy of CFs values were proven by performing a case study in section 4.5. Traditional results obtained from design approaches and converted values($\boldsymbol{m_{c,AGMA}}$ and $F_{c,AGMA}$) using dimensionless numbers obtained are given in Tables 4.17 and 4.18. Comparison of these two values is shown with the value of GVe. The maximum Gear Volume error (GVe) was found as 12.85% for 20-degree pressure given in Table 4.17 and 11,77% for 25-degree pressure given in table 4.18 with the aid of CFs. These values are obtained for 5 kW power transmission value, 1.8:1 speed ratio, and J&M design approach. The reason for this is that it will peak between 0.5 kW and 20 kW, as can be seen in the GRi figures in Section 4.3. Looking at other study cases, the error is less than 10%. The GVe values indicate that the traditional and transformed design parameters are almost the same, this result supports the reliability of the CFs obtained in the study.

Briefly, this study can serve as a guide for designers interested in spiral bevel gear design. The designer may select better option to optimize the gearbox design by choosing the size according to the data in the study. Besides, for students who are new to spiral bevel gear design, they can transform the design results of easier methods into the design results of technical standards using conversion formulas without the hassle of using complex formulas. Finally, the results of this study interest all designers, from students who have just begun to gear design to designers who have been engaged in gear design for a long time.

Investigation of conversion factors between spiral bevel gear and spur types of gears are proposed as future work. Especially spur gear design much easier and provide less time-consuming. The second and last future work is to extend this study with different standards and machine element textbooks.

REFERENCES

ANSI/AGMA 2003-B97 Standards, 1997. Fundamental rating factors and calculation methods for involute bevel gear teeth. 59 pages, Virginia, USA.

Argyris, J., Fuentes, A., & Litvin, F. L., 2002. Computerized integrated approach for design and stress analysis of spiral bevel gears. Computer methods in applied mechanics and engineering, Vol 191(11-12), p. 1057-1095.

Babalik F.C., 2010, Makine Elemanları ve Konstrüksiyon Örnekleri. Dora Basım Yayınevi, 4. Baskı, 860 sayfa.

Bibel G.D., Kumar A., Reddy S. and Handschuh R., 1995, Contact Stress Analysis of Spiral Bevel Gears Using Finite Element Analysis. Journal of Mechanical Design, Vol. 117, p 235-240.

Budynas R.G. and Nisbett J.K., 2011. Shigley's Mechanical Engineering Design. Ninth Edition, McGraw-Hill, 1120 pages.

Dhavale A.S. and Utpat A., 2013. Study of Stress Relief Features at Root of Teeth of Spur Gear. International Journal of Engineering Research and Applications Vol. 3, Issue 3, p.895-899.

DIN 3991 Standard, 1988. Calculation of load capacity of bevel gears - Part 1: Introduction and general influence factors, 19 pages, Germany.

DIN 3991 Standard, 1988. Calculation of load capacity of bevel gears - Part 2: Calculation of surface durability (pitting), 9 pages, Germany.

DIN 3991 Standard, 1988. Calculation of load capacity of bevel gears - Part 3: Calculation of tooth root strength, 15 pages, Germany.

Galina I. S., Andrey E. V. and Vladimir I. M., 2007. Algorithms for analysis of meshing and contact of spiral bevel gears. Mechanics and Machine Theory, Vol.42, p 198-215.

Geren N. and Baysal M.M., 2000. Expert System Development for Spur Gear Design. 9. International Conference on Machine Design and Production.

Geren N., Uzay Ç., 2016. "A Translation Technique: Dimensionless Ratings and Conversion Factors Between ISO and AGMA Gear Standards", ASME 2016 International Mechanical Engineering Congress and Exposition, 8 pages, Arizona, USA.

Geren N., Uzay Ç., Bayramoğlu M., 2017. "Introducing gear ratings and AGMA conversion factors for the steel spur gear design under bending fatigue", Materials Testing-Materials and Components Technology and application, vol.59, pp.1043-1053.

Geren N., Uzay Ç., Bayramoğlu M., 2020. "A proposal to improve the competence of students within the unnecessarily complex mechanical engineering design", International Journal of Technology and Design Education, 30 pages.

Gologlu C. and Zeyveli M., 2009. A Genetic Approach to Automate Preliminary Design of Gear Drives. Computers & Industrial Engineering, 57, p. 1043–1051.

Gökçek M., 2012, Mechanical Engineering. First Published by In Tech, 670 pages.

Kapelevich A.L., 2013. Direct Gear Design. CRC Press, Taylor & Francis Group. 324 pages.

ISO 10300 Standard, 2001. Calculation of load capacity of bevel gears - Part 1: Introduction and general influence factors, 49 pages, Switzerland.

ISO 10300 Standard, 2001. Calculation of load capacity of bevel gears - Part 2: Calculation of surface durability (pitting), 17 pages, Switzerland.

ISO 10300 Standard, 2003. Calculation of load capacity of bevel gears - Part 3: Calculation of tooth root strength, 37 pages, Switzerland.

ISO Standards 6336 – Part 5, 2003. Calculation of load capacity of spur and helical gears – Strength and quality of materials. 43 pages, Switzerland.

Juvinall R.C., Marshek K.M., 2011. Fundamentals of Machine Component Design. Wiley 5th Edition, 928 pages.

Mendi F., Başkal T., Boran K. and Boran F.E., 2010. Optimization of Module, Shaft Diameter and Rolling Bearing for Spur Gear through Genetic Algorithm. Expert Systems with Applications, 37, 8058–8064.

Parthiban A., Raju P.R., Sreenivasulu V., Rao P.D. and Kiran C.U., 2013. Profile Modification for Increasing the Tooth Strength in Spur Gear using CAD & CAE. International Journal of Innovations in Engineering and Technology, Vol.2, Issue 1, p. 231-241.

Sgihley J.E., 1985. Mechanical Engineering Design: First Metric Edition.Mcgraw-Hill, 698 pages.

Wu, Y., Wang, J., Han, Q., 2012. Static/dynamic contact FEA and experimental study for tooth profile modification of helical gears. Journal of Mechanical Science and Technology, 26.5: 1409-1417.

Ugural A.C., 2003. Mechanical Design an Integrated Approach 1st Edition. McGraw Hill, 864 pages.

Vijayarangan, S., and Ganesan N., 1994. Static Contact Stress Analysis of a Spur Gear Tooth Using the Finite Element Method, Including Frictional Effects. Computers & Structures Vol. 51, Issue 6, p. 765-770.

Zhang H. and Tie X. ,2012. Meshing Performance Analysis of New Non-zero-positive Modification Spiral Bevel Gear. Advanced Materials Research Vols 479-481, p 1457-1462.

http://khkgears.net/ , Kohara Gear Industry Co., Ltd.

BIOGRAPHY

Mehmet Onur OĞULATA was born in 11.04.1992 on Adana. He graduated from Adana College Science High School in 2010. In the same year, he started Mechanical Engineering at Çukurova University.

He graduated with his Bachelor of Science degree in Mechanical Engineering Department in 2015. He also graduated undergraduate program of Automotive Engineering with double major in 2016. Since 2017, he has been working as a Research Assistant at Mechanical Engineering Department of Karamanoğlu Mehmetbey University.

APPENDIX

APPENDIX A

A.1. Comparison of Face With and Module Results for α_n=20°, Material type 2

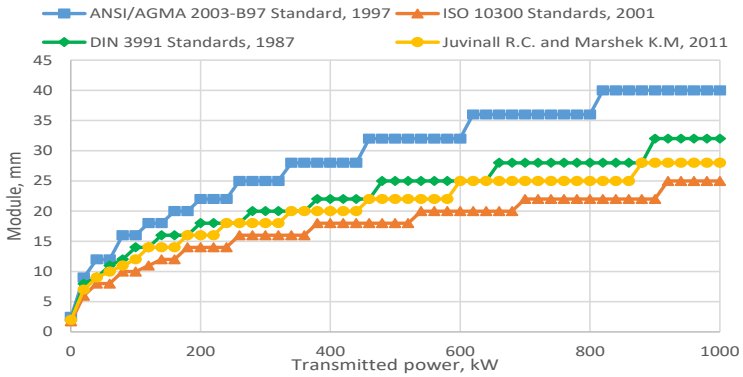

Figure A.1. Module values under various transmitted power at 1:1 speed ratio for α_n=20° and material type 2

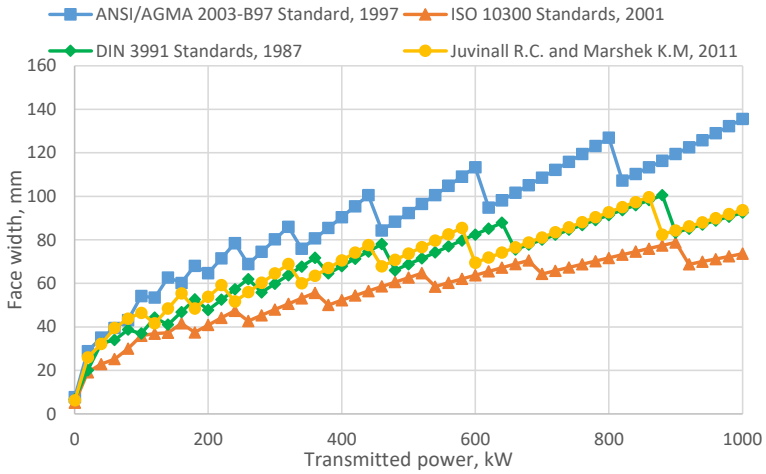

Figure A.2. Face width values under various transmitted power at 1:1 speed ratio for α_n=20° and material type 2

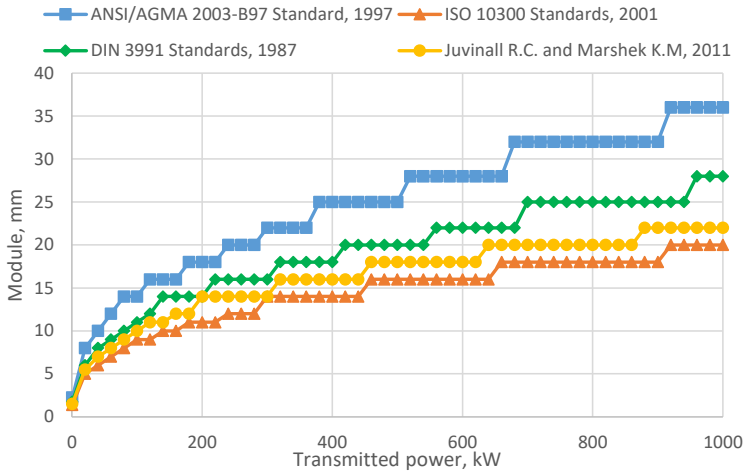

Figure A.3. Module values under various transmitted power at 2:1 speed ratio for α_n=20° and material type 2

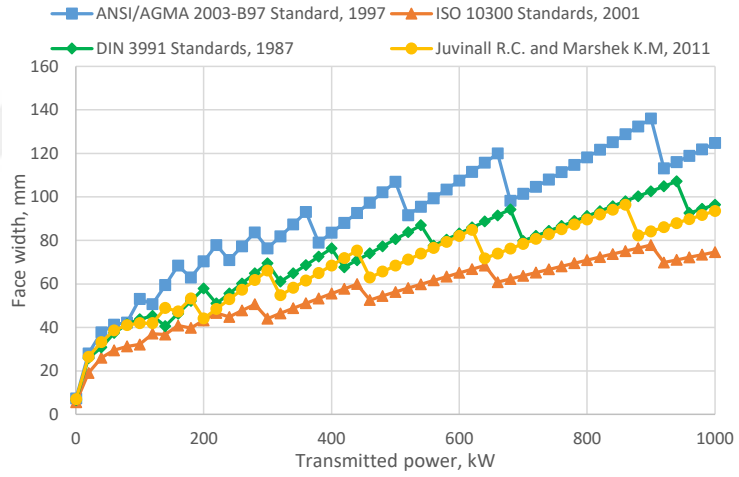

Figure A.4. Face width values under various transmitted power at 2:1 speed ratio for α_n=20° and material type 2

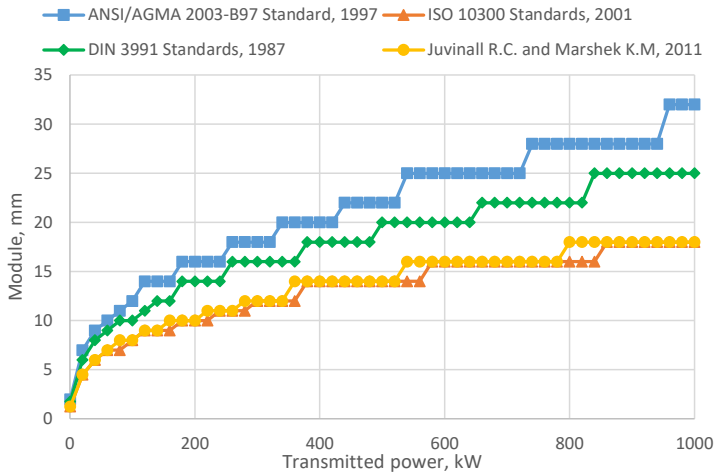

Figure A.5. Module values under various transmitted power at 3:1 speed ratio for α_n=20° and material type 2

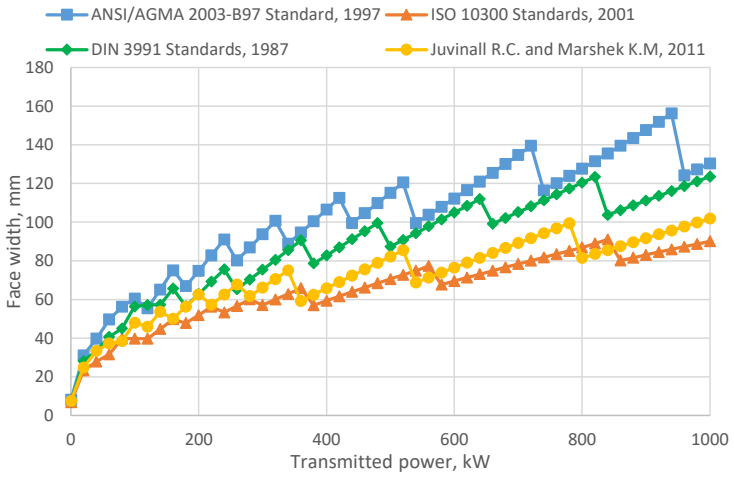

Figure A.6. Face width values under various transmitted power at 3:1 speed ratio for α_n=20° and material type 2

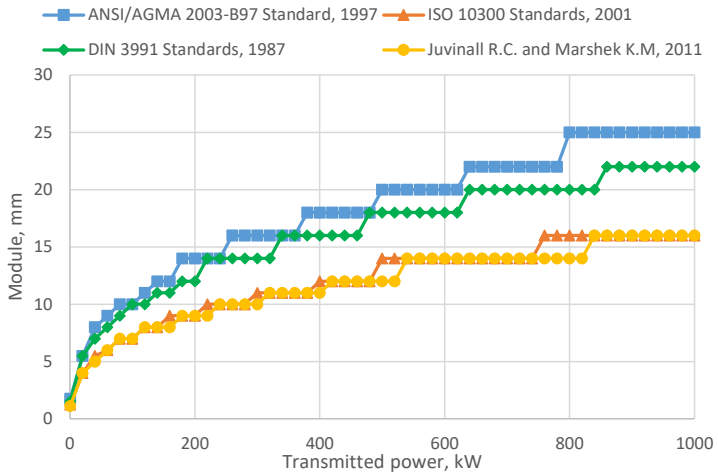

Figure A.7. Module values under various transmitted power at 4:1 speed ratio for α_n=20° and material type 2

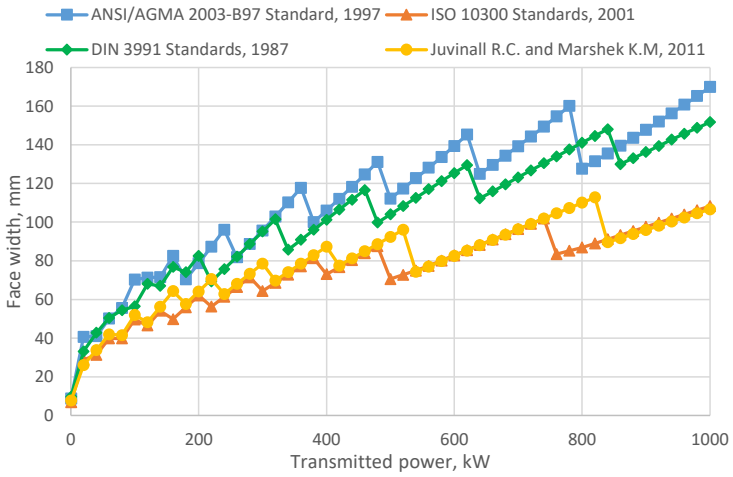

Figure A.8. Face width values under various transmitted power at 1:1 speed ratio for α_n=20° and material type 2

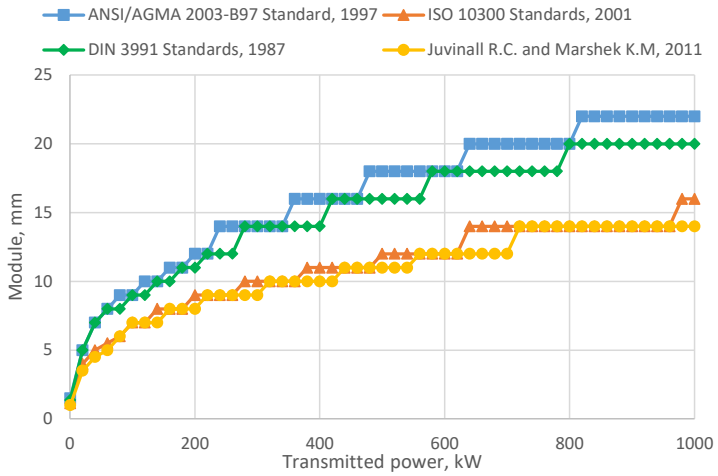

Figure A.9. Module values under various transmitted power at 5:1 speed ratio for α_n=20° and material type 2

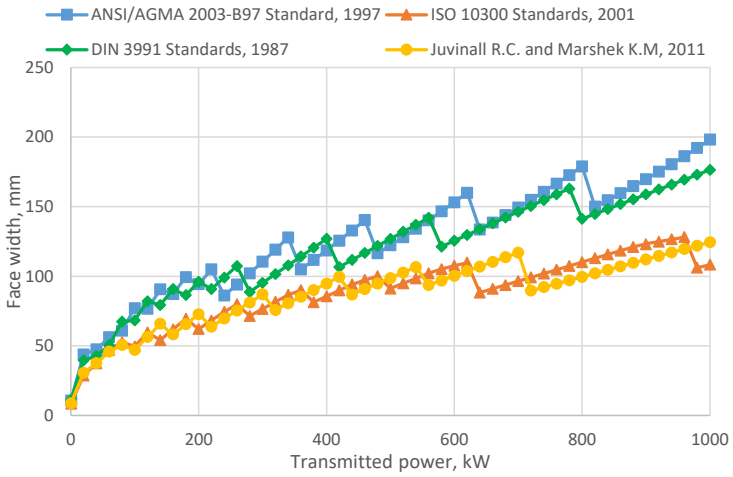

Figure A.10. Face width values under various transmitted power at 5:1 speed ratio for α_n=20° and material type 2

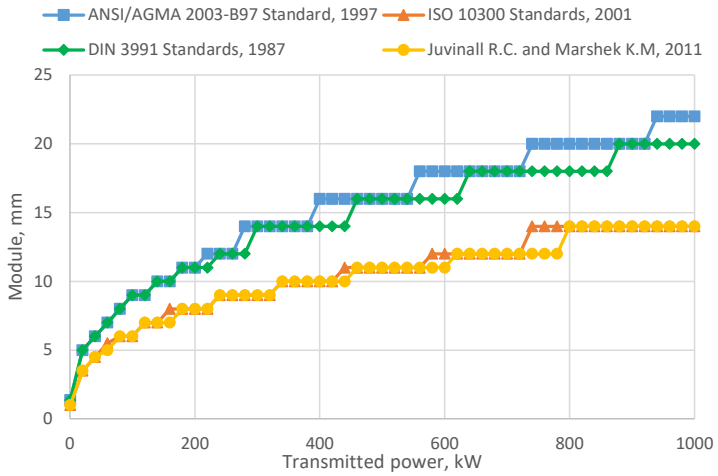

Figure A.11. Module values under various transmitted power at 6:1 speed ratio for α_n=20° and material type 2

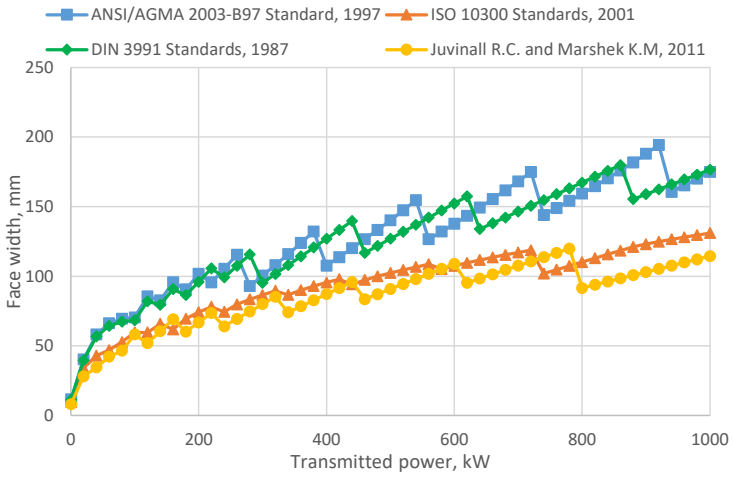

Figure A.12. Face width values under various transmitted power at 6:1 speed ratio for α_n=20° and material type 2

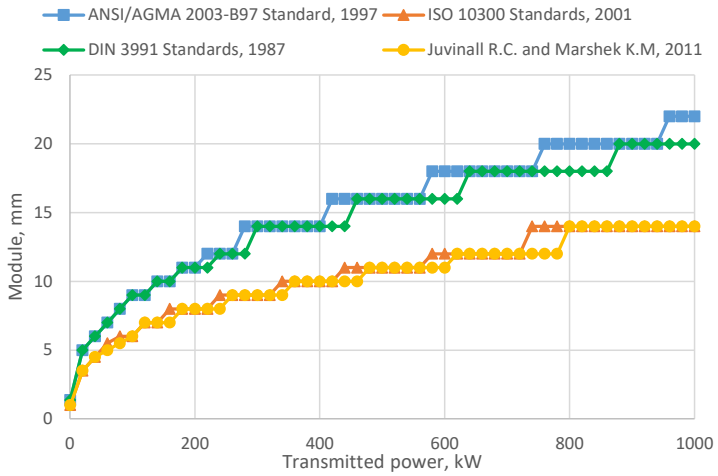

Figure A.13. Module values under various transmitted power at 7:1 speed ratio for α_n=20° and material type 2

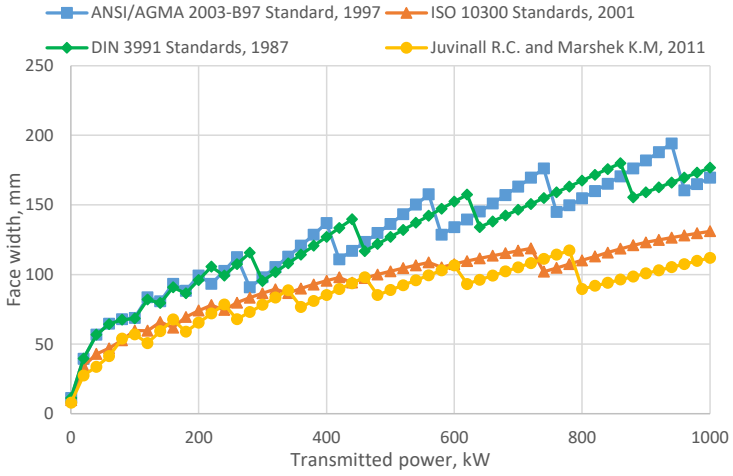

Figure A.14. Face width values under various transmitted power at 7:1 speed ratio for α_n=20° and material type 2

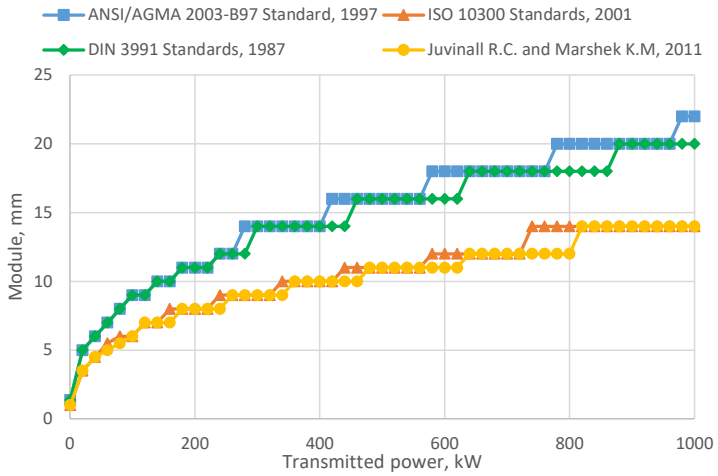

Figure A.15. Module values under various transmitted power at 8:1 speed ratio for α_n=20° and material type 2

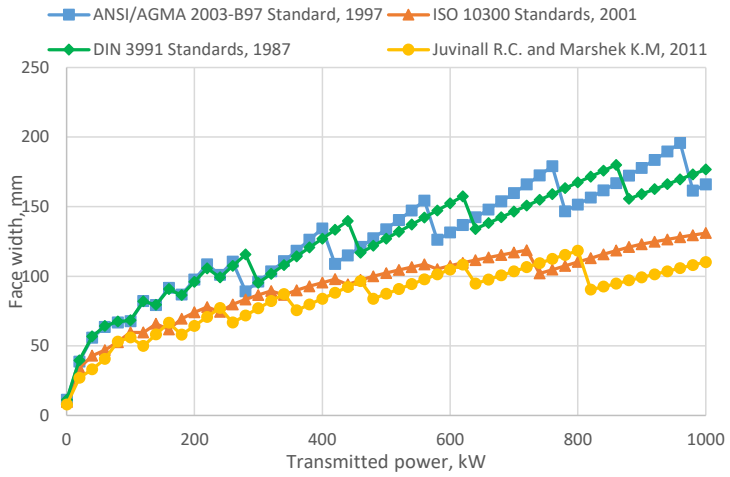

Figure A.16. Face width values under various transmitted power at 8:1 speed ratio for α_n=20° and material type 2

A.2. Comparison of the Module Results Considering Speed Ratio for the Selected Power Transmissions for α_n=20° and Material type 2

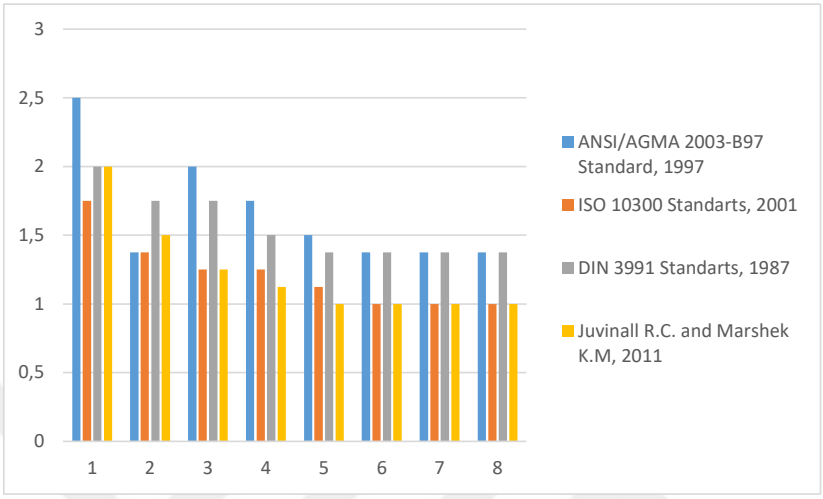

Figure A.17. The speed ratio effect on the module at 0,5 kW power transmission for α_n=20° and material type 2

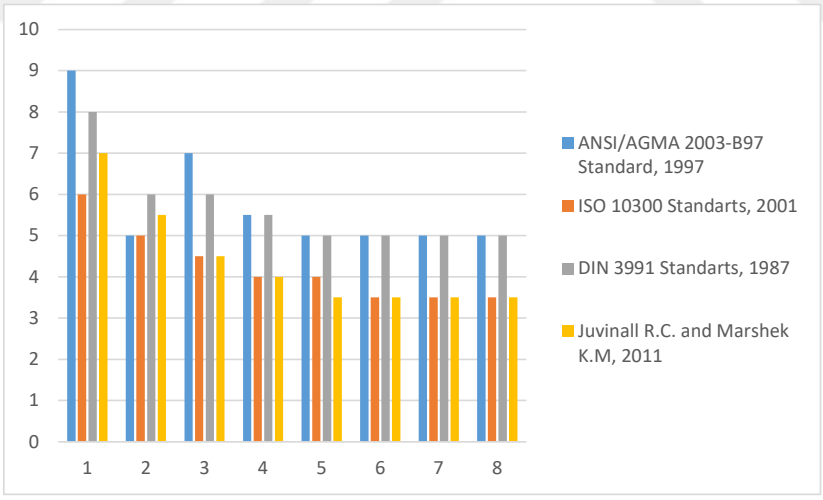

Figure A.18. The speed ratio effect on the module at 20 kW power transmission for α_n=20° and material type 2

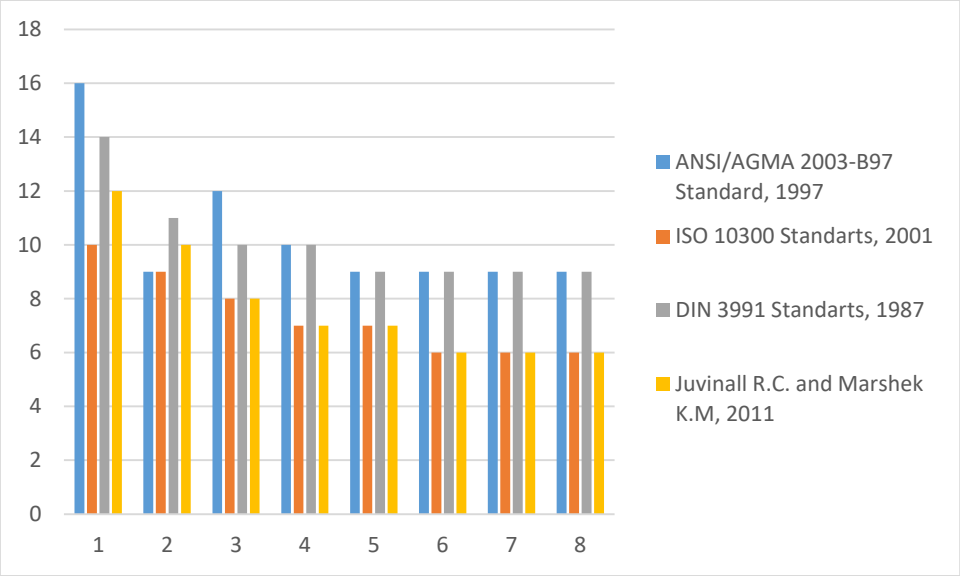

Figure A.19. The speed ratio effect on the module at 100 kW power transmission for α_n=20° and material type 2

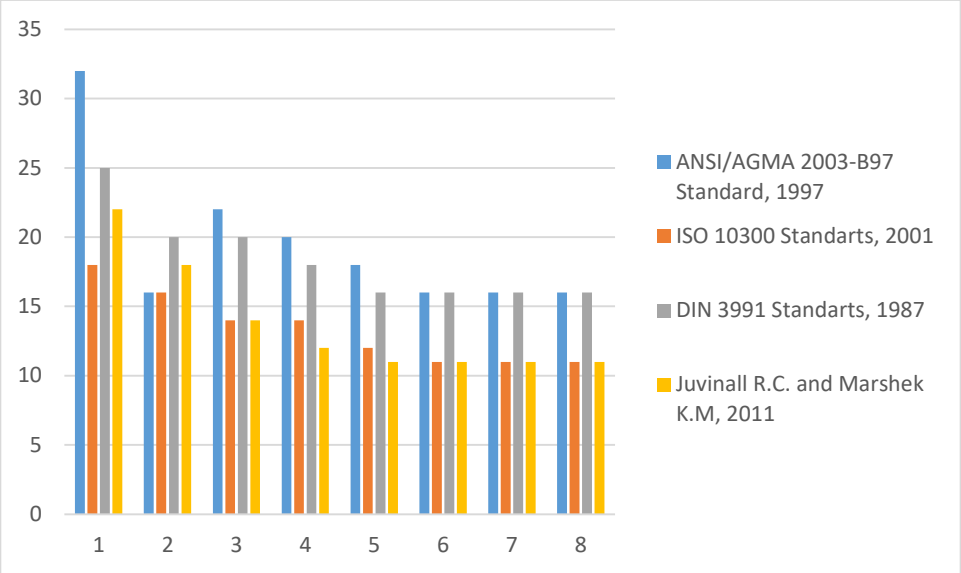

Figure A.20. The speed ratio effect on the module at 500 kW power transmission for α_n=20° and material type 2

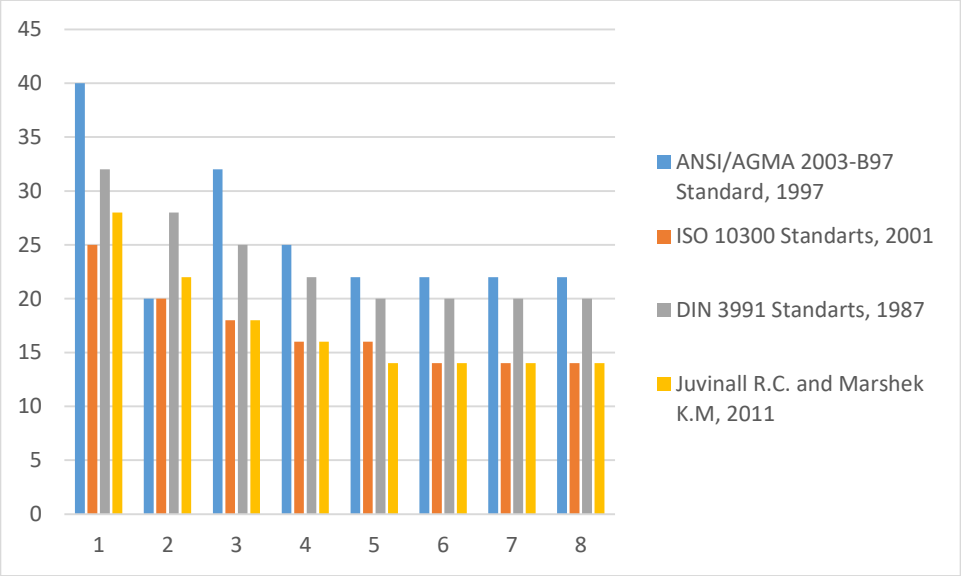

Figure A.21. The speed ratio effect on the module at 1000 kW power transmission for α_n=20° and material type 2

A.3. Obtaining Geometric Rating Number (GRi) for All Design Approaches and α_n=20°, Material type 2

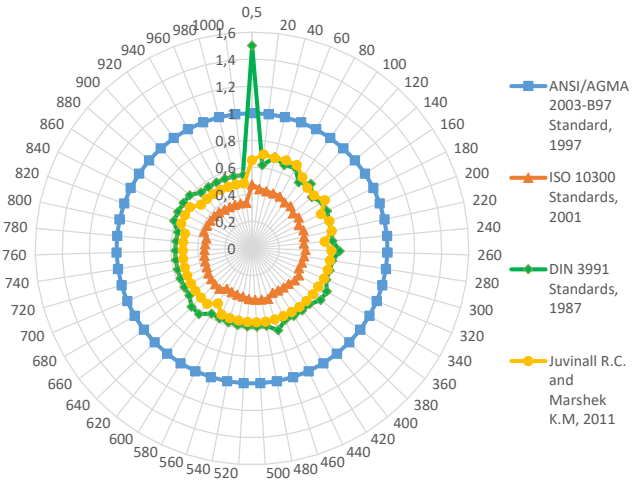

Figure A.22. Results of GR_i for all approaches at 1:1 speed ratio for α_n=20° and material type 2

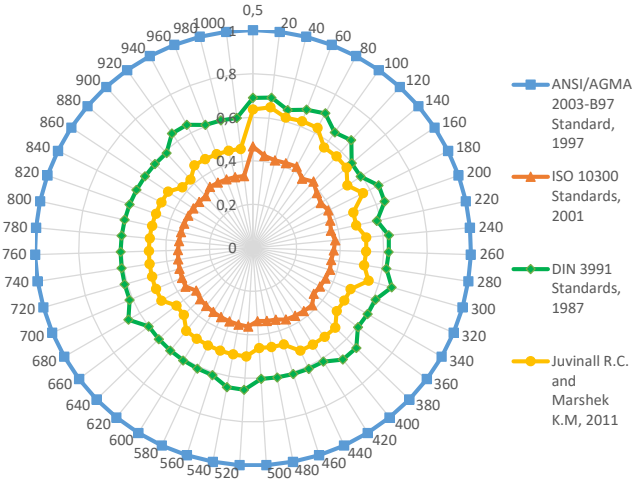

Figure A.23. Results of GR_i for all approaches at 2:1 speed ratio for α_n=20° and material type 2

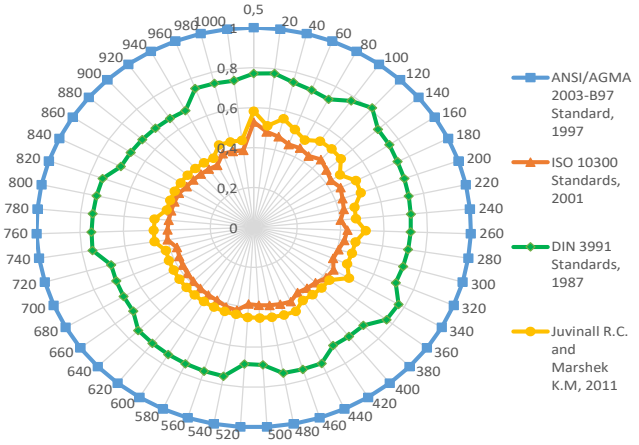

Figure A.24. Results of GR_i for all approaches at 3:1 speed ratio for α_n=20° and material type 2

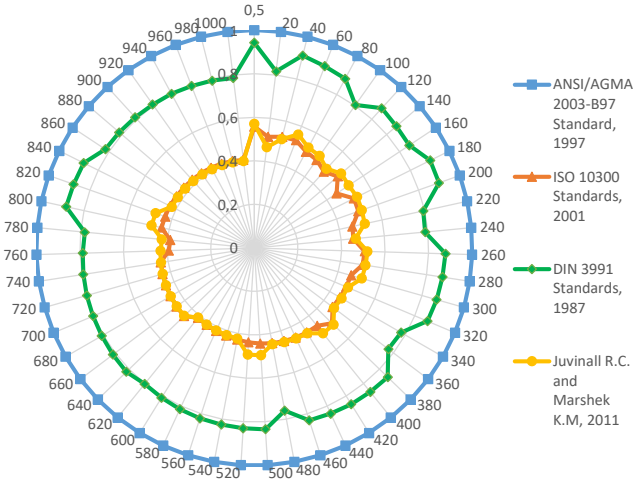

Figure A.25. Results of GR_i for all approaches at 4:1 speed ratio for α_n=20° and material type 2

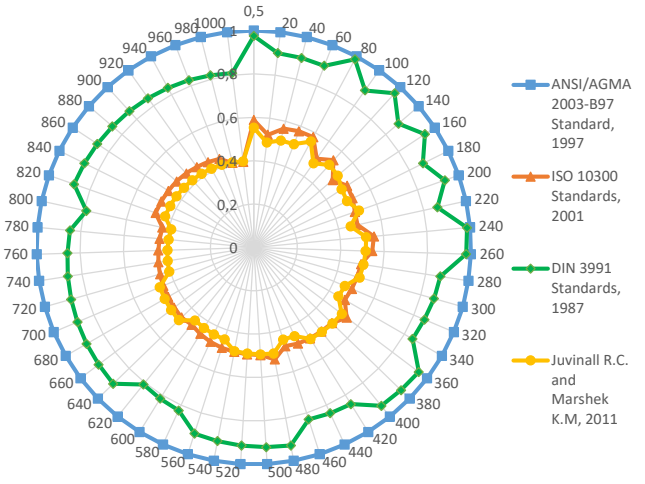

Figure A.26. Results of GR_i for all approaches at 5:1 speed ratio for α_n=20° and material type 2

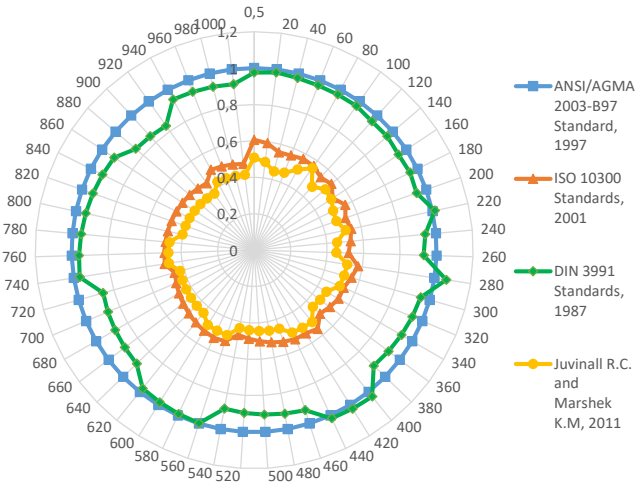

Figure A.27. Results of GR_i for all approaches at 6:1 speed ratio for α_n=20° and material type 2

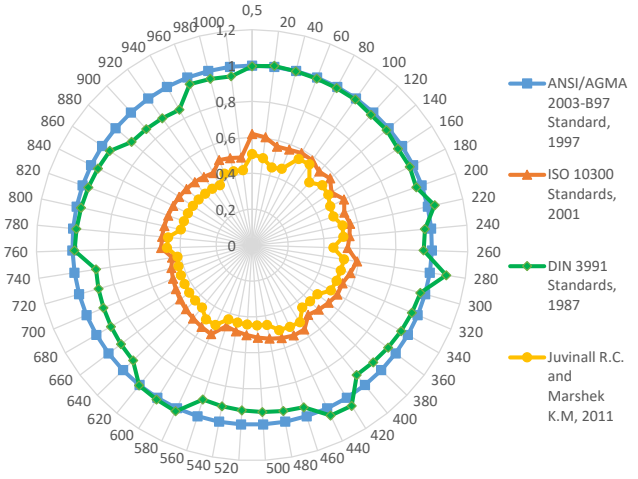

Figure A.28. Results of GR_i for all approaches at 7:1 speed ratio for α_n=20° and material type 2

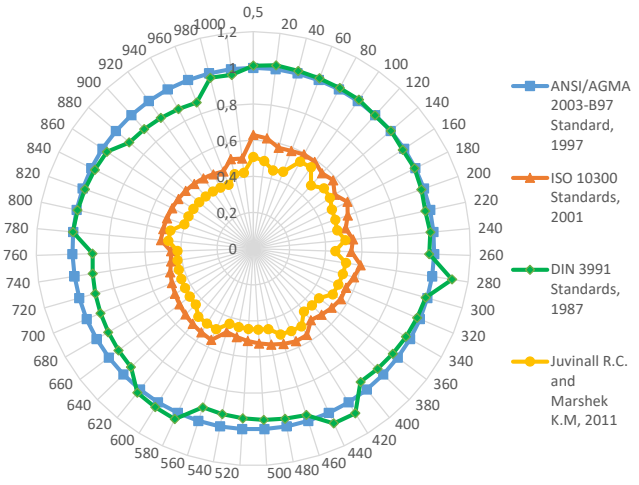

Figure A.29. Results of GR_i for all approaches at 8:1 speed ratio for α_n=20° and material type 2

APPENDIX B

B.1. Comparison of Face With and Module Results for α_n=20°, Material type 3

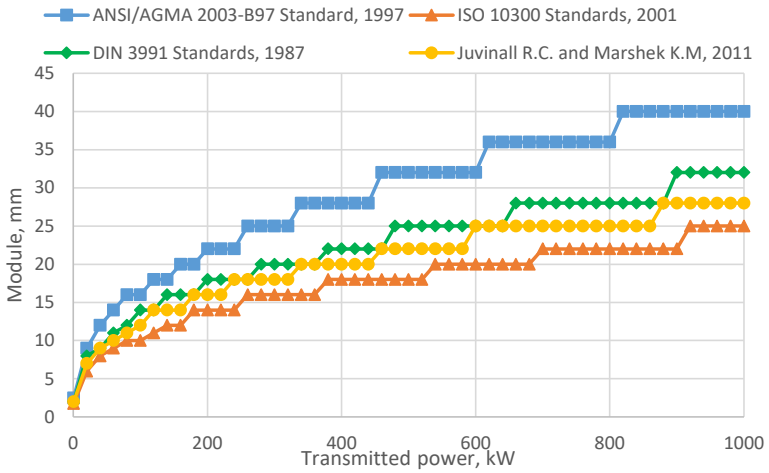

Figure B.1. Module values under various transmitted power at 1:1 speed ratio for α_n=20° and material type 3

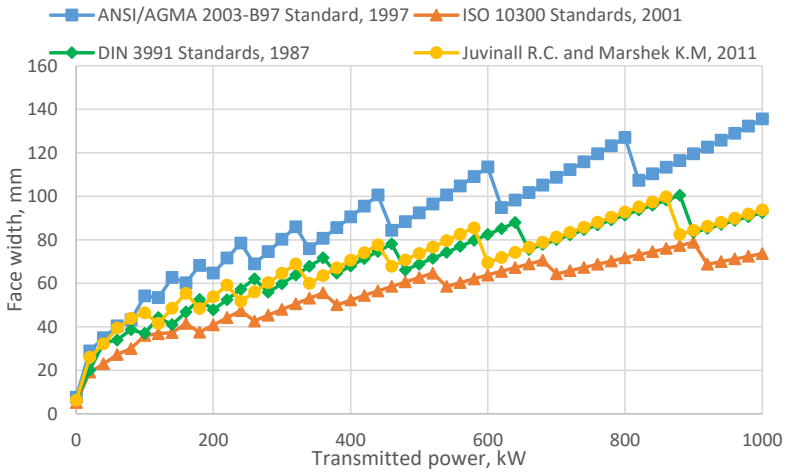

Figure B.2. Face width values under various transmitted power at 1:1 speed ratio for α_n=20° and material type 3

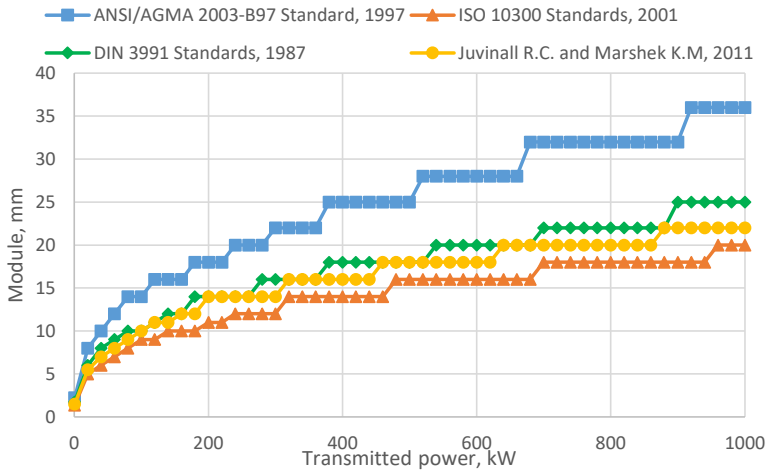

Figure B.3. Module values under various transmitted power at 2:1 speed ratio for α_n=20° and material type 3

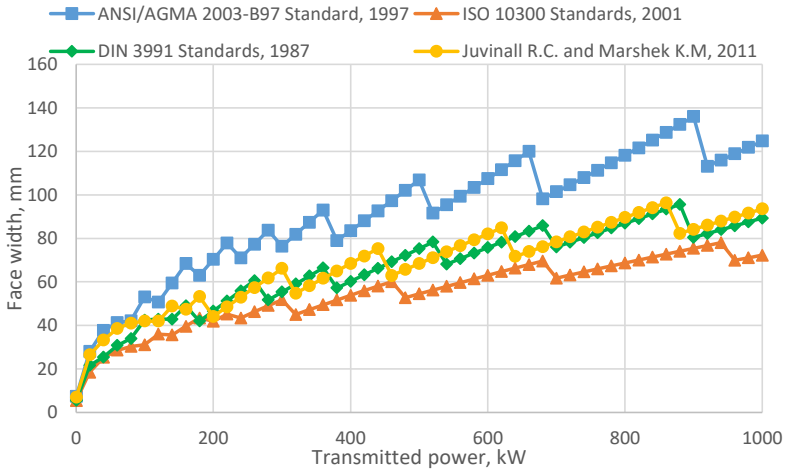

Figure B.4. Face width values under various transmitted power at 2:1 speed ratio for α_n=20° and material type 3

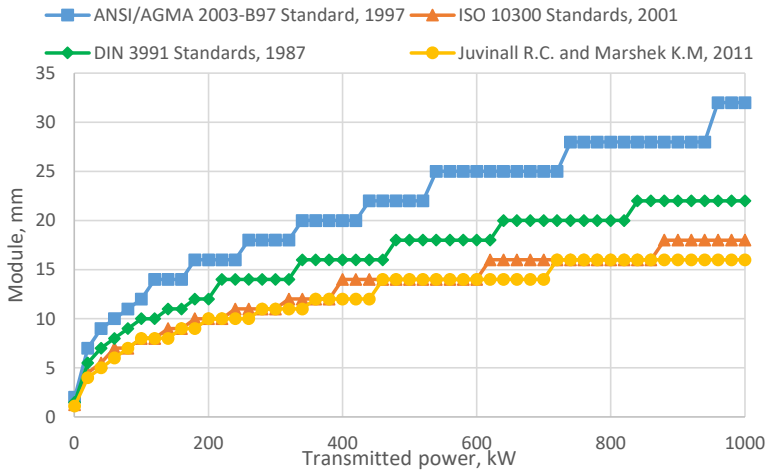

Figure B.5. Module values under various transmitted power at 3:1 speed ratio for α_n=20° and material type 3

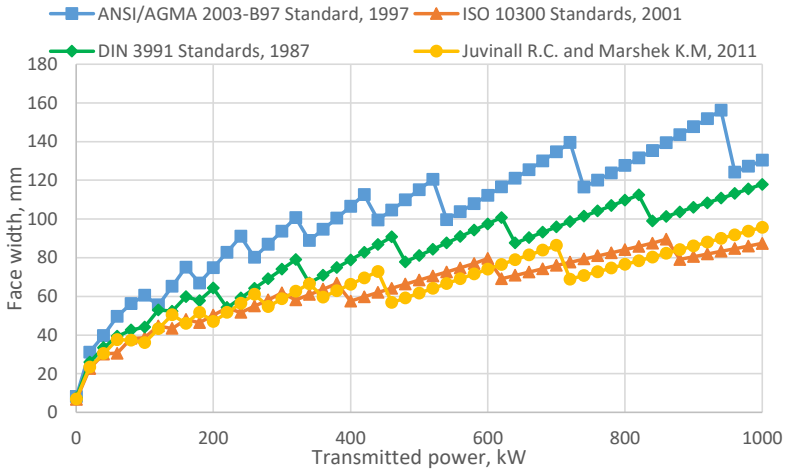

Figure B.6. Face width values under various transmitted power at 3:1 speed ratio for α_n=20° and material type 3

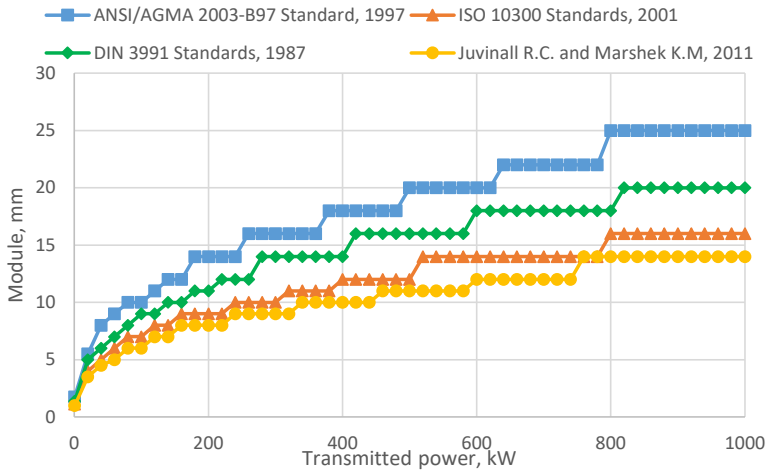

Figure B.7. Module values under various transmitted power at 4:1 speed ratio for α_n=20° and material type 3

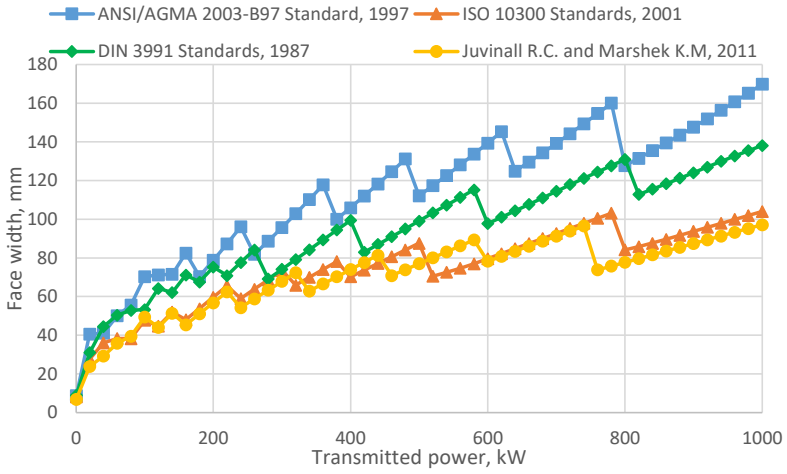

Figure B.8. Face width values under various transmitted power at 4:1 speed ratio for α_n=20° and material type 3

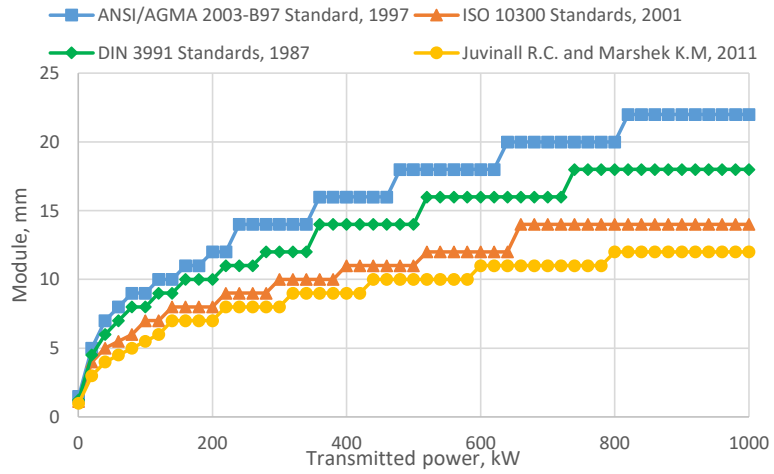

Figure B.9. Module values under various transmitted power at 5:1 speed ratio for α_n=20° and material type 3

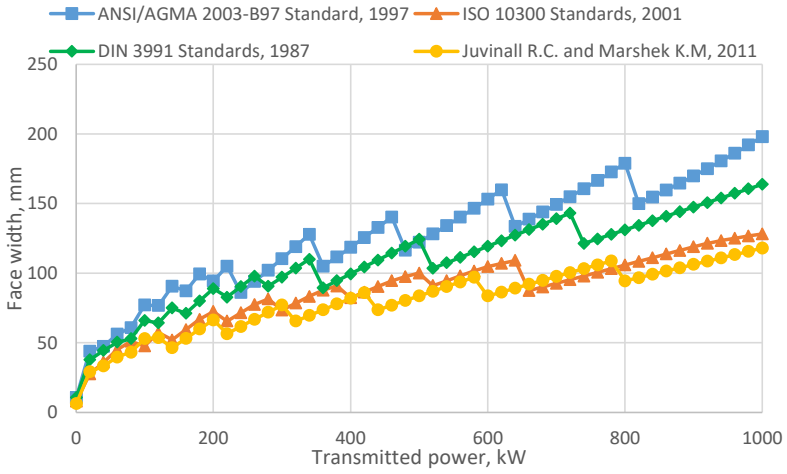

Figure B.10. Face width values under various transmitted power at 5:1 speed ratio for α_n=20° and material type 3

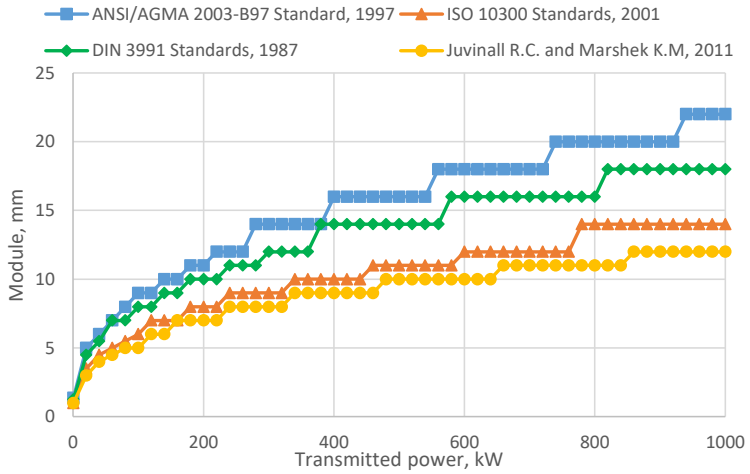

Figure B.11. Module values under various transmitted power at 6:1 speed ratio for α_n=20° and material type 3

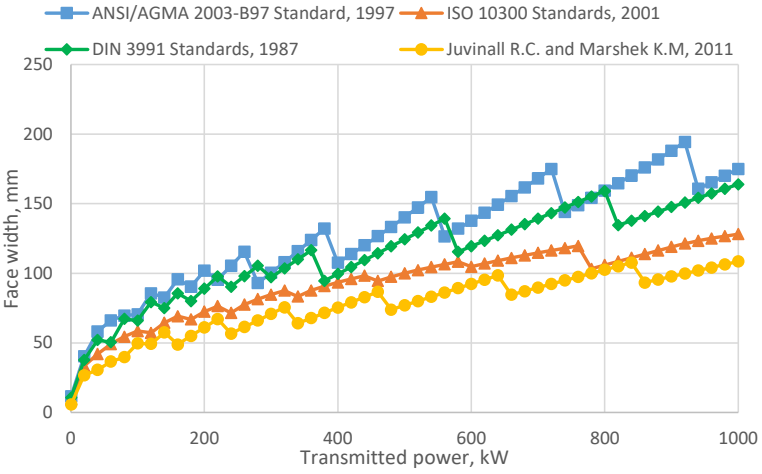

Figure B.12. Face width values under various transmitted power at 6:1 speed ratio for α_n=20° and material type 3

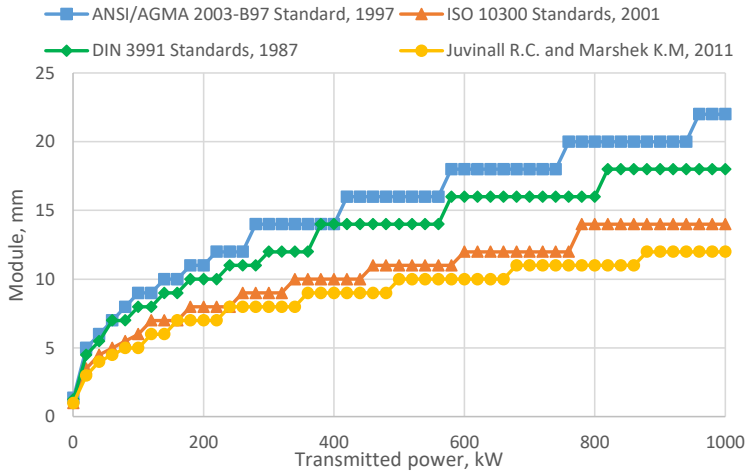

Figure B.13. Module values under various transmitted power at 7:1 speed ratio for α_n=20° and material type 3

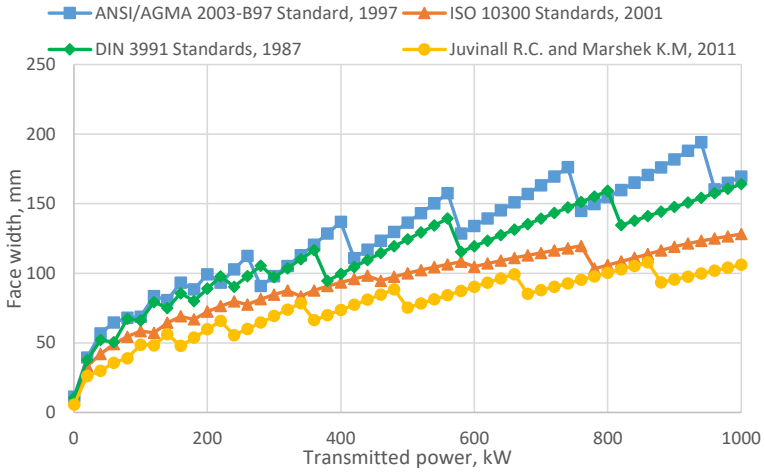

Figure B.14. Face width values under various transmitted power at 7:1 speed ratio for α_n=20° and material type 3

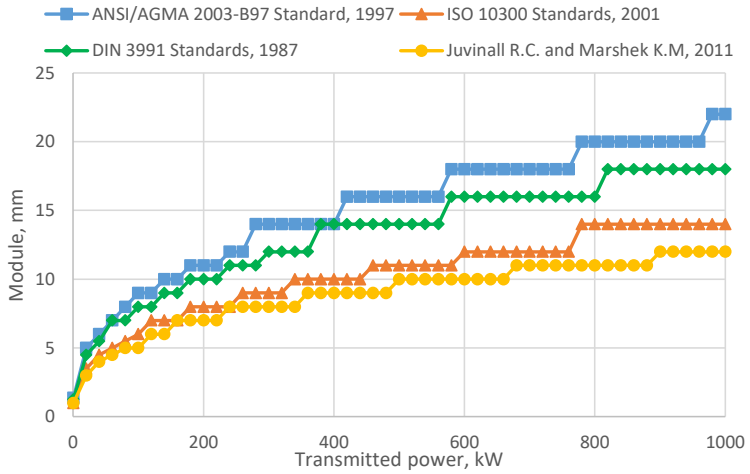

Figure B.15. Module values under various transmitted power at 8:1 speed ratio for α_n=20° and material type 3

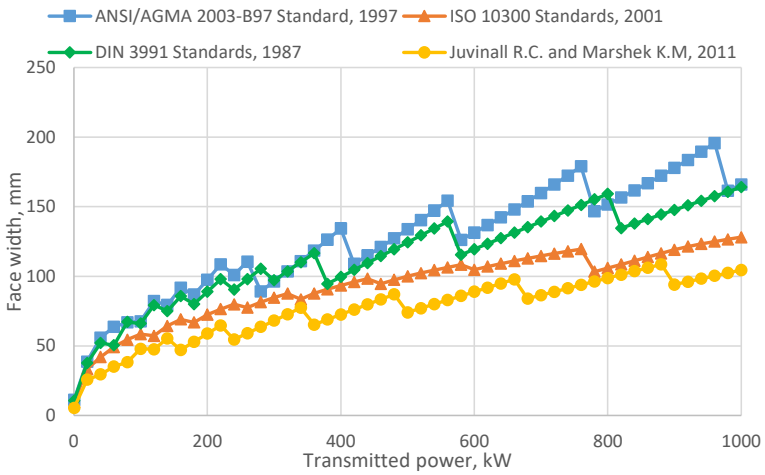

Figure B.16. Face width values under various transmitted power at 8:1 speed ratio for α_n=20° and material type 3

B.2. Comparison of the Module Results Considering Speed Ratio for the Selected Power Transmissions for α_n=20° and Material type 3

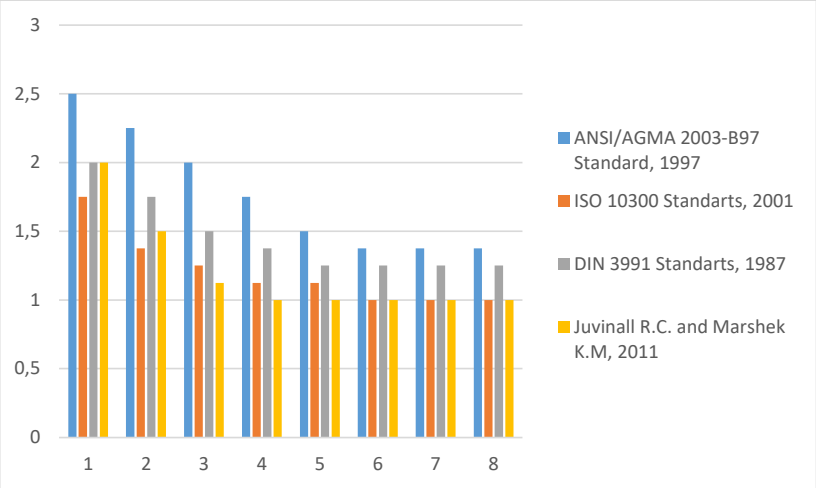

Figure B.17. The speed ratio effect on the module at 0,5 kW power transmission for α_n=20° and material type 3

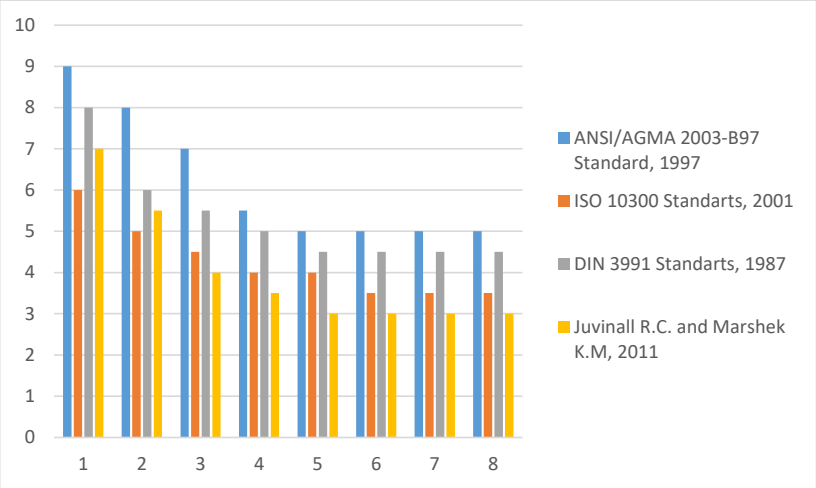

Figure B.18. The speed ratio effect on the module at 20 kW power transmission for α_n=20° and material type 3

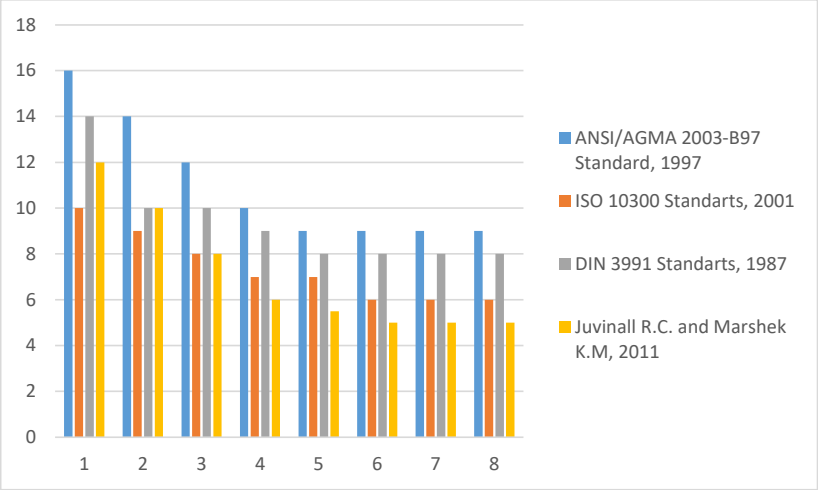

Figure B.19. The speed ratio effect on the module at 100 kW power transmission for α_n=20° and material type 3

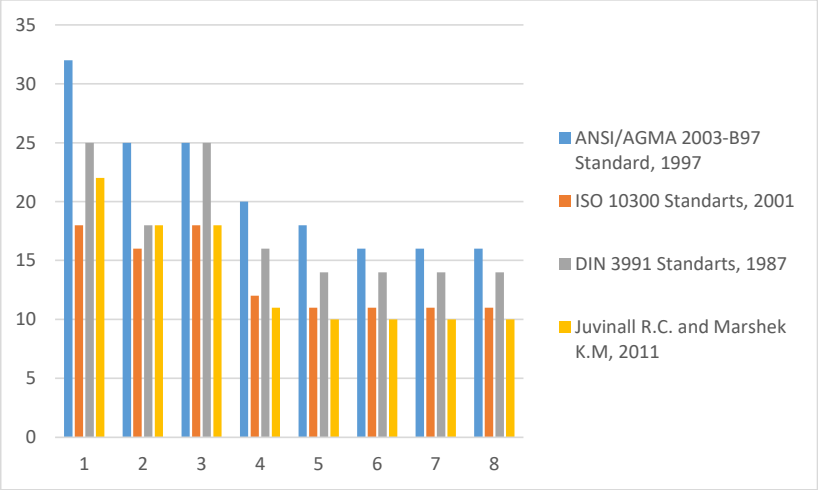

Figure B.20. The speed ratio effect on the module at 500 kW power transmission for α_n=20° and material type 3

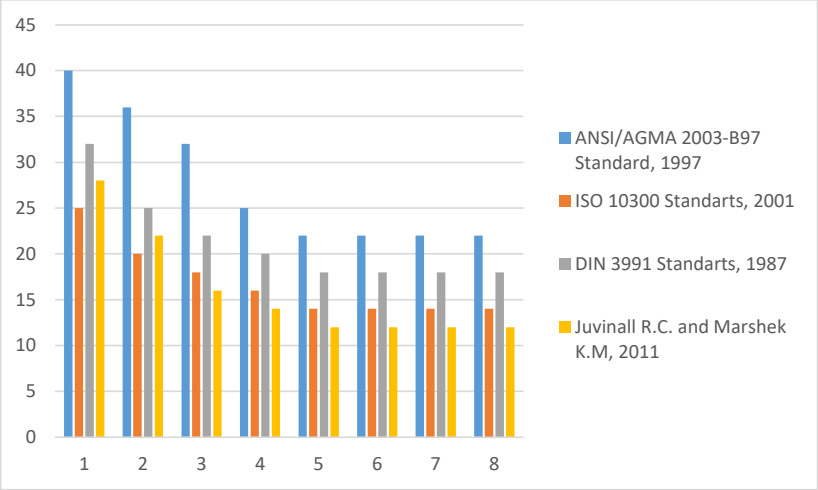

Figure B.21. The speed ratio effect on the module at 1000 kW power transmission for α_n=20° and material type 3

B.3. Obtaining Geometric Rating Number (GRi) for All Design Approaches and α_n=20°, Material type 3

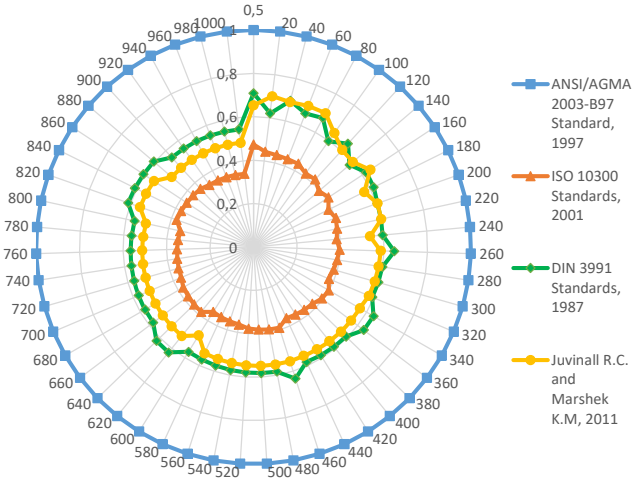

Figure B.22. Results of GR_i for all approaches at 1:1 speed ratio for α_n=20° and material type 3

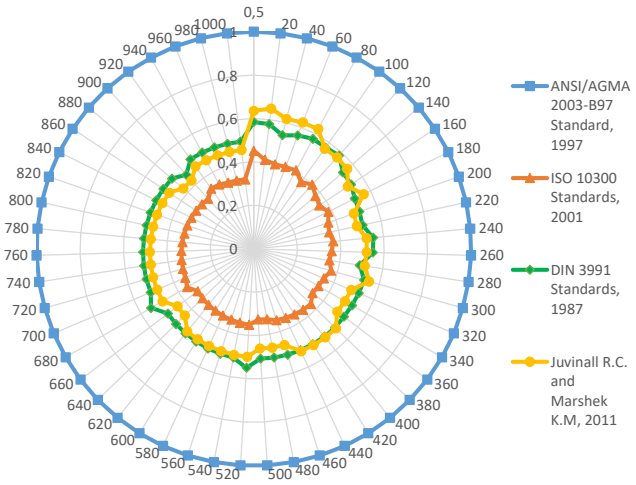

Figure B.23. Results of GR_i for all approaches at 2:1 speed ratio for α_n=20° and material type 3

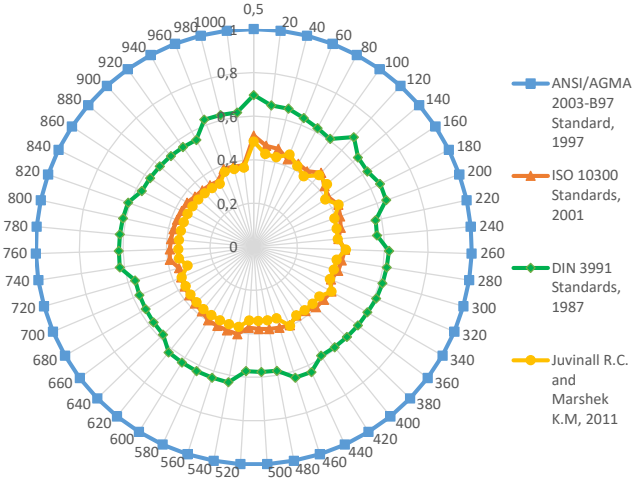

Figure B.24. Results of GR_i for all approaches at 3:1 speed ratio for α_n=20° and material type 3

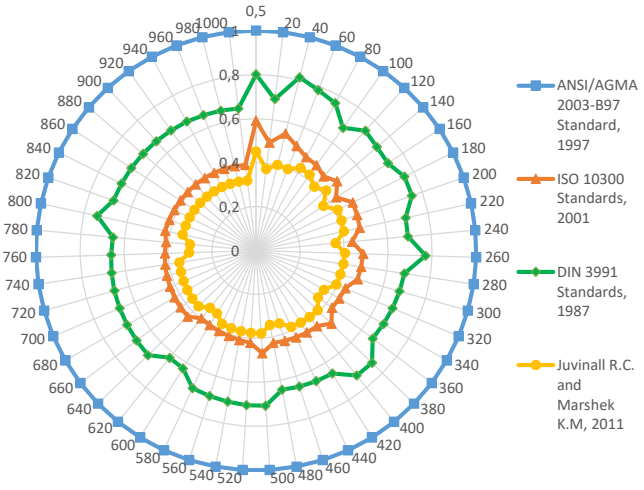

Figure B.25. Results of GR_i for all approaches at 4:1 speed ratio for α_n=20° and material type 3

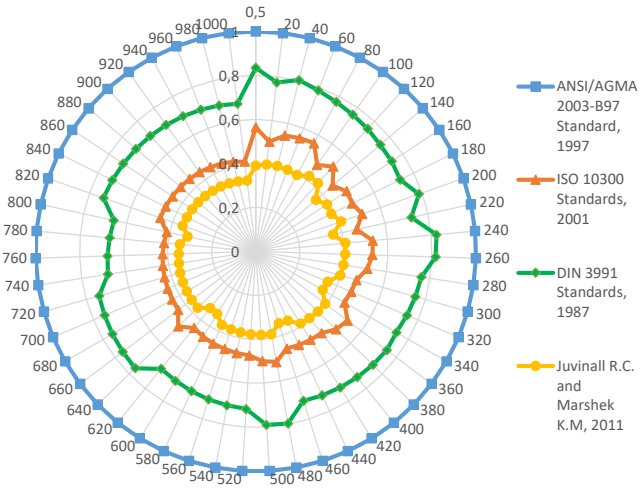

Figure B.26. Results of GR_i for all approaches at 5:1 speed ratio for α_n=20° and material type 3

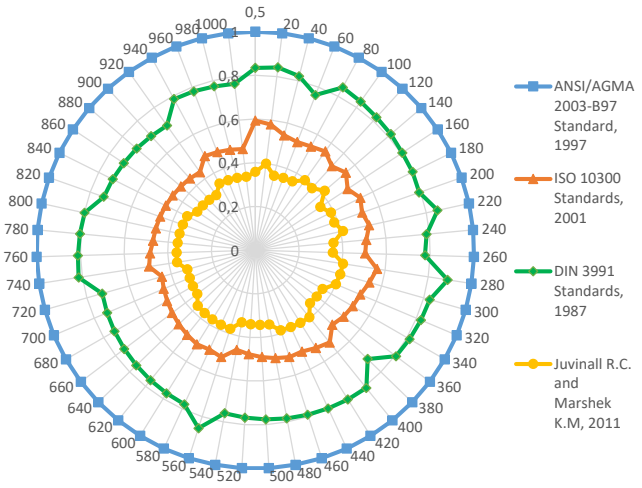

Figure B.27. Results of GR_i for all approaches at 6:1 speed ratio for α_n=20° and material type 3

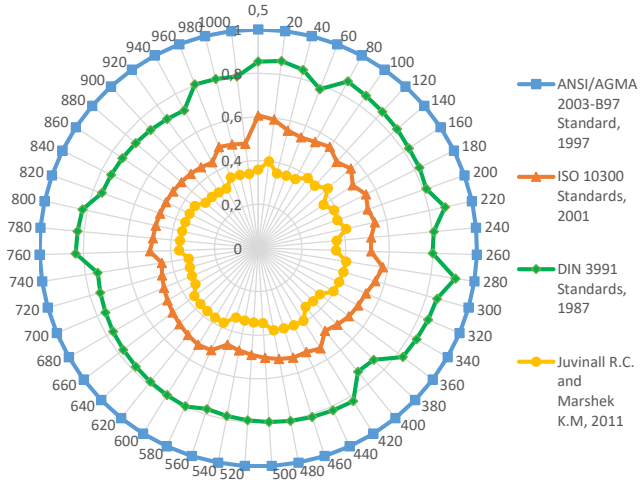

Figure B.28. Results of GR_i for all approaches at 7:1 speed ratio for α_n=20° and material type 3

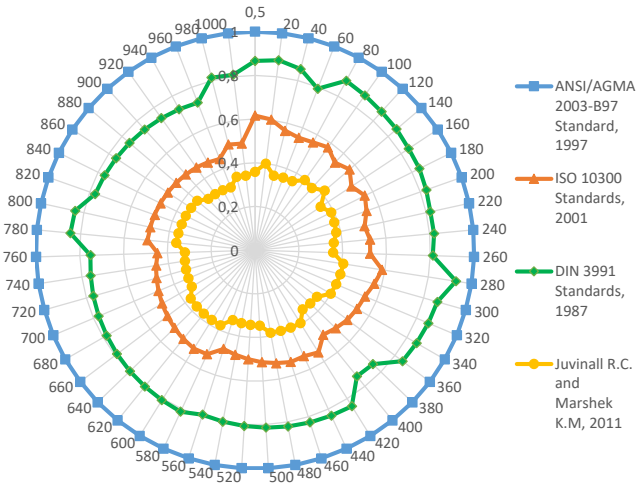

Figure B.29. Results of GR_i for all approaches at 8:1 speed ratio for α_n=20° and material type 3

APPENDIX C

C.1. Comparison of Face With and Module Results for α_n=25°, Material type 1

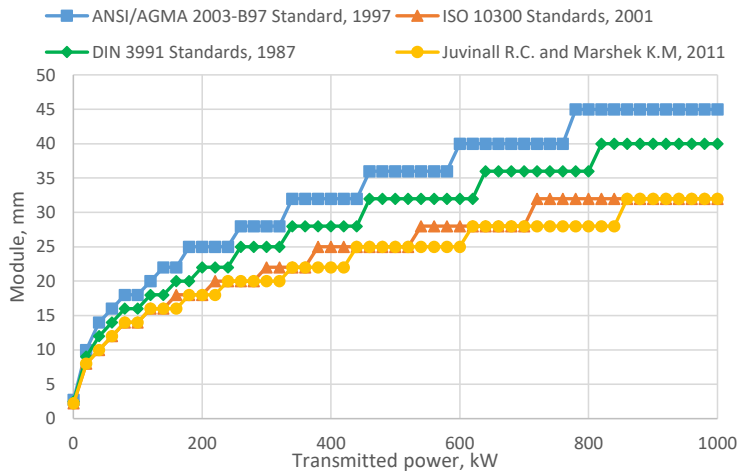

Figure C.1. Module values under various transmitted power at 1:1 speed ratio for α_n=25° and material type 1

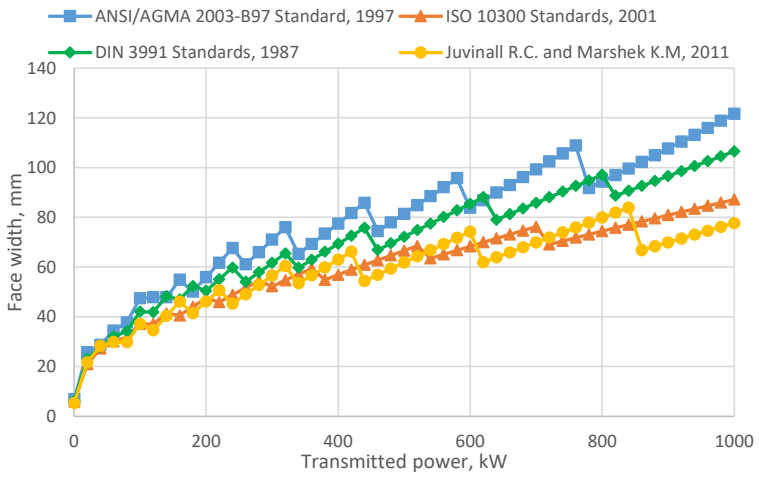

Figure C.2. Face width values under various transmitted power at 1:1 speed ratio for α_n=25° and material type 1

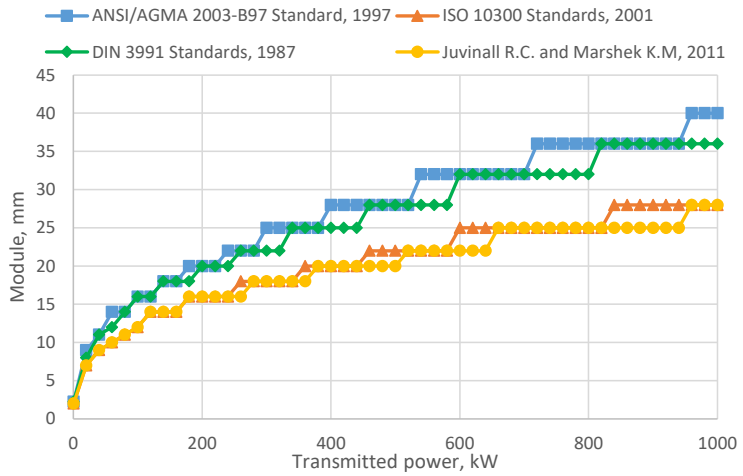

Figure C.3. Module values under various transmitted power at 2:1 speed ratio for α_n=25° and material type 1

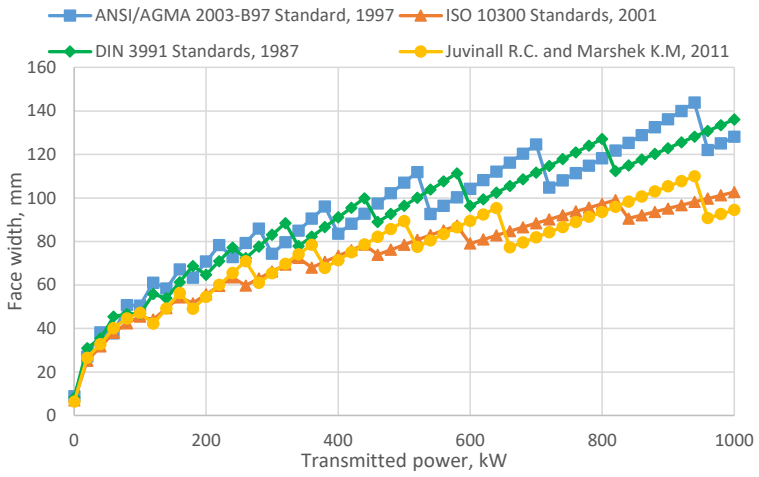

Figure C.4. Face width values under various transmitted power at 2:1 speed ratio for α_n=25° and material type 1

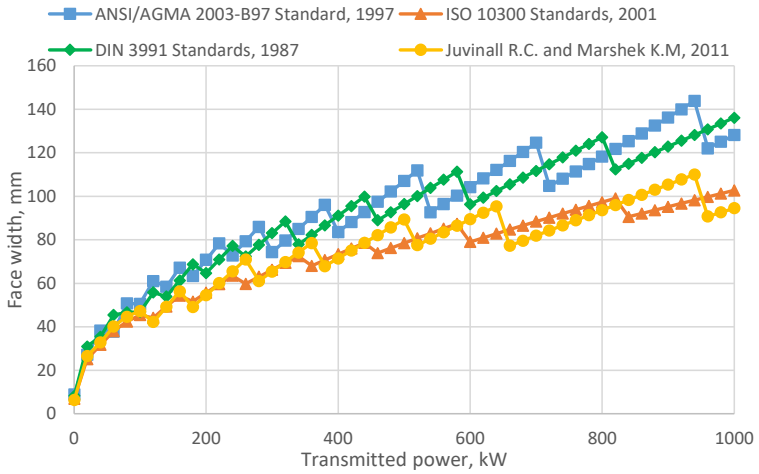

Figure C.5. Module values under various transmitted power at 3:1 speed ratio for α_n=25° and material type 1

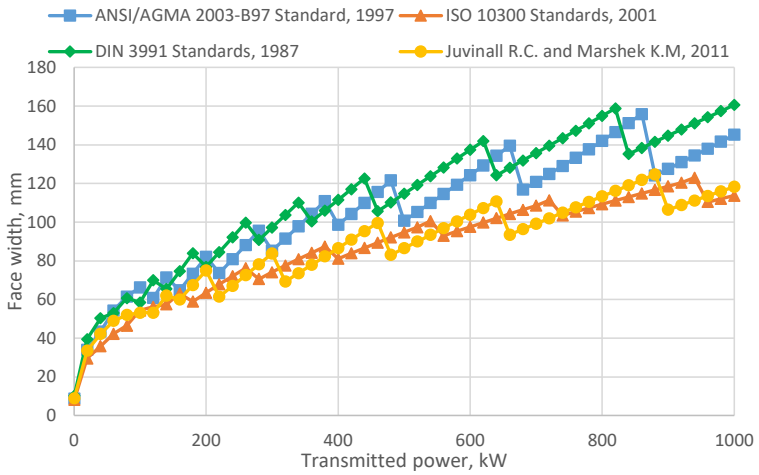

Figure C.6. Face width values under various transmitted power at 3:1 speed ratio for α_n=25° and material type 1

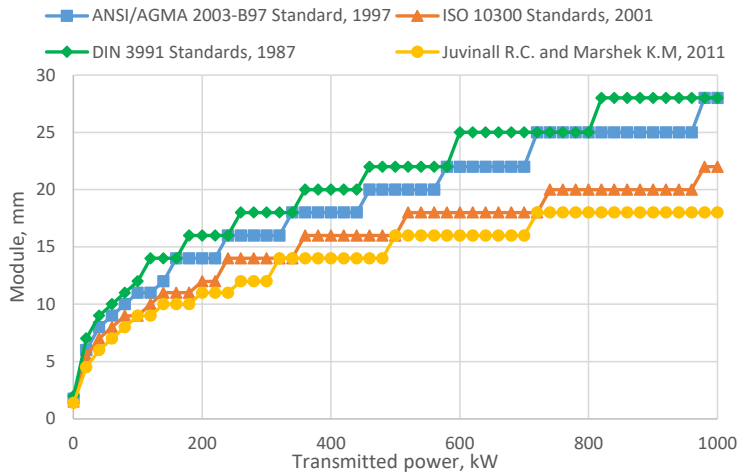

Figure C.7. Module values under various transmitted power at 4:1 speed ratio for α_n=25° and material type 1

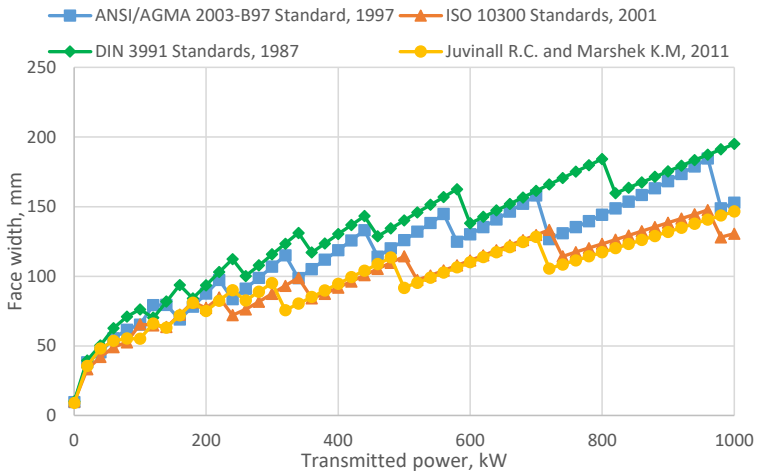

Figure C.8. Face width values under various transmitted power at 4:1 speed ratio for α_n=25° and material type 1

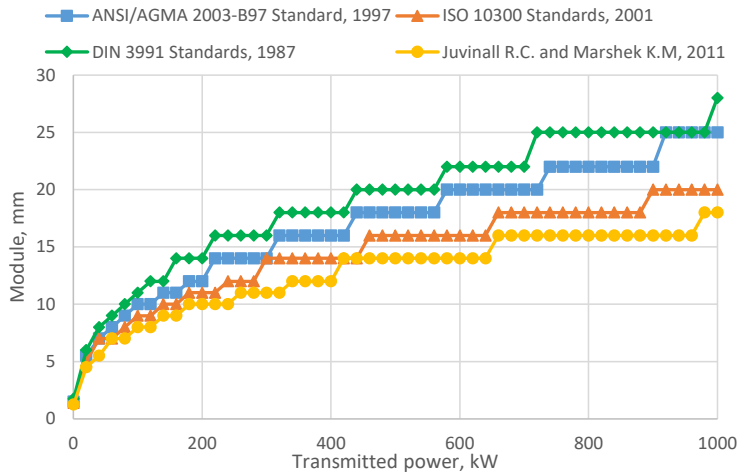

Figure C.9. Module values under various transmitted power at 5:1 speed ratio for α_n=25° and material type 1

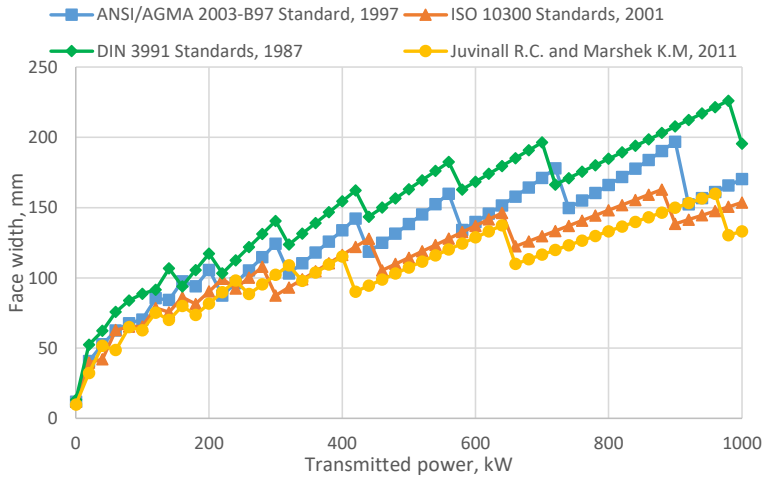

Figure C.10. Face width values under various transmitted power at 5:1 speed ratio for α_n=25° and material type 1

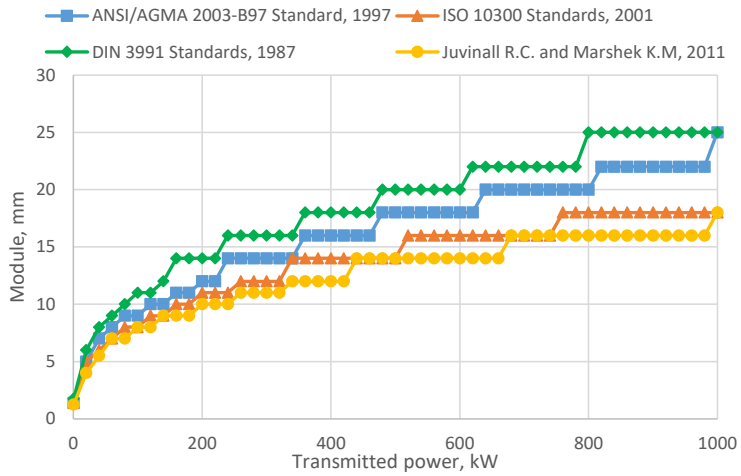

Figure C.11. Module values under various transmitted power at 6:1 speed ratio for α_n=25° and material type 1

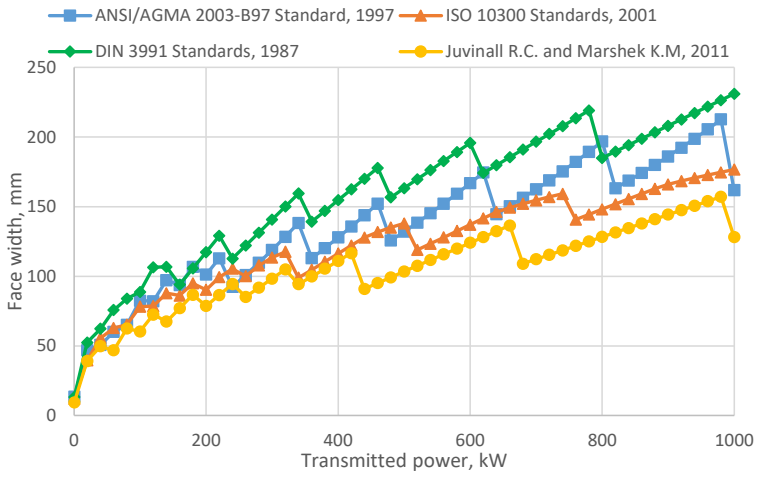

Figure C.12. Face width values under various transmitted power at 6:1 speed ratio for α_n=25° and material type 1

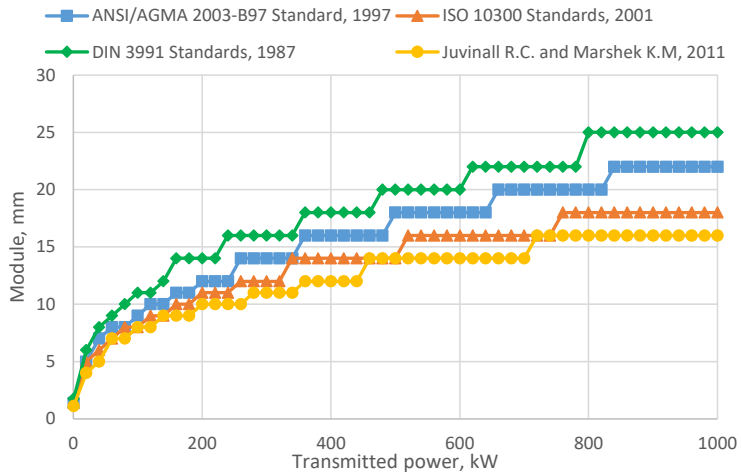

Figure C.13. Module values under various transmitted power at 7:1 speed ratio for α_n=25° and material type 1

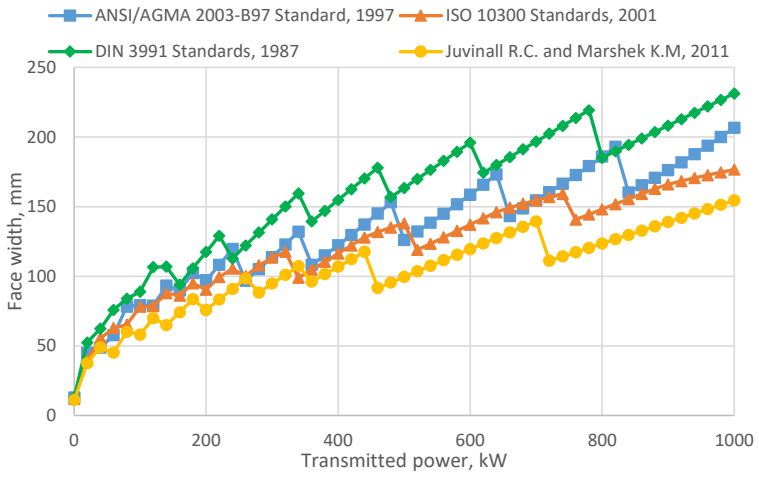

Figure C.14. Face width values under various transmitted power at 7:1 speed ratio for α_n=25° and material type 1

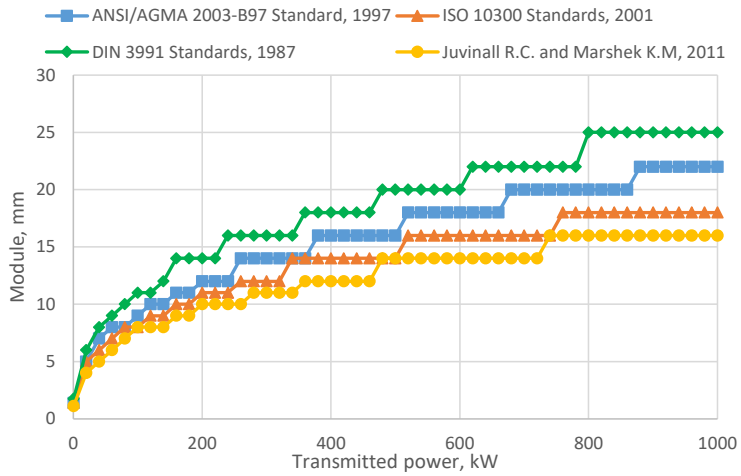

Figure C.15. Module values under various transmitted power at 8:1 speed ratio for α_n=25° and material type 1

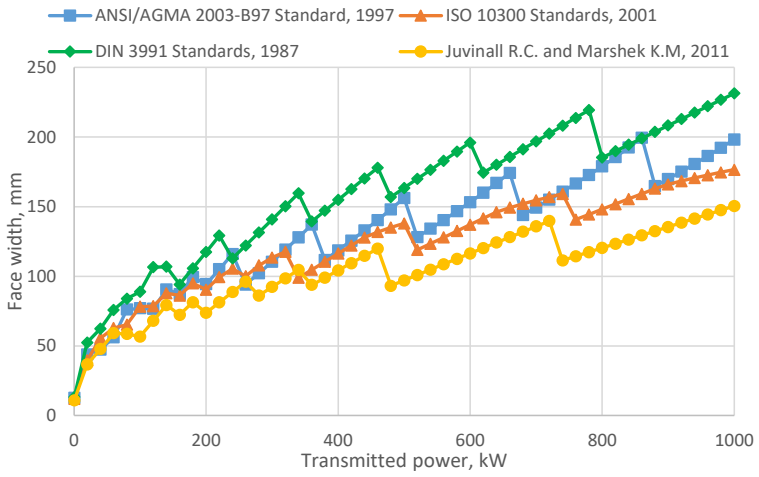

Figure C.16. Face width values under various transmitted power at 8:1 speed ratio for α_n=25° and material type 1

C.2. Comparison of the Module Results Considering Speed Ratio for the Selected Power Transmissions for α_n=25° and Material type 1

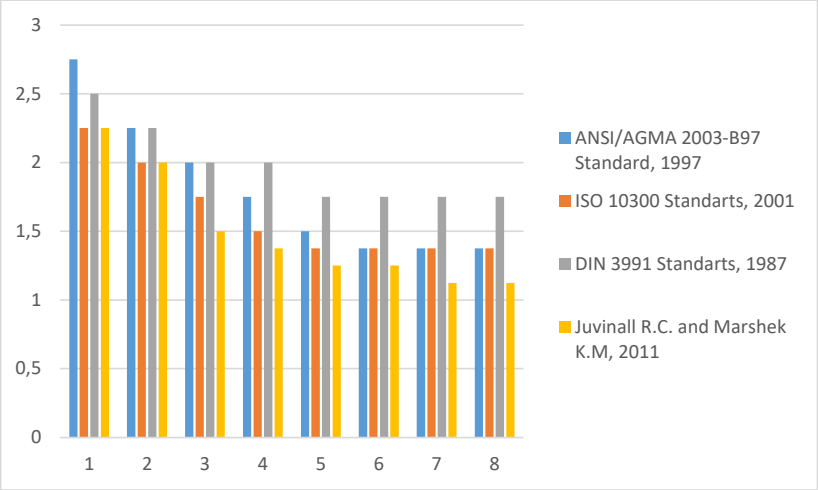

Figure C.17. The speed ratio effect on the module at 0,5 kW power transmission for α_n=25° and material type 1

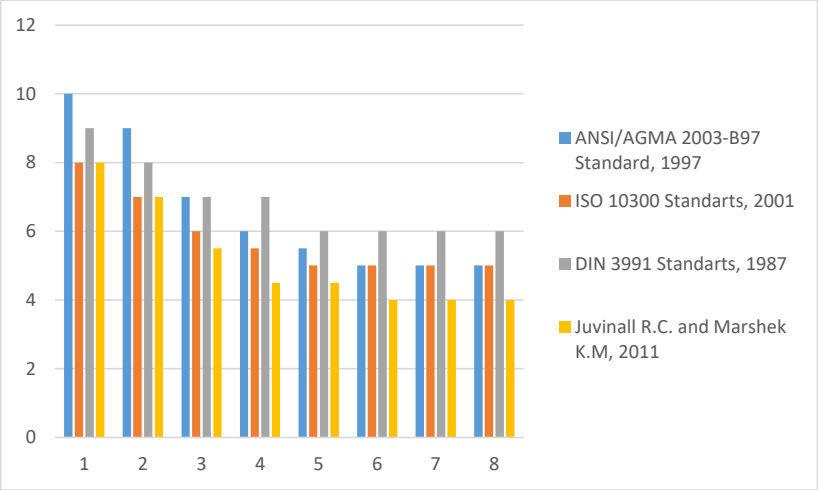

Figure C.18. The speed ratio effect on the module at 20 kW power transmission for α_n=25° and material type 1

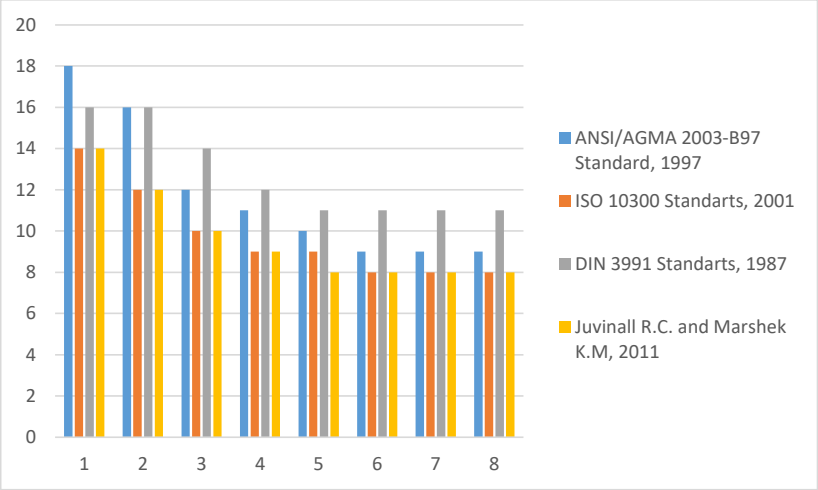

Figure C.19. The speed ratio effect on the module at 100 kW power transmission for α_n=25° and material type 1

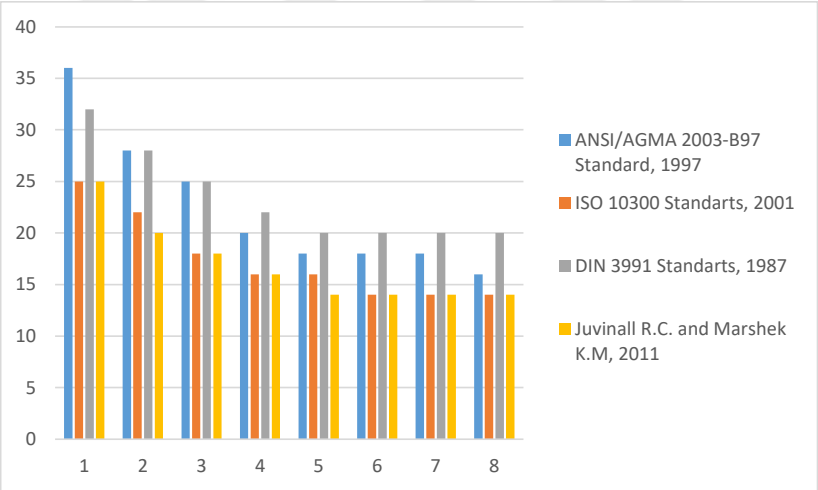

Figure C.20. The speed ratio effect on the module at 500 kW power transmission for α_n=25° and material type 1

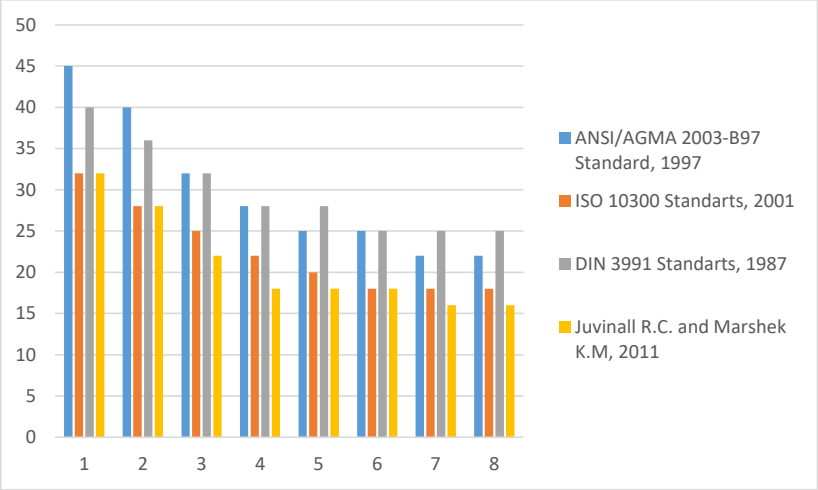

Figure C.21. The speed ratio effect on the module at 1000 kW power transmission for α_n=25° and material type 1

C.3. Obtaining Geometric Rating Number (GRi) for All Design Approaches and α_n=25°, Material type 1

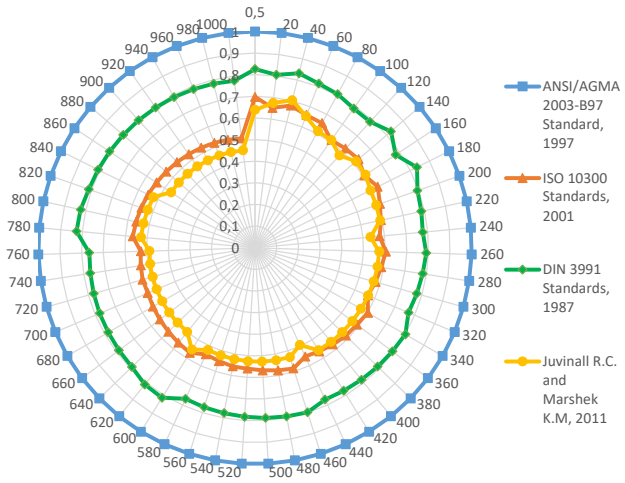

Figure C.22. Results of GR_i for all approaches at 1:1 speed ratio for α_n=25° and material type 1

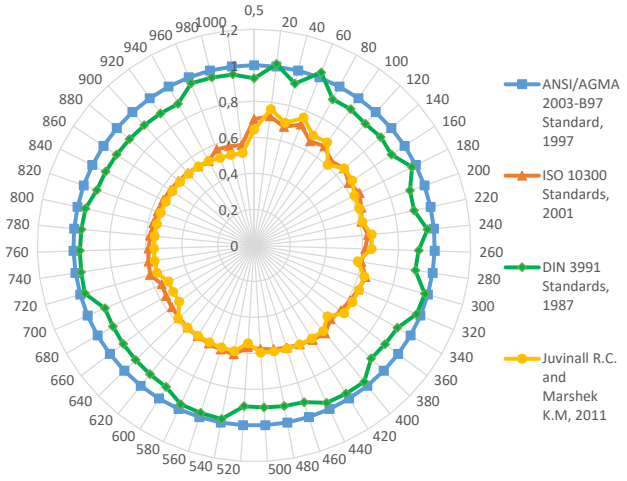

Figure C.23. Results of GR_i for all approaches at 2:1 speed ratio for α_n=25° and material type 1

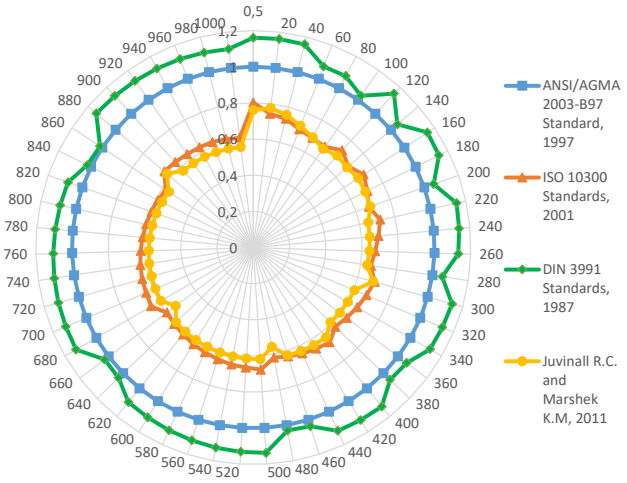

Figure C.24. Results of GR_i for all approaches at 3:1 speed ratio for α_n=25° and material type 1

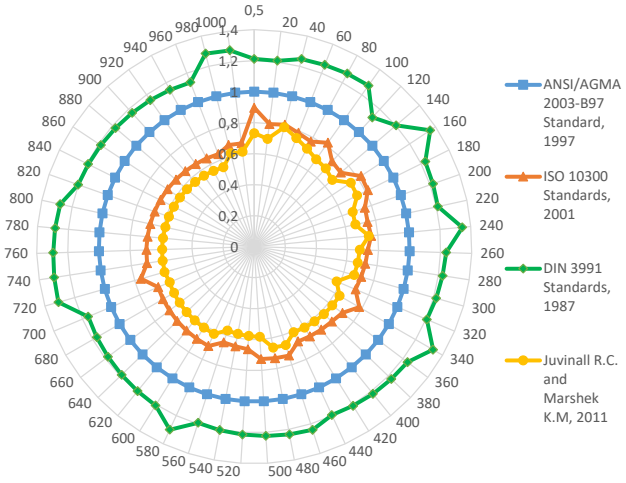

Figure C.25. Results of GR_i for all approaches at 4:1 speed ratio for α_n=25° and material type 1

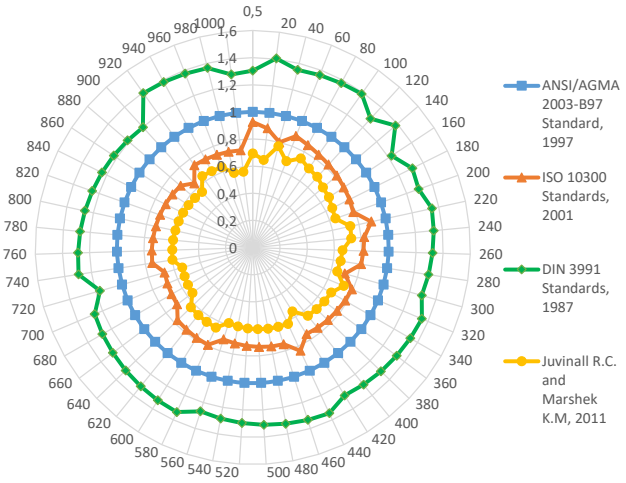

Figure C.26. Results of GR_i for all approaches at 5:1 speed ratio for α_n=25° and material type 1

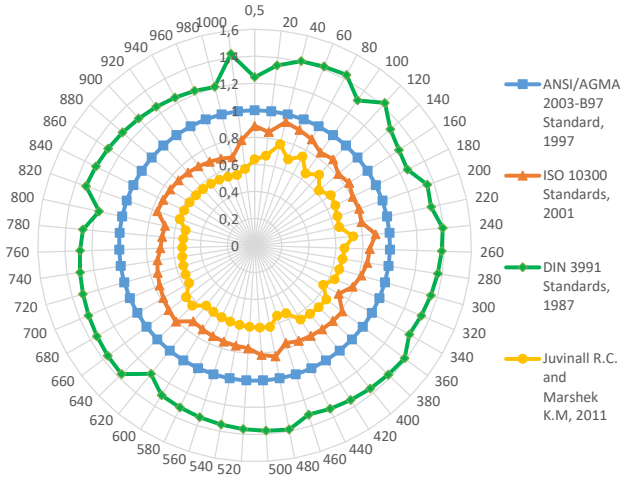

Figure C.27. Results of GR_i for all approaches at 6:1 speed ratio for α_n=25° and material type 1

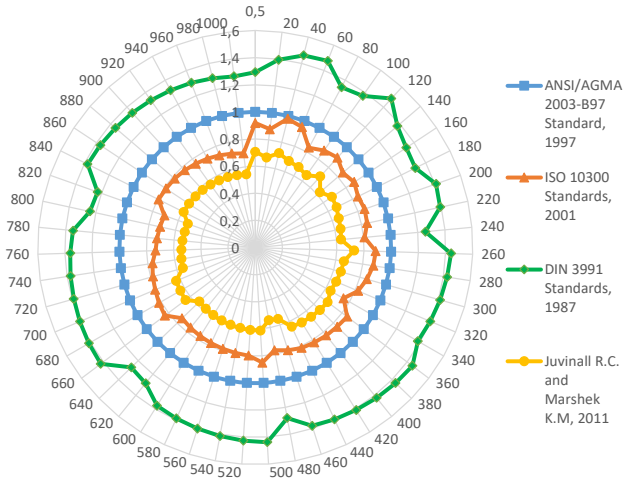

Figure C.28. Results of GR_i for all approaches at 7:1 speed ratio for α_n=25° and material type 1

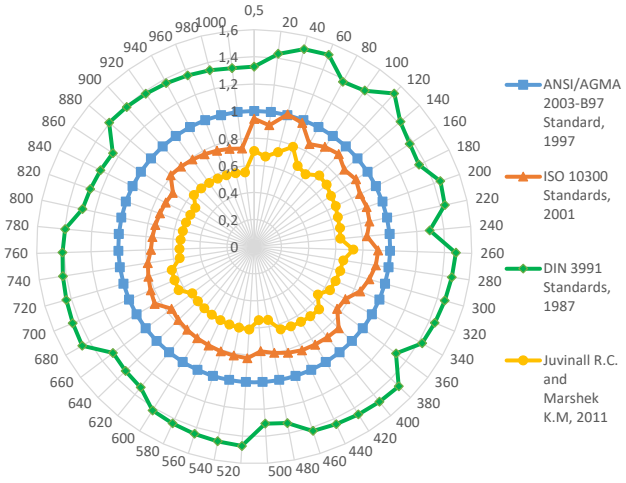

Figure C.29. Results of GR_i for all approaches at 8:1 speed ratio for α_n=25° and material type 1

APPENDIX D

D.1. Comparison of Face With and Module Results for α_n=25°, Material type 2

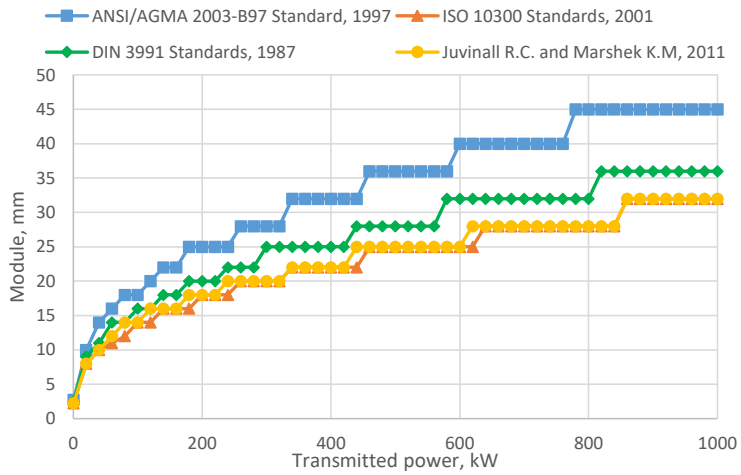

Figure D.1. Module values under various transmitted power at 1:1 speed ratio for α_n=25° and material type 2

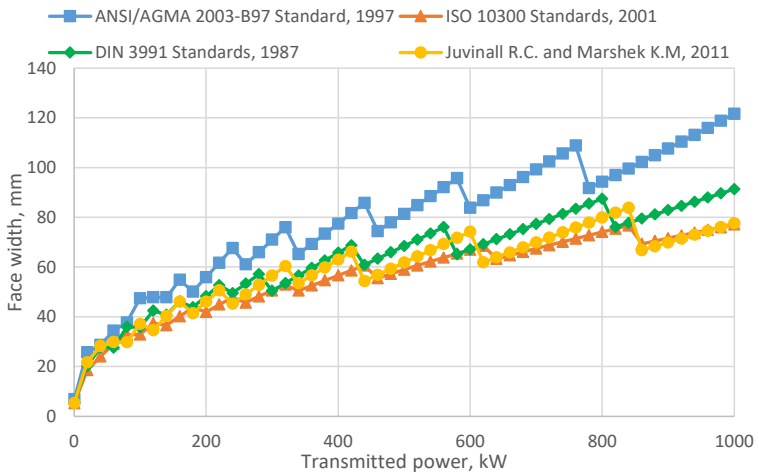

Figure D.2. Face width values under various transmitted power at 1:1 speed ratio for α_n=25° and material type 2

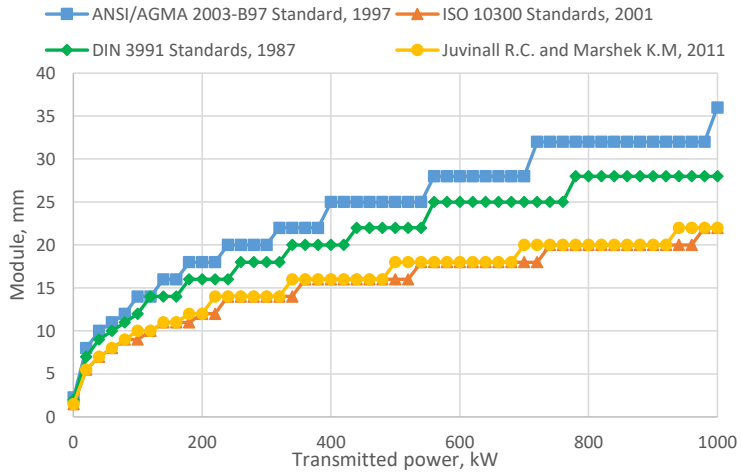

Figure D.3. Module values under various transmitted power at 2:1 speed ratio for α_n=25° and material type 2

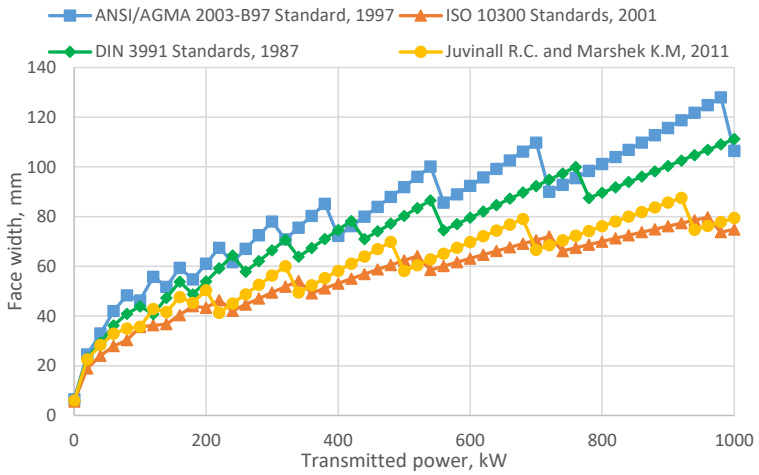

Figure D.4. Face width values under various transmitted power at 2:1 speed ratio for α_n=25° and material type 2

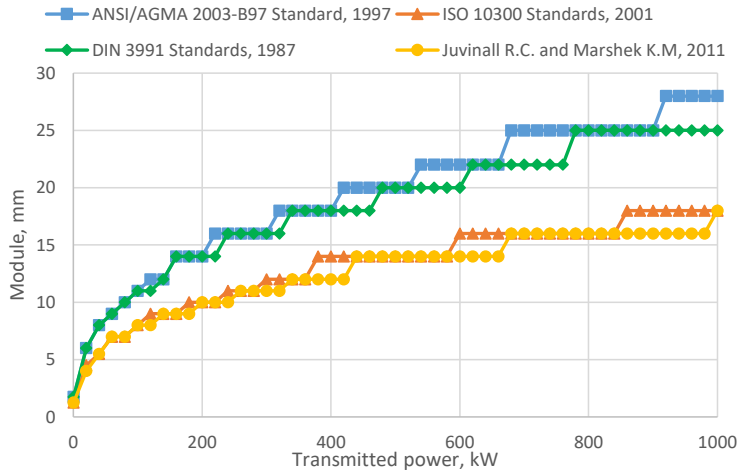

Figure D.5. Module values under various transmitted power at 3:1 speed ratio for α_n=25° and material type 2

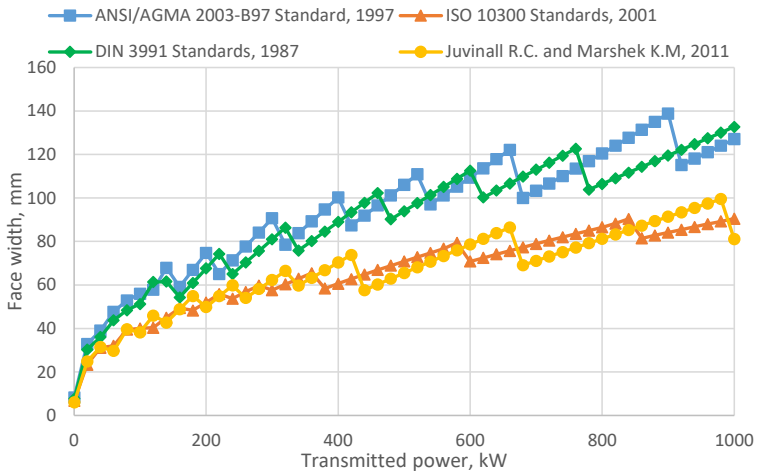

Figure D.6. Face width values under various transmitted power at 3:1 speed ratio for α_n=25° and material type 2

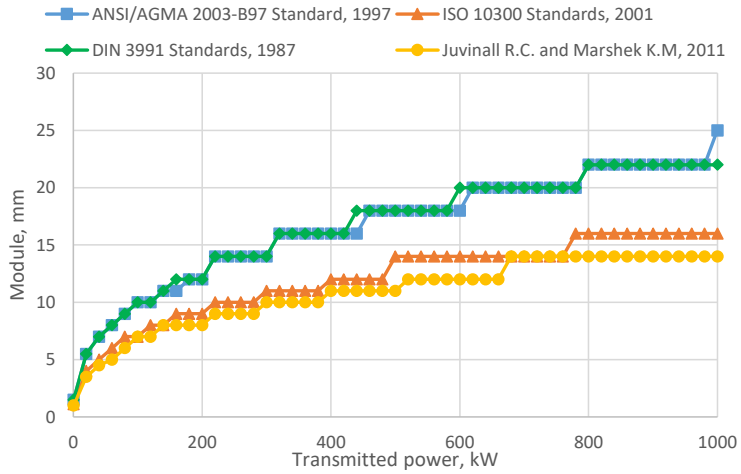

Figure D.7. Module values under various transmitted power at 4:1 speed ratio for α_n=25° and material type 2

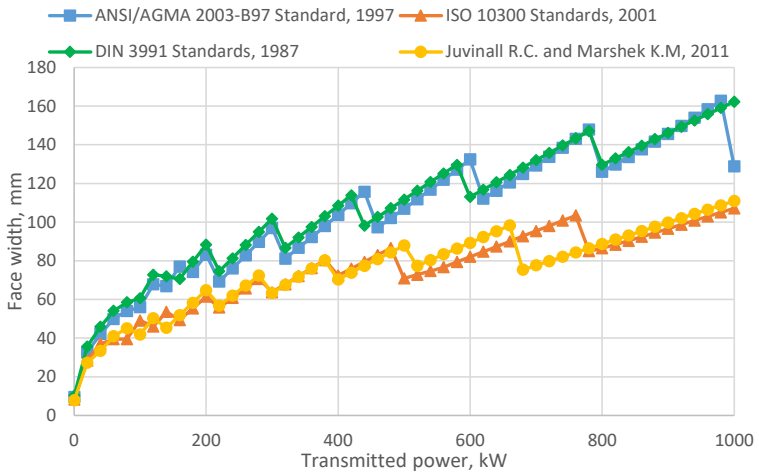

Figure D.8. Face width values under various transmitted power at 4:1 speed ratio for α_n=25° and material type 2

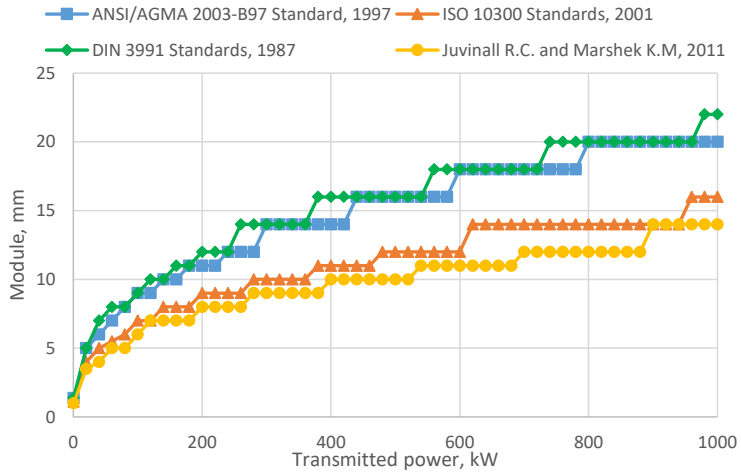

Figure D.9. Module values under various transmitted power at 5:1 speed ratio for α_n=25° and material type 2

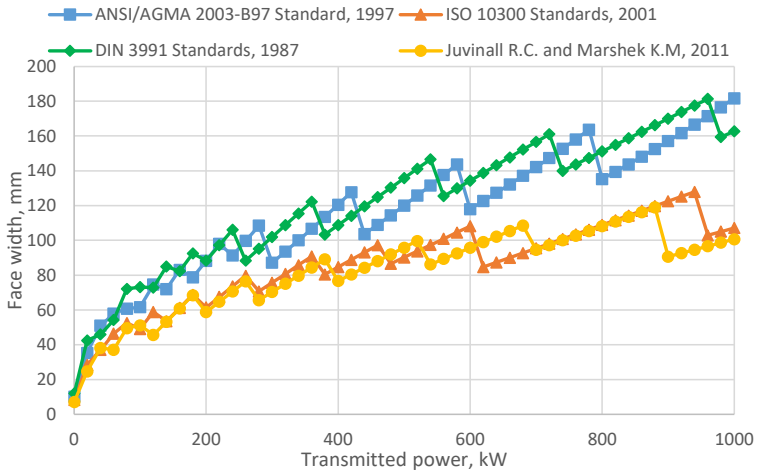

Figure D.10. Face width values under various transmitted power at 5:1 speed ratio for α_n=25° and material type 2

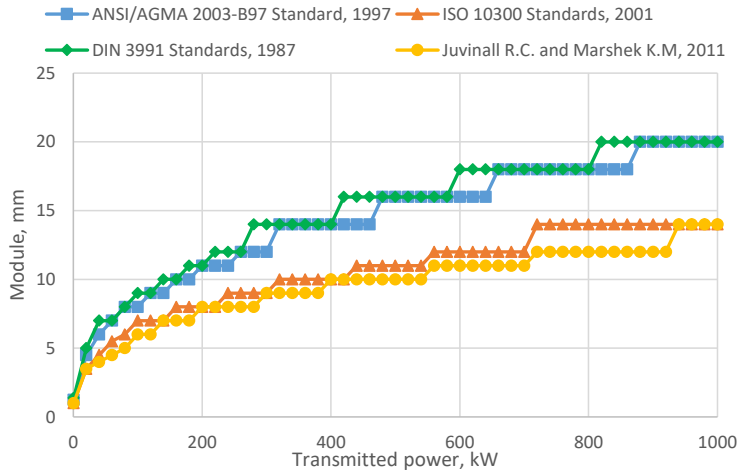

Figure D.11. Module values under various transmitted power at 6:1 speed ratio for α_n=25° and material type 2

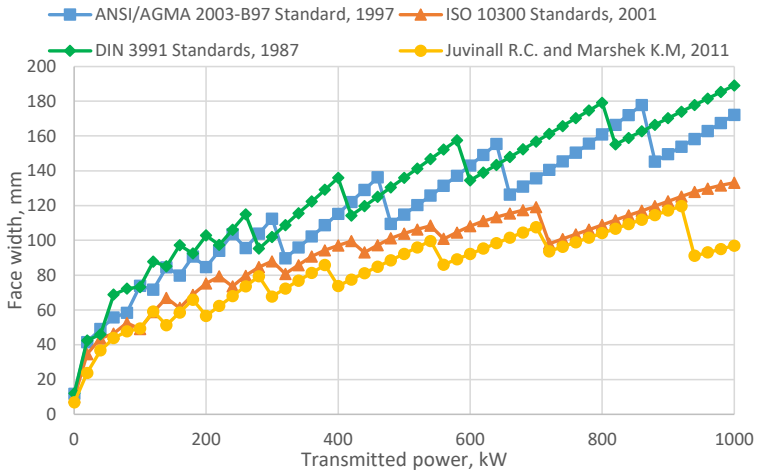

Figure D.12. Face width values under various transmitted power at 6:1 speed ratio for α_n=25° and material type 2

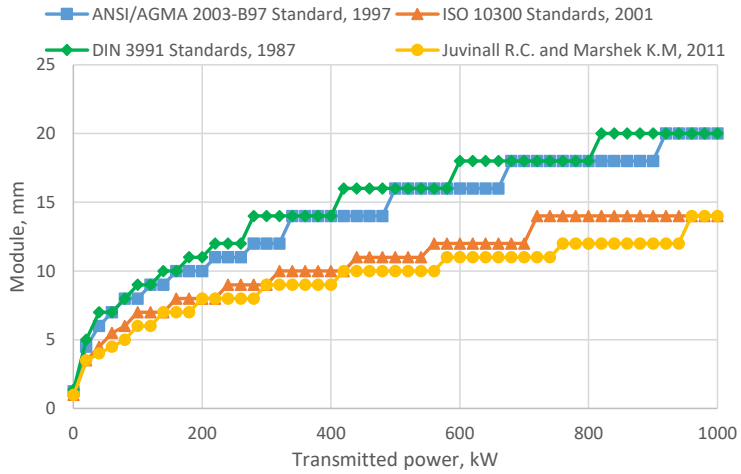

Figure D.13. Module values under various transmitted power at 7:1 speed ratio for α_n=25° and material type 2

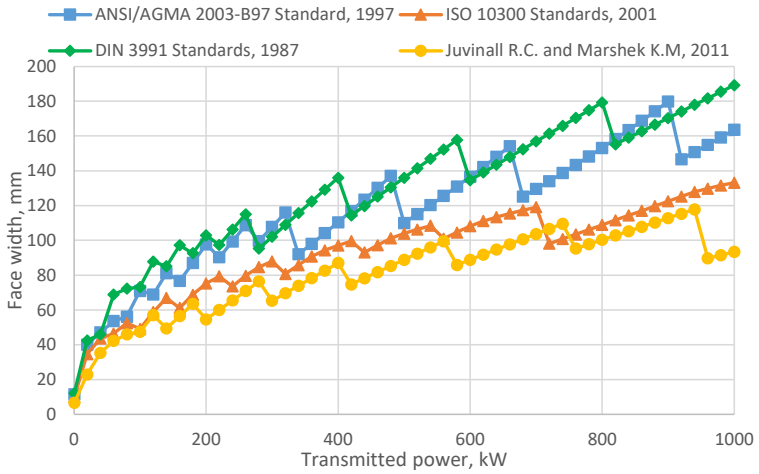

Figure D.14. Face width values under various transmitted power at 7:1 speed ratio for α_n=25° and material type 2

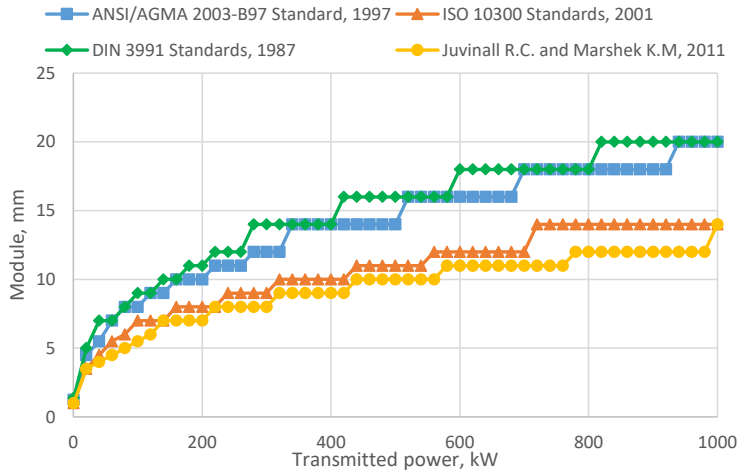

Figure D.15. Module values under various transmitted power at 8:1 speed ratio for α_n=25° and material type 2

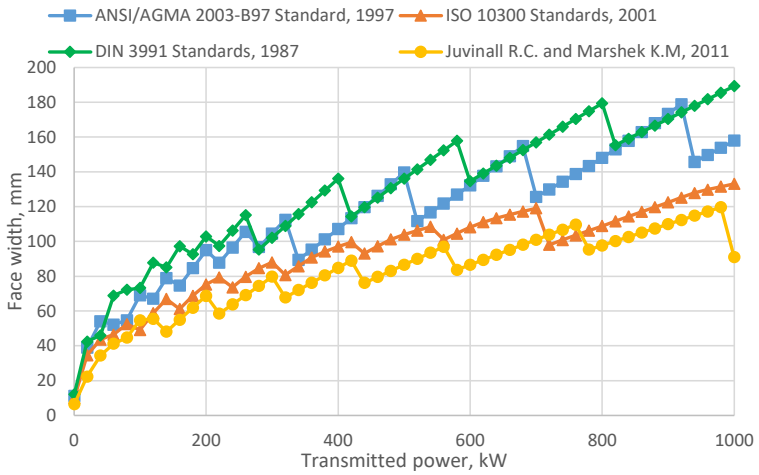

Figure D.16. Face width values under various transmitted power at 8:1 speed ratio for α_n=25° and material type 2

D.2. Comparison of the Module Results Considering Speed Ratio for the Selected Power Transmissions for α_n=25° and Material type 2

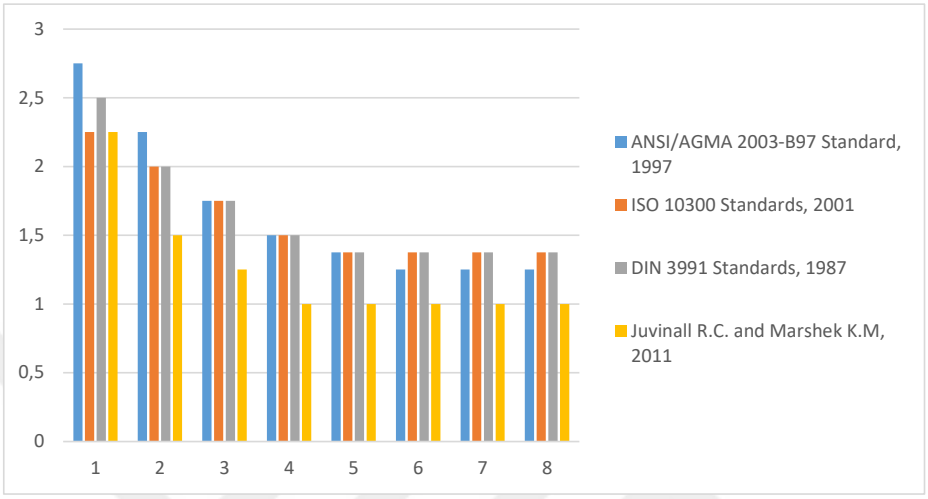

Figure D.17. The speed ratio effect on the module at 0,5 kW power transmission for α_n=25° and material type 2

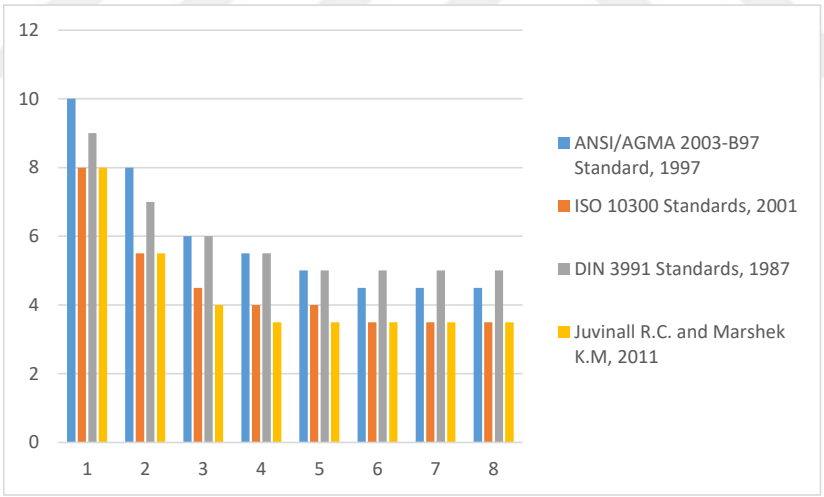

Figure D.18. The speed ratio effect on the module at 20 kW power transmission for α_n=25° and material type 2

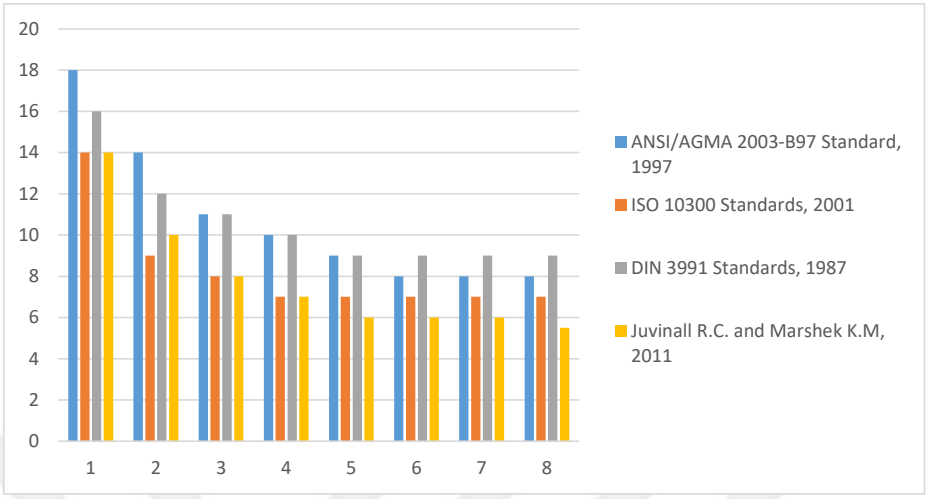

Figure D.19. The speed ratio effect on the module at 100 kW power transmission for α_n=25° and material type 2

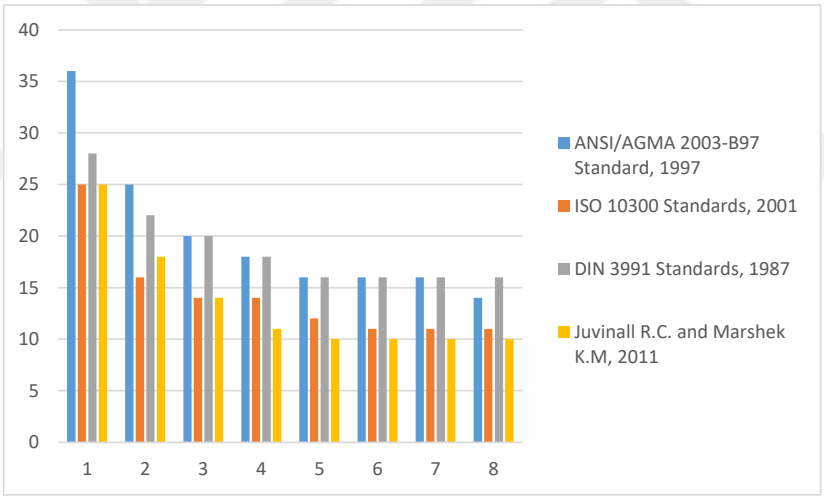

Figure D.20. The speed ratio effect on the module at 500 kW power transmission for α_n=25° and material type 2

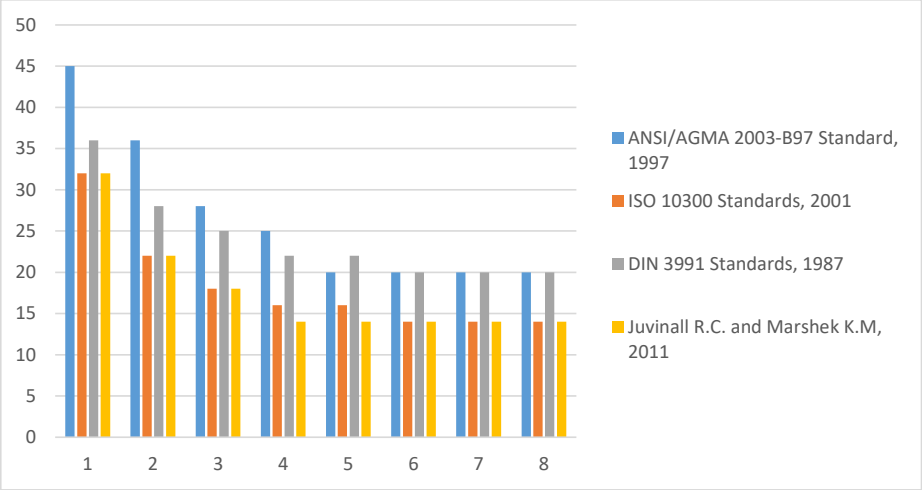

Figure D.21. The speed ratio effect on the module at 1000 kW power transmission for α_n=25° and material type 2

D.3. Obtaining Geometric Rating Number (GRi) for All Design Approaches and α_n=25°, Material type 2

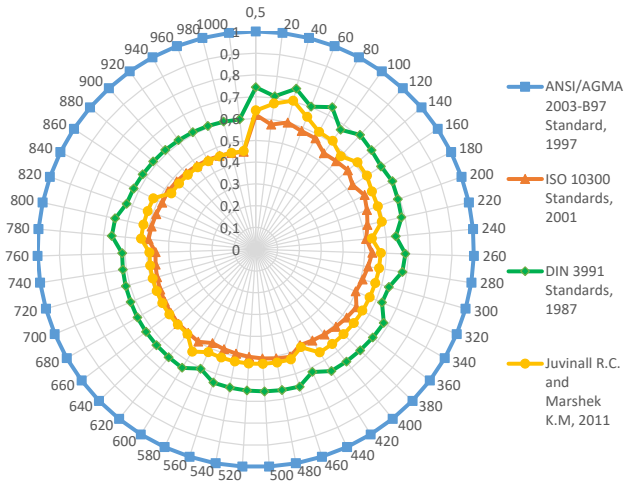

Figure D.22. Results of GR_i for all approaches at 1:1 speed ratio for α_n=25° and material type 2

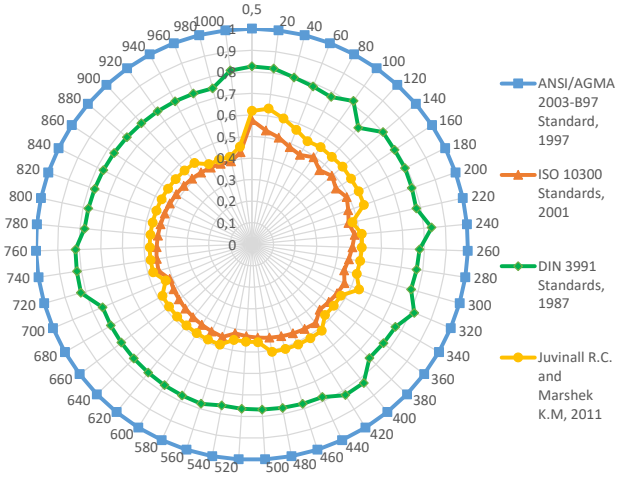

Figure D.23. Results of GR_i for all approaches at 2:1 speed ratio for α_n=25° and material type 2

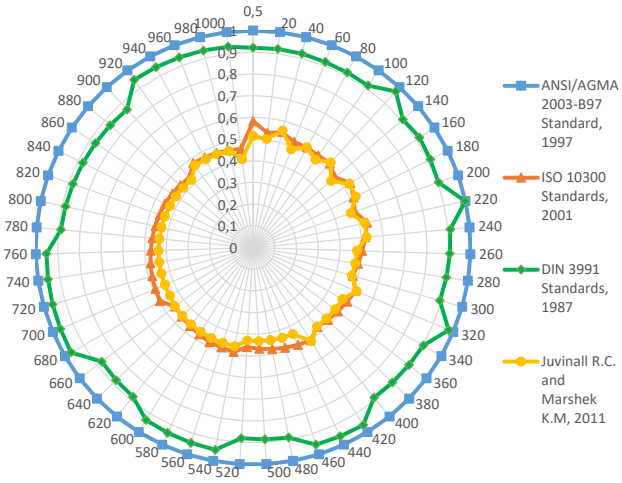

Figure D.24. Results of GR_i for all approaches at 3:1 speed ratio for α_n=25° and material type 2

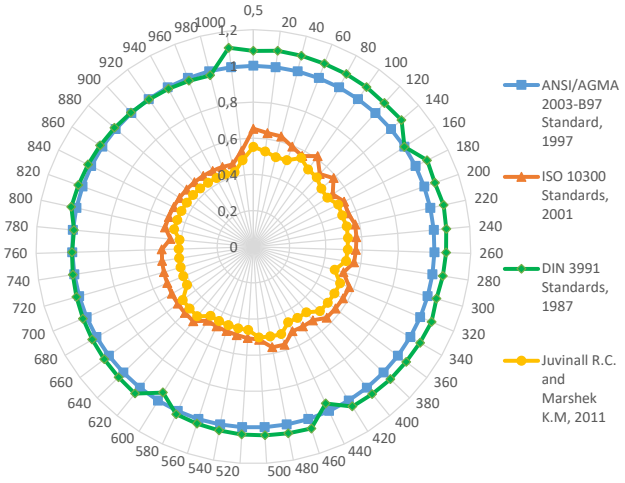

Figure D.25. Results of GR_i for all approaches at 4:1 speed ratio for α_n=25° and material type 2

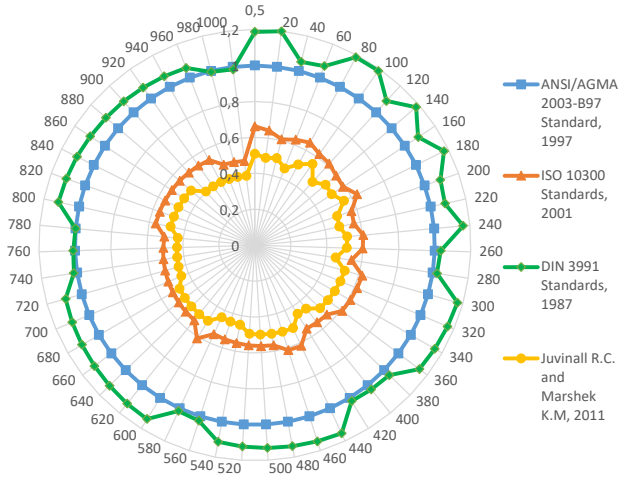

Figure D.26. Results of GR_i for all approaches at 5:1 speed ratio for α_n=25° and material type 2

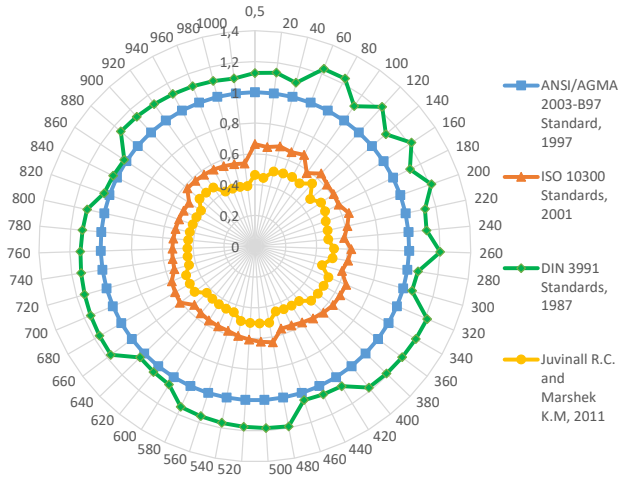

Figure D.27. Results of GR_i for all approaches at 6:1 speed ratio for α_n=25° and material type 2

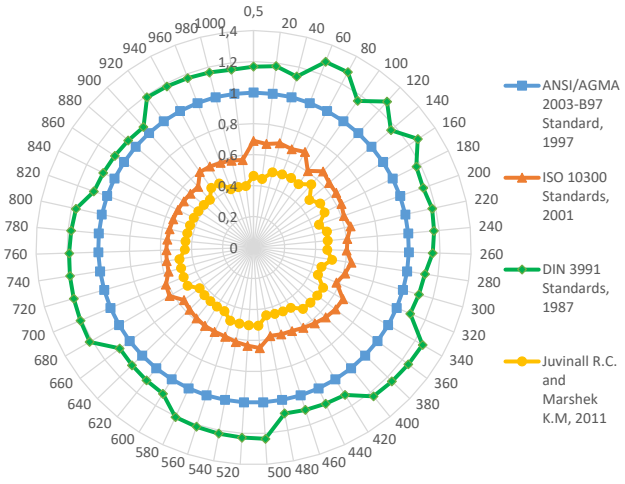

Figure D.28. Results of GR_i for all approaches at 7:1 speed ratio for α_n=25° and material type 2

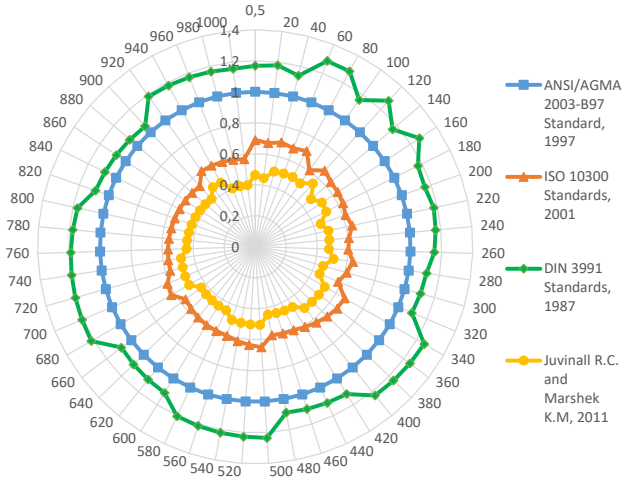

Figure D.29. Results of GR_i for all approaches at 8:1 speed ratio for α_n=25° and material type 2

APPENDIX E

E.1. Comparison of Face With and Module Results for α_n=25°, Material type 3

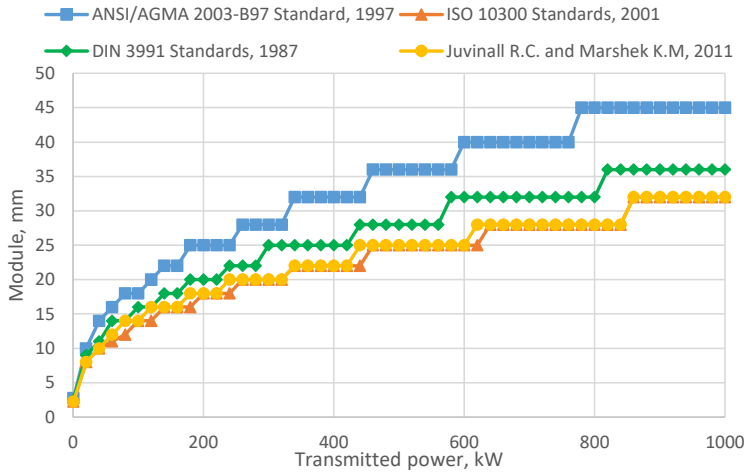

Figure E.1. Module values under various transmitted power at 1:1 speed ratio for α_n=25° and material type 3

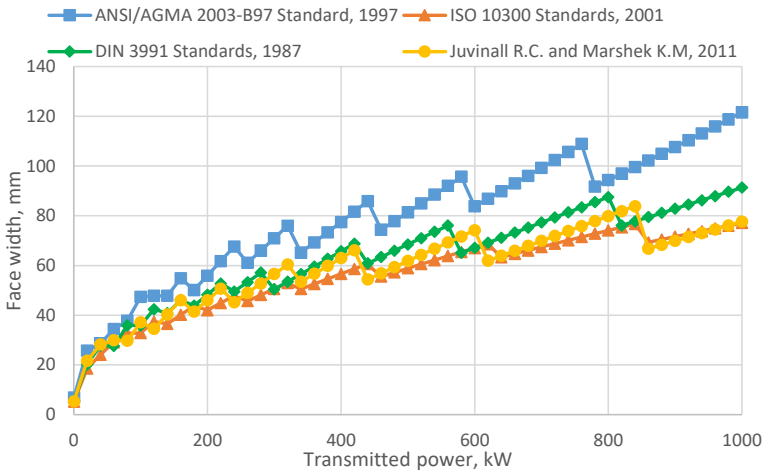

Figure E.2. Face width values under various transmitted power at 1:1 speed ratio for α_n=25° and material type 3

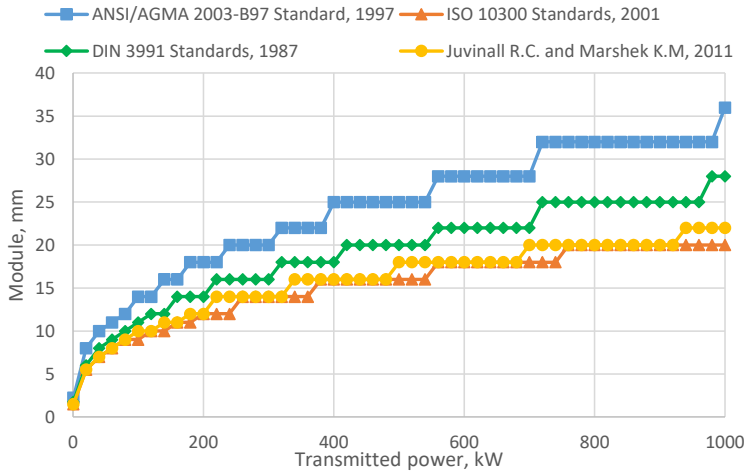

Figure E.3. Module values under various transmitted power at 2:1 speed ratio for α_n=25° and material type 3

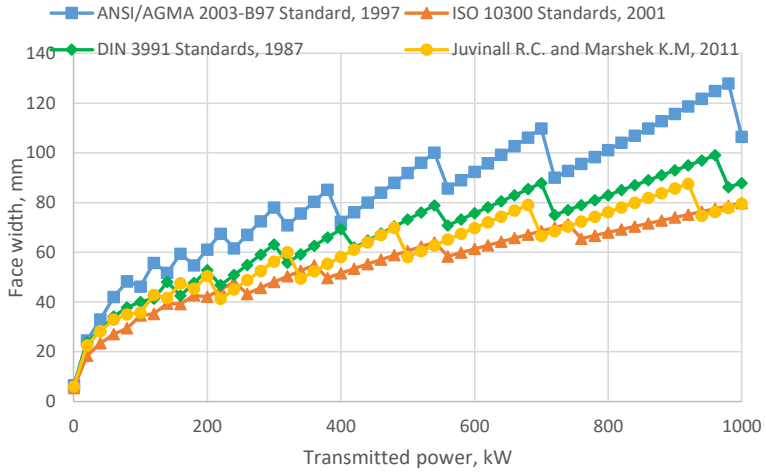

Figure E.4. Face width values under various transmitted power at 2:1 speed ratio for α_n=25° and material type 3

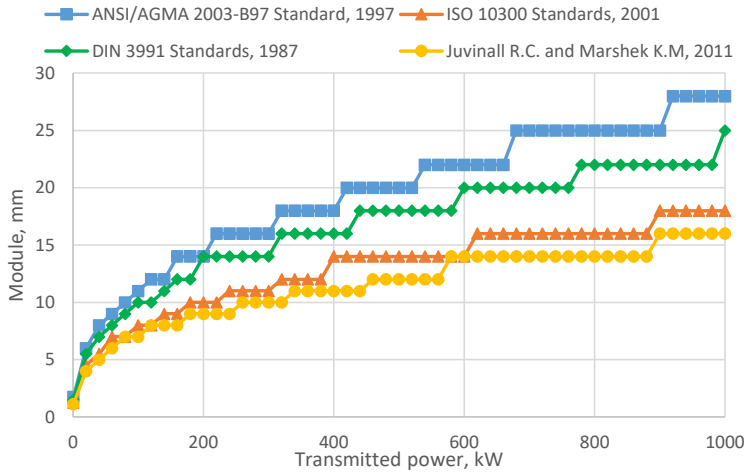

Figure E.5. Module values under various transmitted power at 3:1 speed ratio for α_n=25° and material type 3

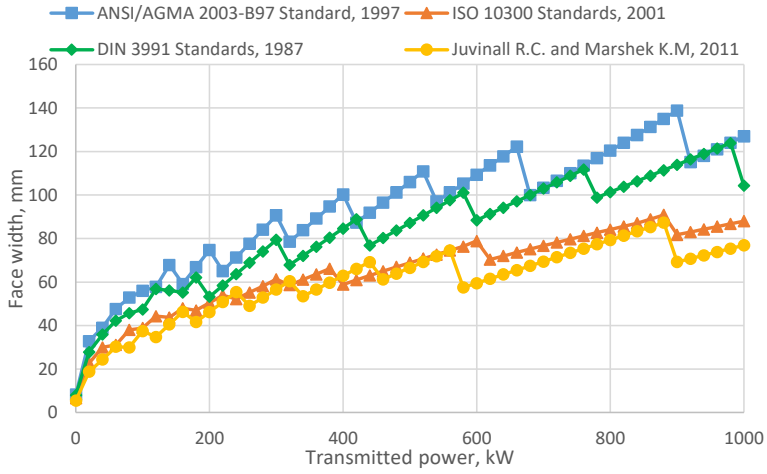

Figure E.6. Face width values under various transmitted power at 3:1 speed ratio for α_n=25° and material type 3

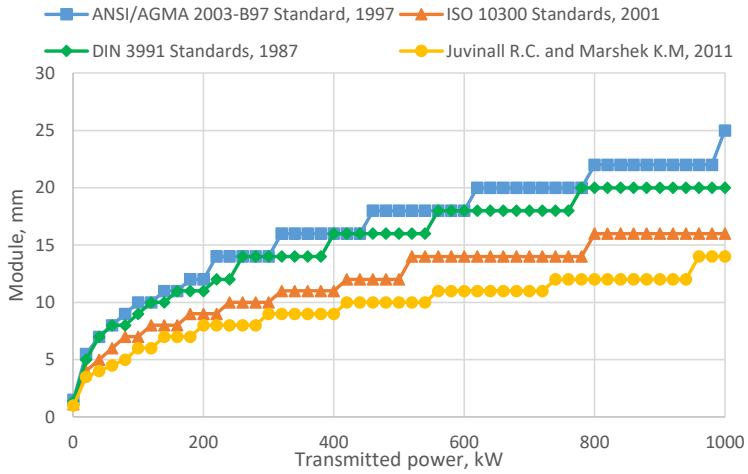

Figure E.7. Module values under various transmitted power at 4:1 speed ratio for α_n=25° and material type 3

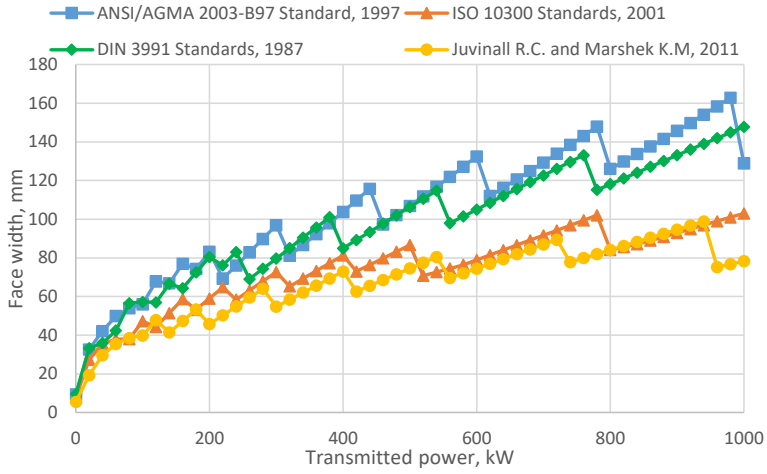

Figure E.8. Face width values under various transmitted power at 4:1 speed ratio for α_n=25° and material type 3

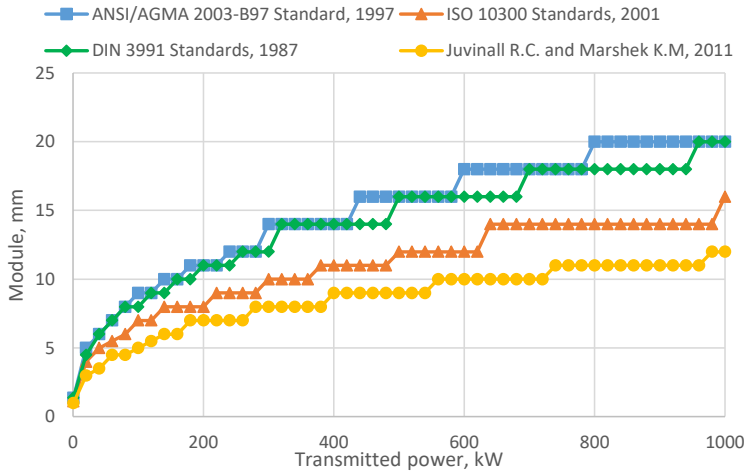

Figure E.9. Module values under various transmitted power at 5:1 speed ratio for α_n=25° and material type 3

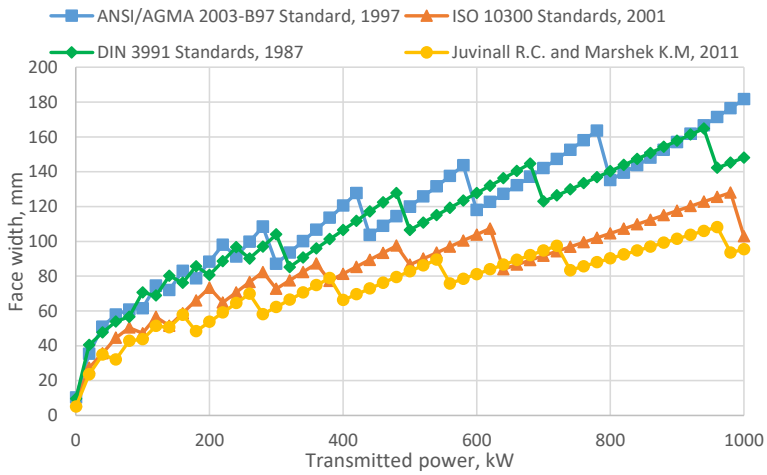

Figure E.10. Face width values under various transmitted power at 5:1 speed ratio for α_n=25° and material type 3

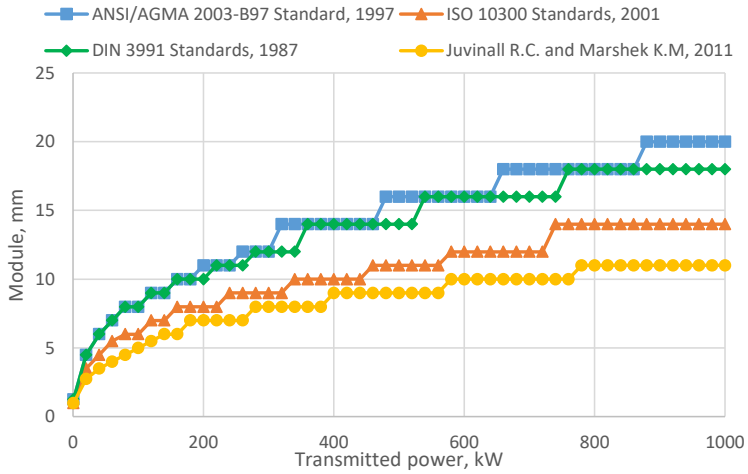

Figure E.11. Module values under various transmitted power at 6:1 speed ratio for α_n=25° and material type 3

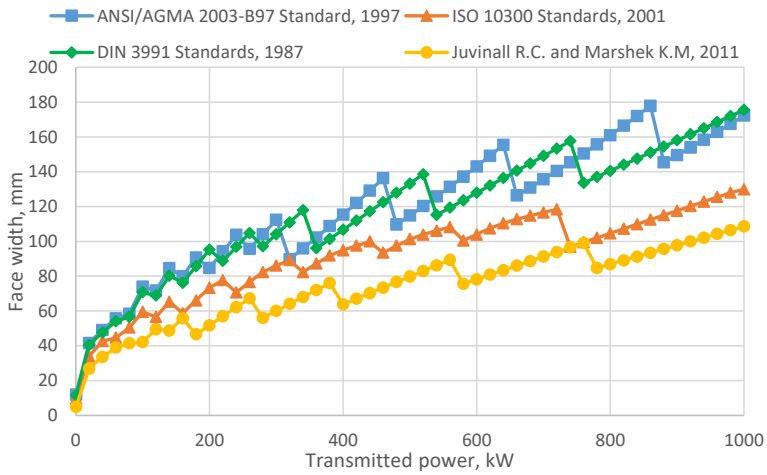

Figure E.12. Face width values under various transmitted power at 6:1 speed ratio for α_n=25° and material type 3

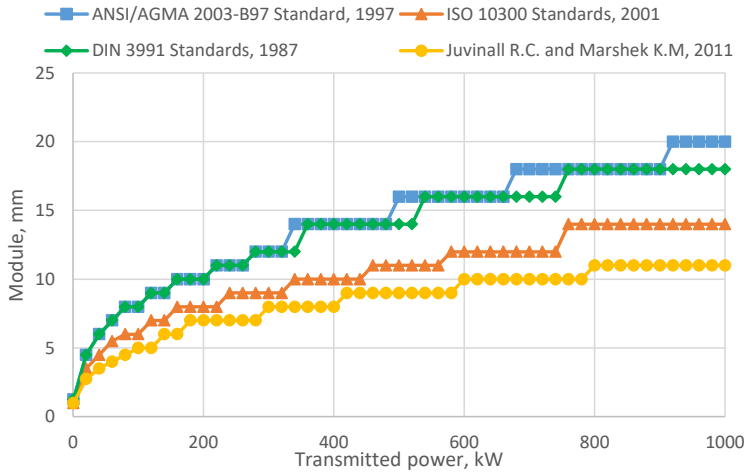

Figure E.13. Module values under various transmitted power at 7:1 speed ratio for α_n=25° and material type 3

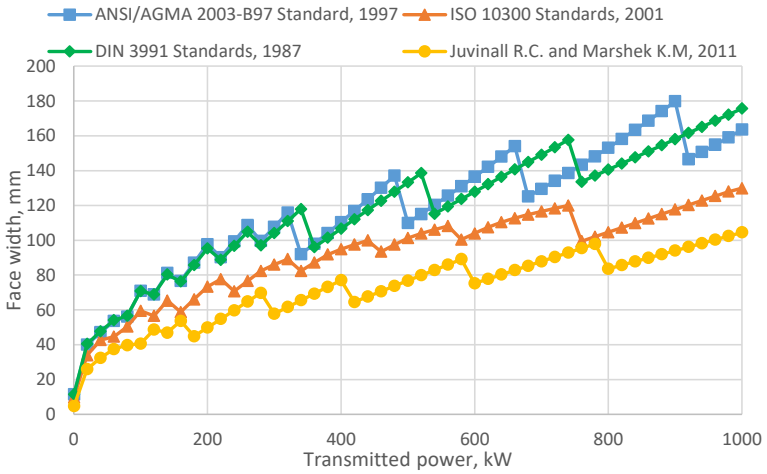

Figure E.14. Face width values under various transmitted power at 7:1 speed ratio for α_n=25° and material type 3

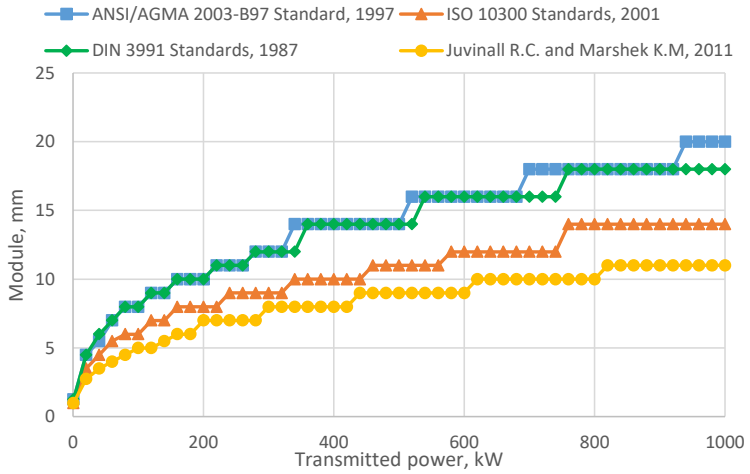

Figure E.15. Module values under various transmitted power at 8:1 speed ratio for α_n=25° and material type 3

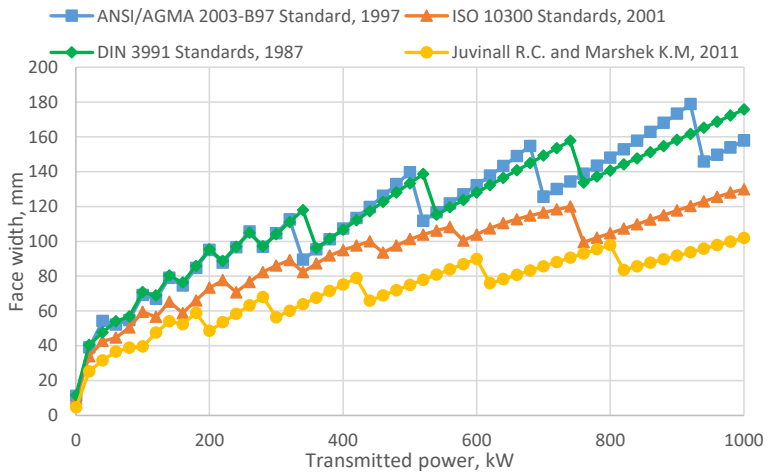

Figure E.16. Face width values under various transmitted power at 8:1 speed ratio for α_n=25° and material type 3

E.2. Comparison of the Module Results Considering Speed Ratio for the Selected Power Transmissions for α_n=25° and Material type 3

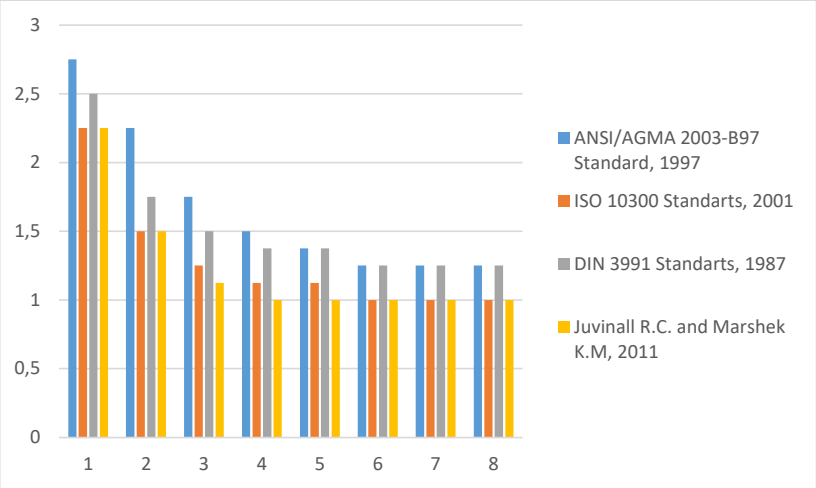

Figure E.17. The speed ratio effect on the module at 0,5 kW power transmission for α_n=25° and material type 3

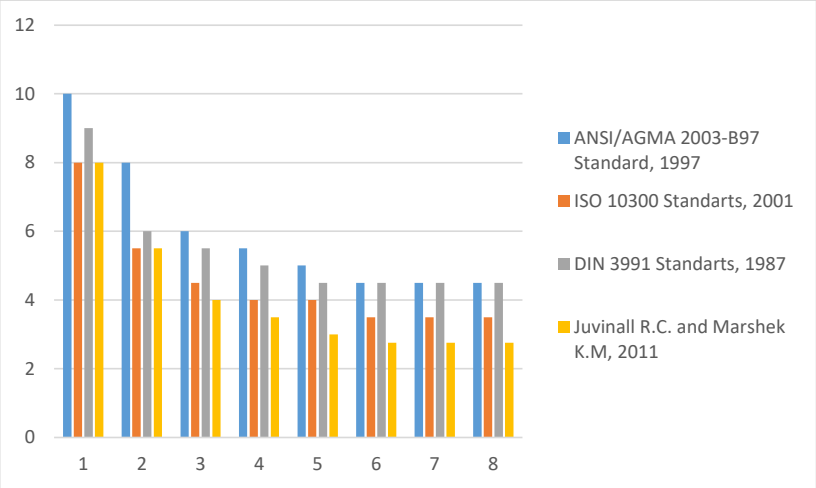

Figure E.18. The speed ratio effect on the module at 20 kW power transmission for α_n=25° and material type 2

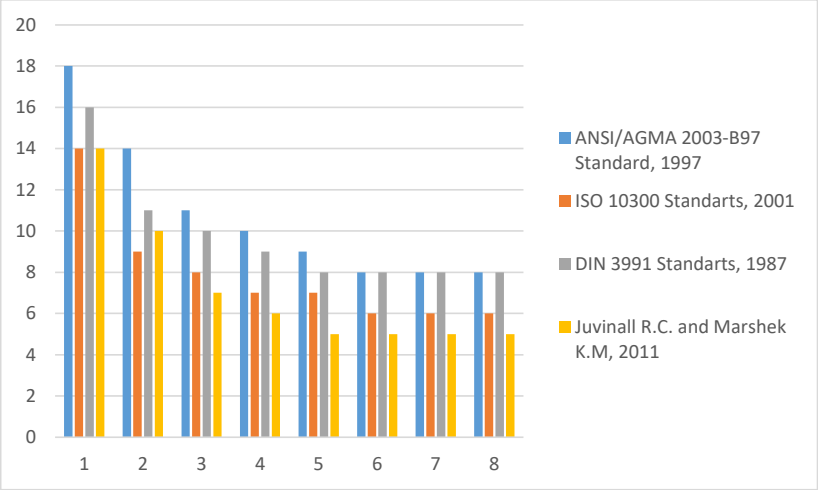

Figure E.19. The speed ratio effect on the module at 100 kW power transmission for α_n=25° and material type 2

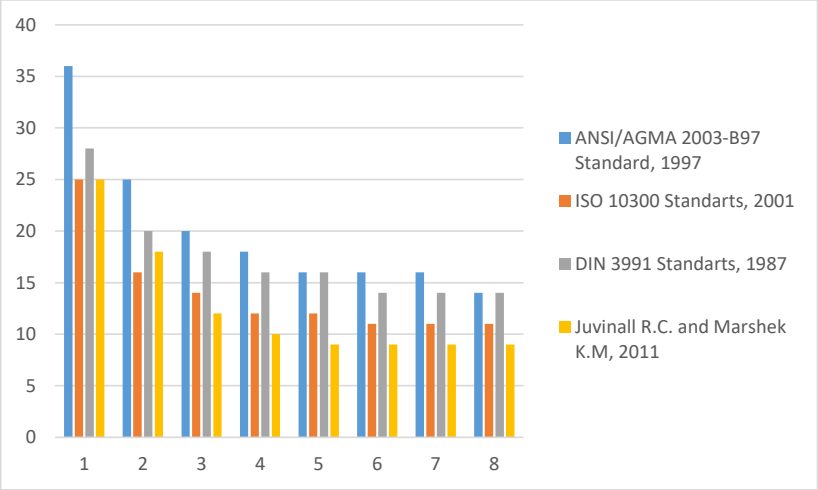

Figure E.20. The speed ratio effect on the module at 500 kW power transmission for α_n=25° and material type 2

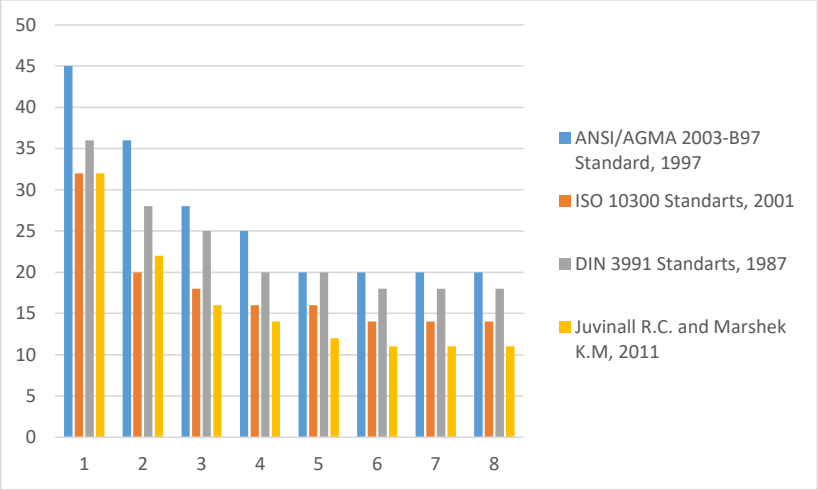

Figure E.21. The speed ratio effect on the module at 1000 kW power transmission for α_n=25° and material type 2

E.3. Obtaining Geometric Rating Number (GRi) for All Design Approaches and α_n=25°, Material type 3

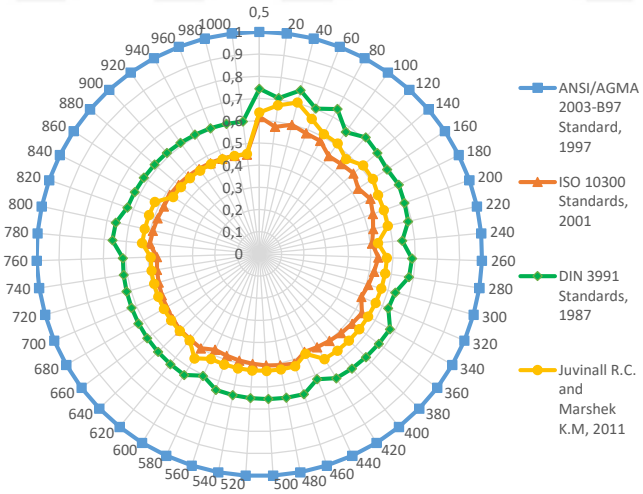

Figure E.22. Results of GR_i for all approaches at 1:1 speed ratio for α_n=25° and material type 3

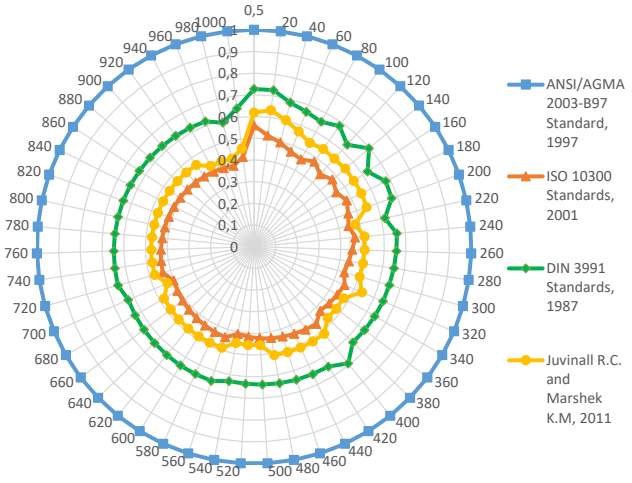

Figure E.23. Results of GR_i for all approaches at 2:1 speed ratio for α_n=25° and material type 3

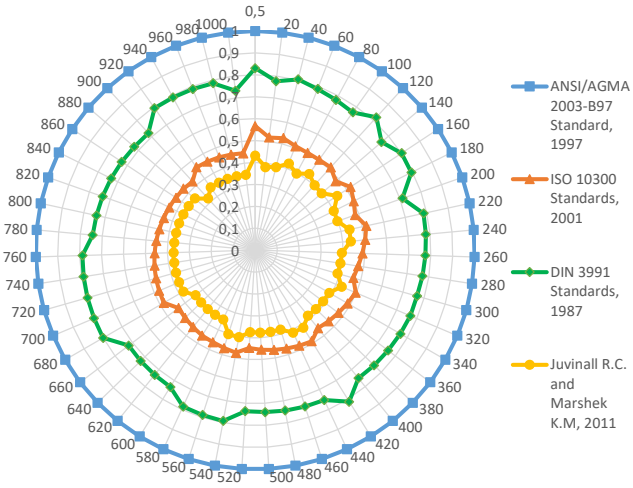

Figure E.24. Results of GR_i for all approaches at 3:1 speed ratio for α_n=25° and material type 3

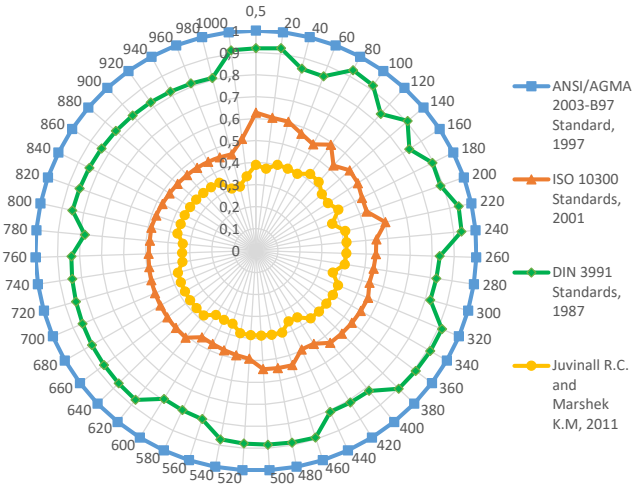

Figure E.25. Results of GR_i for all approaches at 4:1 speed ratio for α_n=25° and material type 3

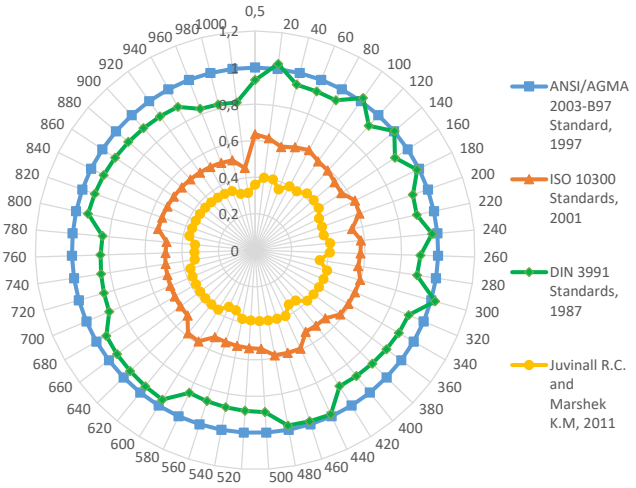

Figure E.26. Results of GR_i for all approaches at 5:1 speed ratio for α_n=25° and material type 3

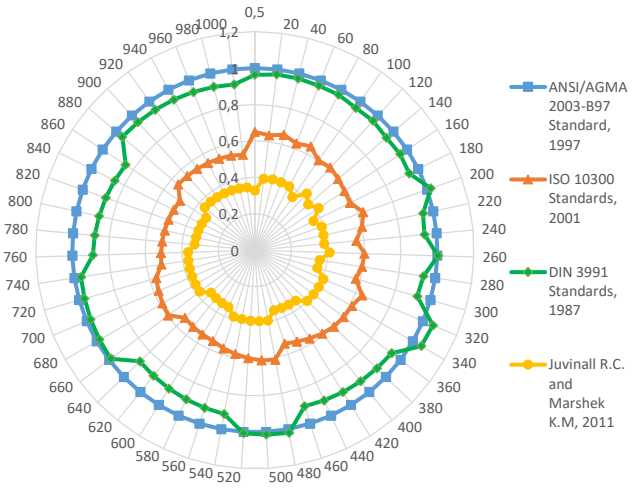

Figure E.27. Results of GR_i for all approaches at 6:1 speed ratio for α_n=25° and material type 3

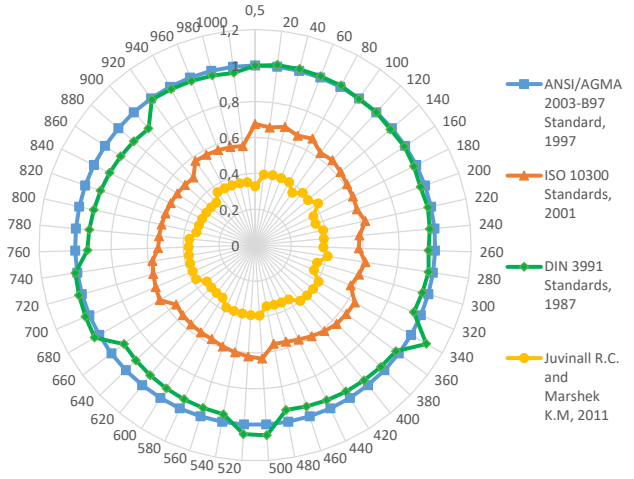

Figure E.28. Results of GR_i for all approaches at 7:1 speed ratio for α_n=25° and material type 3

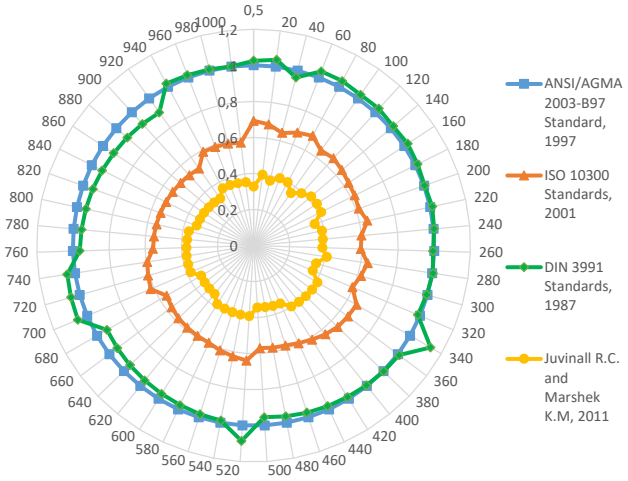

Figure E.29. Results of GR_i for all approaches at 8:1 speed ratio for α_n=25° and material type 3